THE UNIVERSITY OF CHICAGO

INTRINSIC NEURONAL EXCITABILITY AND LEARNED TEMPORAL FEATURES OF BEHAVIOR IN ZEBRA FINCHES

A DISSERTATION SUBMITTED TO

THE FACULTY OF THE DIVISION OF THE BIOLOGICAL SCIENCES

AND THE PRITZKER SCHOOL OF MEDICINE

IN CANDIDACY FOR THE DEGREE OF

DOCTOR OF PHILOSOPHY

COMMITTEE ON NEUROBIOLOGY

BY

NELSON DAVID MEDINA

CHICAGO, ILLINOIS

MARCH 2023

En el borde del camino hay una silla.

— Silvio Rodriguez, Historia de las Sillas

TABLE OF CONTENTS

LIST OF FIGURES v
LIST OF TABLES vii
ACKNOWLEDGEMENTS viii
ABSTRACT x
CHAPTER 1 INTRODUCTION 1
Fundamental properties of information processing in neurons 1
Synapses, neurons, and networks 2
Intrinsic Plasticity 6
Birdsong as a model system 10
The Song System: motor and basal ganglia pathways 13
HVC Network Properties 15
Intrinsic Properties of HVC neurons 18
Fundamental units of song 21
Syllable combination selectivity 22
Goals of this thesis 23
CHAPTER 2 TEMPORAL FEATURES OF SONG CORRELATE WITH HVC_X REBOUND EXCITABILITY 25
Introduction 25
Timing is critical 27
Investigating plasticity of IPs in vitro 28
Methods 28
Animals and housing 28
Natural and instrumental song learning 29
Song analysis and segmentation 33
Slice preparation 35
Whole-cell recordings 35
Inclusion and analysis criteria 38
Retrograde labeling 38
Data Processing and Analysis 38
Results 39
Within-individual uniformity of IPs 40

IP expression is determined by song learning 42
Plasticity of intrinsic excitability in vitro 44
HVC_X IPs are learned and related to temporal features song. 50
Discussion 62
Reflections on Daou and Margoliash, 2020 63
Activity dependent changes to excitability in vitro 66
HVC_X IPs are learned and related to temporal features song. 67
CHAPTER 3 MODELING HVC_X NEURONS NETWORK PROPERTIES 69
Introduction: A coordinated orchestra keeps time 69
Modeling methods and results 71
Discussion 79
CHAPTER 4 REPLICATION OF SONGBIRD METRONOMICS 83
Introduction 83
Methods 84
Replication 85
Discussion 85
CHAPTER 5 SEEING SONG AND OTHER FUTURE DIRECTIONS 88
Introduction 88
Methods 89
Results 89
Discussion 91
CHAPTER 6 GENERAL DISCUSSION 93
A conductor is not a metronome 94
Summary and Interpretation of results 94
Reflections on Neuroethology 104
REFERENCES 105

LIST OF FIGURES

1.1. The action potential 5
1.2. Ion channel conductances affect neuron firing properties 9
1.3. Zebra finch song is highly stereotyped 12
1.4. Diagram of the song system nuclei 15
1.5. HVC projection neurons have distinct IPS 20
2.1. Diagram of experimental designs 31
2.2. A juvenile listening to song playback 32
2.3. Automatic detection of harmonic stacks 34
2.4. A brain slice containing HVC 37
2.5. Features of recordings covary with series resistance 40
2.6. Within-bird similarity of intrinsic properties 41
2.7. Time and activity dependent loss of evoked firing 45
2.8. Somatic stimulation protocol 45
2.9. Stimulation decreases evoked firing frequency 46
2.10. Example traces from a stimulated neuron 47
2.11. Stimulation induced hyperpolarization 47
2.12. Summary of rapid resting membrane potential hyperpolarization 48
2.13. Post-stimulation changes in afterhyperpolarization 48
2.14. Post-stimulation changes in I/V relationship 49
2.15. HVC_X IPs evaluated from the raw data 51
2.16. HVC_{RA} and HVC_X are distinguishable by their membrane capacitance 51
2.17. Correlations of spectral song features with HVC_X IPs 53
2.18. Harmonic stacks have lower pitches than other syllable types 54
2.19. Harmonic stacks reflect temporal structure 55
2.20. Features of rebound excitation relate to temporal song features 57
2.21. Revisiting data from Daou and Margoliash, 2020 58
2.22. Duration of song motif and longest harmonic stacks covary 59
2.23. Instrumental tutoring with modified songs produces changes in HVC_X IPs 60
2.24. Evoked inward currents relate to song duration 61
2.25. Verified HCN currents for one cell from two birds 62

3.1. HVC_X can function as coincidence detectors in vitro 70
3.2. Rebound excitation shifts the range of integration 71
3.3. The fundamental circuit module of my Hodgkin-Huxley network model 75
3.4. A network model uses intrinsic rebound excitation to detect sequences 77
3.5. Example traces of sequence selective model neurons 78
4.1. Replication of the guess and test method (GAT) 86
4.2 Root mean squared error summary plots for one song 87
5.1. Setup for CaMPARI2 photoconversion during song playback 89
5.2. Examples of viral expression 90
5.3. In vitro CaMPARI2 photoconversion 91
6.1. Uniformity of intrinsic properties promotes precision in population spike timing 96
6.2. Modular network structure supports multiple bursts 101
6.3. Multi-bursting model neurons produce parallel burst sequences 102

LIST OF TABLES

1. Mixed linear model results for sag ratios 43
2. Mixed linear model results for firing frequency..... 43

ACKNOWLEDGEMENTS

First of all, I would like to acknowledge my advisor, Daniel Margoliash, who has an unyielding optimism and confidence in the people he accepts into his lab. I could not have succeeded without Dan's support throughout the many challenges of graduate school, scientific or otherwise. For that, and for all I've learned from you about being a careful and resilient scientist, thank you, Dan.

My labmates created a culture of solidarity and scientific curiosity that made going into lab a happy experience, always. They encouraged me at every step, helped troubleshoot every setback, and celebrated each success. Kyler Brown was my first mentor in the lab, withstood my endless barrage of questions as a rotation student, and impressed in me that 'the truth can wait' – something that I found comforting and told myself many times throughout graduate school. Sofija Canavan showed me the pinnacle of efficient zebra finch breeding colonies and lab notebook organization. Graham Fetterman explained almost any concept on the drop of a hat and gave me unfettered advice. Sofija and Graham taught me how to code and kept me honest in my analyses. I cannot count the hours we spent by a whiteboard discussing each other's latest scientific challenges or ideas. From them, I learned what it means to be a good coworker and labmate. Arij Daou made invaluable contributions to my work and is an irreplaceable electrophysiologist and companion. In many ways, Arij's contagious passion for neuroscience contributed to my perseverance through the process of data collection. Conversations with Andrew Savoy stimulated a lot of thinking and contributed to the discussions of the results within this thesis. Andy has also been an ideal colleague, who fearlessly delved into many side projects with me, always bringing ingenious practical solutions to equipment limitations. Daniel Baleckaitis provided technical and emotional support at every step, taught me how to do surgeries and injections, and to not sweat the small

things. Daniel also taught me how to use the espresso machine in lab, a skill that many a lab member has benefited from, none more than me.

David Koren taught me the fundamentals of patch clamp electrophysiology and provided me with guidance through my first years of graduate school. I will always remember the excitement of my first whole cell recording, which I did with David (Thursday, November 24th, 2016, circa 2:00 am). David is an exceptional mentor and a dear friend. Giorgio Grasselli and Heather Titley trained me in whole cell recordings in Christian Hansel's lab and instilled in me the attention to detail (not superstitions) required to keep a patch rig operational. Daniel Gill was always willing to entertain my ideas and provide grounding perspective. While I cannot name each and every person, I would be remiss if I didn't acknowledge the members of the Hansel and Eatock labs who over the years, collectively, have so generously shared their time and equipment to help improve the quality of my experiments and thinking. I must also thank the members of my committee, Ruth Anne Eatock, Christian Hansel, and Jason Maclean, for their general support and for their contributions to my experimental design and interpretation of my results.

Lastly, I want to thank my family. My brother, Alejandro, who has been a beacon of reason and intellectual honesty all of my life. My cousins (and close friends) who have stuck with me despite international and geographical challenges. My wonderful partner, Anastasia Sorokina, without whom I could not have survived graduate school. And most of all, I want to thank my parents, Nelson David Medina Sr. and Ana Lilia Jimenez, for whom words can't begin to approximate the appreciation I feel. My parents left behind everyone and everything they knew, on two occasions, to give my brother and I the opportunity to write this very document and live a life with intellectual freedom. I hope to continue to carry my gratitude into everything I that I do, always. Gracias Papi y Mami.

ABSTRACT

The study of plasticity in the intrinsic properties (IPs) of neurons is unveiling mechanisms beyond synaptic plasticity that relate network activity and learning. Prior results in zebra finches establish a relationship between the IPs of forebrain neurons and learned song. Within the premotor nucleus HVC, the IPs of HVC basal-ganglia-projecting neurons (HVC_X) are developmentally regulated and differ across birds in a way that is related to their learned songs.

In my PhD project I investigated the role of song learning in regulating HVC_X IPs. I used a counterbalanced design to raise siblings or unrelated birds to sing natural or modified songs. I patched onto HVC_X neurons in slice and evaluated their firing properties in relation to the bird's song. I found that various features of HVC_X IPs, and their variation, were related to the songs the birds sang.

Examining the relation between IPs and learned song allowed me to delve deeper into the relation between HVC_X and song features. I discovered a correlation between timing features of song and the rebound excitation of HVC_X: neurons from birds who sang longer songs with long harmonic stacks had a combination of IPs that reflected stronger rebound excitation. This demonstrates an explicit link between neuronal IPs and features of learned behavior. Given that harmonic stacks are spectrally unchanging over their duration, this result also suggests a mechanism underlying HVC_X neurons' documented ability to integrate over long periods of time.

To explore the possible mechanisms quantitatively, I used my results, along with established work, to develop a Hodgkin-Huxley-based network model of HVC that related in vitro IPs with in vivo bursting properties during singing. I conceptualized HVC_X as interval encoders that detect sequences by summing rebound depolarization triggered by the removal of inhibition with monosynaptic excitatory events that occur later in time. In the network,

HVC_X are connected in a nested fashion to encode increasingly complex sequences. This model serves as a hypothesis linking neuronal IPs to network structure and behavior.

In the course of these studies, I performed a number of experiments focused on bringing viral tools to the experimental toolbelt in the Margoliash lab (viral tracing, calcium imaging, and activity dependent fluorescent labeling), and replicated work showing internal temporal structure within zebra finch song. Altogether, my work focused on linking fundamental neural mechanisms of information processing to network structure, and learned behavior, and hypothesized how they might relate to temporal integration. My work accentuates the importance of including neuronal IPs when developing realistic network-level descriptions of neural circuits.

CHAPTER 1

INTRODUCTION

Fundamental properties of information processing in neurons

In 1894, Santiago Ramon y Cajal told the Royal Society of London that "the ability of neurons to grow in an adult and their power to make new connections can explain learning". His work, summarized by Heinrich Waldeyer-Hartz as the 'neuron doctrine' provided the fundamental infrastructure that blossomed into the field of neuroscience. Through his detailed drawings and descriptions of neuron morphology, Cajal discovered that neurons are discrete cells that make connections with each other to form elaborate networks. He hypothesized that information was exchanged through gaps between neurons, called synapses (Higgins and George, 2013).

Cajal was right to pay close attention to neurons' morphology, and to their connections. Synapses are critical for information processing in neural networks and express an expansive diversity of structure and function. Neurons communicate with each other across synapses via transmission of molecules called neurotransmitters. At each synapse, specialized post-synaptic receptors for neurotransmitters open transmembrane channels in the receiving neuron that allow the flow of ions towards electrochemical equilibrium. This is the main method of communication between neurons. However, connectivity is only part of the story of information processing in neurons (chemical transmission). This thesis aims to explore how non-synaptic mechanisms contribute to how individual neurons, and therefor networks, process information.

Neurons spend most of their energy maintaining a precise concentration for different ions (Cl^-, Na^+, Ca^{+2}, K^+), thereby regulating the electrochemical gradients that define the direction in which each ion flows across the cell membrane. The differences in ionic concentrations result in

neuronal membranes that are electrically charged. A neuron's steady-state voltage, or resting potential, is roughly 70 millivolts negative relative to the outside. In this configuration, neurons behave as entropy-fighting machines, working to maintain their resting membrane potential. This might seem like a Sisyphean task, but this maintenance is the underpinning of neurons' essential function, which orchestrates behavior: the timing, the shape of, and the numbers and temporal structure of emitted action potentials.

Neurons 'spike', sending electrical impulses propagating throughout their cell bodies, causing a unidirectional wave of depolarization down their axon at speeds upwards of 150 meters per second. This is an action potential; a behavior which is only possible because of the electrochemical gradient and specialized voltage-gated proteins. The first experiments that quantitatively described and modeled the action potential were done by Alan Hodgkin and Andrew Huxley (1952), who recorded from an unmyelinated axon from the giant squid. They developed a series of differential equations that defined a dynamical system whose output replicated that of the squid axon. Their model included voltage-gated parameters for $sodium^{+}$ and $potassium^{+}$ channels with their corresponding reversal potentials. That biophysical model provided the first mechanistic explanation of the 'all-in-one' behavior of the action potential. This work defined a second foundational pillar for neuroscience: intrinsic functional properties, and signal processing within neurons. And just as there is great diversity in synaptic morphology and function, a world of complexity in ion channel types and properties has since been unveiled.

Synapses, neurons, and networks

As Cajal hypothesized, synaptic connections provide a mechanism for learning. Synapses provide capacity for information storage and are the entry point for information into neural networks. Through Hebbian plasticity, increasing its strength (Hebb, 1949; Caporale and Dan,

2008), a particular synapse can encode the occurrence of specific events that correlate together. Therefore, a subset of synapses within a circuit can encode specific movements or sensations. For example, in context-fear-conditioned mice, activating synapses specific to one context can trigger a fear response in a previously unpaired environment, while inactivating those same synapses can prevent a conditioned fear response (Liu and Tonegawa, 2014). Another experiment elegantly showed that specific inactivation of auditory synapses in the amygdala prevented a previously associated fear response to a tone (Nabavi et al.., 2014). Crucially, in these experiments, it was the specificity and subtlety of the manipulations that highlighted how powerful synaptic plasticity is. Synapses are stable over long periods of time yet remain flexible enough to accommodate the everchanging environment. This kind of investigation of synaptic communication has provided clarity about the brain correlates of learning and memory. Undoubtedly, synaptic plasticity is a fundamental mechanism.

But what are the mechanisms within a neuron to process the post-synaptic signals? These processes depend on the biophysical properties of the cellular membrane. The phospholipid bilayer of a cell behaves as a parallel-plate capacitor, prohibiting the flow of charges across it and storing charges on either side of the membrane. This introduces a capacitive component to all electrical events within a neuron, which then affect the time course of voltage changes within it. Additionally, membranes have embedded proteins that serve important roles for the maintenance and function of cells, many of which are transmembrane proteins that allow the flow of water, ions, and smaller molecules across the membrane. These transmembrane channels introduce a conductive component to the membrane (1/resistance). With Ohm's law (V=IR) we can describe the electrical changes within a neuron that result from synaptic currents. From the time constant (τ = RC), we also understand that the time course of those changes is dependent on the resistive component of the membrane (membrane resistance = M_R), and the capacitive component (membrane capacitance

= M_C). This is a straightforward example of the second fundamental aspect of signal processing in neurons, one highlighted by Hodgkin and Huxley's work: intrinsic functional properties.

The principal function of a neuron (communication with other neurons) hinges on the action potential. Spikes are sudden and transient waves of depolarization that initiate near the cell body at the axon initial segment and travel towards the extremities of the axon. Axons can terminate locally and distally to form synapses with other neurons. At these terminal points exist axon boutons that house the neurotransmitter releasing machinery that forms the presynaptic side of a synapse. Now, consider that a single human pyramidal neuron can form tens of thousands of synapses and that any single postsynaptic event is relatively small. In the postsynaptic neuron, an individual synaptic event dissipates with time and is unlikely to trigger an action potential. This means that the coincidence of multiple inputs is necessary to produce sufficient stimulation to trigger an action potential. Critically, this raises the question of threshold: How much is enough? This is a question of functional properties and is related to the membrane channels that underlie the action potential.

In the simplest description of the action potential, voltage-gated Na^+ channels cause the initial depolarizing phase of the action potential, while voltage-gated K^+ channels with slower kinetics cause the repolarization phase (Figure 1.1). Voltage-gated channels change configuration (open) at fixed voltages determined by their protein structure and occur in a probabilistic manner, not in all-or-non fashion. Because protein thresholds are somewhat fixed, the spike threshold at the neuronal scale depends on the number and density of channels. This gives rise to a source of variability in neuronal functional properties because different neurons can express different amounts and densities of ion channels. Ion channel expression and membrane properties are referred to as intrinsic properties (IPs) and determine the intrinsic excitability of a neuron. Differences in ion channel expression affect how sensitive a neuron is to inputs, and the form of its

response. As such, a neuron's excitability is a product of the expression of its ion channels; its intrinsic excitability.

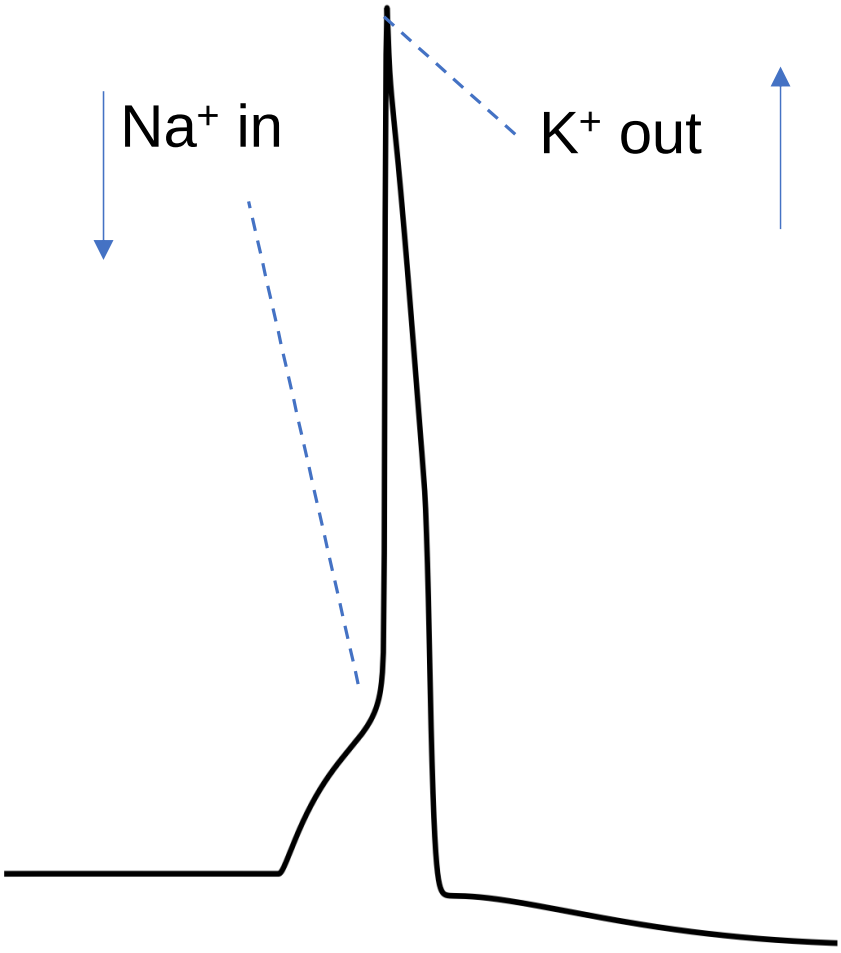

Figure 1.1. The action potential (modeled using Hodgkin-Huxley formulation). The downward blue arrow and associated dashed line points to the moment where the voltage crosses spike threshold and gated sodium channels open to allow sodium ions to flow, which depolarize the neuron. The upward arrow and associated dashed line point to moment where voltage gated potassium channels are maximally open (and voltage gated sodium channels are inactivated) and allow for potassium to flow and repolarize (or hyperpolarize) the neuron.

Intrinsic Plasticity

As it pertains to neuronal plasticity and learning, much of intrinsic excitability remains relatively underappreciated compared to synaptic plasticity. However, even within individual dendrites, activity-dependent plasticity affects dendritic computation and signal propagation to the soma (Sjostrom et al.., 2008; O'Hare et al.., 2022). At the soma and action initial segment, excitability affects whole-neuron bursting properties, giving rise to diverse neuronal behaviors ranging from fast-spiking interneurons to phasic onset encoding neurons.

Consider the following examples: Specialized 'OFF' ganglion cells in the retina rely on hyperpolarization activated cyclic nucleotide (HCN) channels, and an inhibitory response to light, to encode loss of signal (Margolis and Detwiler, 2007; Mitra and Miller, 2007). In cerebellar Purkinje cells, the regulation of the calcium-dependent potassium channel (SK) is associated with eye-blink conditioning, and its knock-out leads to mice with motor learning deficiencies (Grasselli, et al.., 2019; Titley et al.., 2020). Importantly, IPs also contribute to global features like resting membrane potential and can give rise to neurons that express patterned activity, as with rhythmic oscillators (Prinz et al.., 2004). In the lobster stomatogastric ganglion, intrinsic plasticity contributes to circuit output and stability (Marder and Prinz, 2002).

From here, it becomes clear that to understand a network we must understand the firing properties of its individual neurons and model them, as well as their connections. These properties of a neuron's excitability, or intrinsic properties (IPs), are a manifestation of the collage of ion channels expressed by the neuron and can be modeled mathematically as Hodgkin and Huxley did (Prinz et al.., 2004; Daou et al.., 2013; Daou and Margoliash, 2020). Experience–dependent changes of intrinsic excitability have been observed in many systems (Mitra and Miller, 2007; Marder and

Prinz, 2002; Ross et al.., 2017, 2019), but how to integrate these findings into models of complex learning and memory is still being discussed (Daou and Margoliash, 2020; Titley et al., 2017).

Ion channel expression is a major factor of intrinsic excitability in neurons. Depending on which channels, and their relative proportions, neurons can have very different responses to identical stimuli. Below, I present two examples of ion channels that have markedly different properties and effects on neuronal excitability. These examples should emphasize a useful analogy: That each kind of ion channel in a cell is itself a 'knob' that can be tweaked to alter signal processing, and that none of them exist independently of the other. Each neuron behaves as a dynamical system that incorporates all the ion channels (and their dynamics) that it expresses.

The first example is the small conductance calcium-dependent potassium channel (SK). SK channels allow the passage of potassium cations across the membrane but only in the presence of calcium ions. Calcium is typically only present in high intracellular concentration during potent activation, making it an effective proxy signal for activation within the neuron. This means that SK channels only open during moments of strong depolarization. When they do open, they allow potassium to flow towards its equilibrium potential, resulting in potassium ions leaving the neuron and hyperpolarizing it. In this way, the SK channel is a knob that decreases excitability. As neurons spike, calcium floods the cell opening potassium channels and driving the membrane potential away from spiking threshold. This means that two otherwise identical neurons that receive the same suprathreshold inputs would produce outputs that are inversely related to their respective SK channel maximal conductance.

The second example is the hyperpolarization activated cyclic nucleotide (HCN) channel. Like the SK channel, HCN channels open under specific conditions. Contrastingly, HCN channels open when the membrane is strongly hyperpolarized, then they permit the flow of multiple cations (K^+, Na^+). The resulting effect is a depolarizing current that is conditional on strong inhibition or

hyperpolarization. Thus, HCN channels act to counteract inhibition, preventing the neuron from becoming strongly hyperpolarized. HCN channels are sensitive to temperature and are modulated by secondary messengers like calcium and cyclic nucleotides.

Ion channels and their properties can be incorporated into a mathematical Hodgkin-Huxley (HH) model of neurons, which can then be used to illustrate their effects. Below, I show two model neurons who received an identical input (square pulse of 50 pA). Neuron 1 has twice the SK conductance of neuron 2, which results in neuron 1 expressing a lower evoked firing frequency (Figure 1.2). In two other neurons injected with a hyperpolarizing input (square pulse of -20 pA), we can see the effect of the HCN channel (Figure 1.2). Neuron 4 has a modest HCN conductance, while neuron 3 has none. Neuron 4 initially hyperpolarizes to the current injection, then the HCN channels begin to open and provide an opposing depolarizing current that manifests as a ramp-up in the membrane voltage (voltage sag). This is referred to as the 'sag' current, or Ih. Additionally, neuron 4, also has a more depolarized resting membrane potential because HCN channels have a probability to open at this neuron's resting potential, and therefore provide a continuous depolarizing current.

From these examples, we can appreciate that ion channel expression directly impacts the input-output relationship of neurons. If neurons change their ion channel expression, they change their signal processing. And just as changes in synaptic strength represent a method of information encoding, plasticity in intrinsic excitability is a powerful cellular mechanism underlying learning and memory. In reality, however, it is impossible to separate the two (synaptic and intrinsic) contributions within a brain in action, yet both are critical and influence one another.

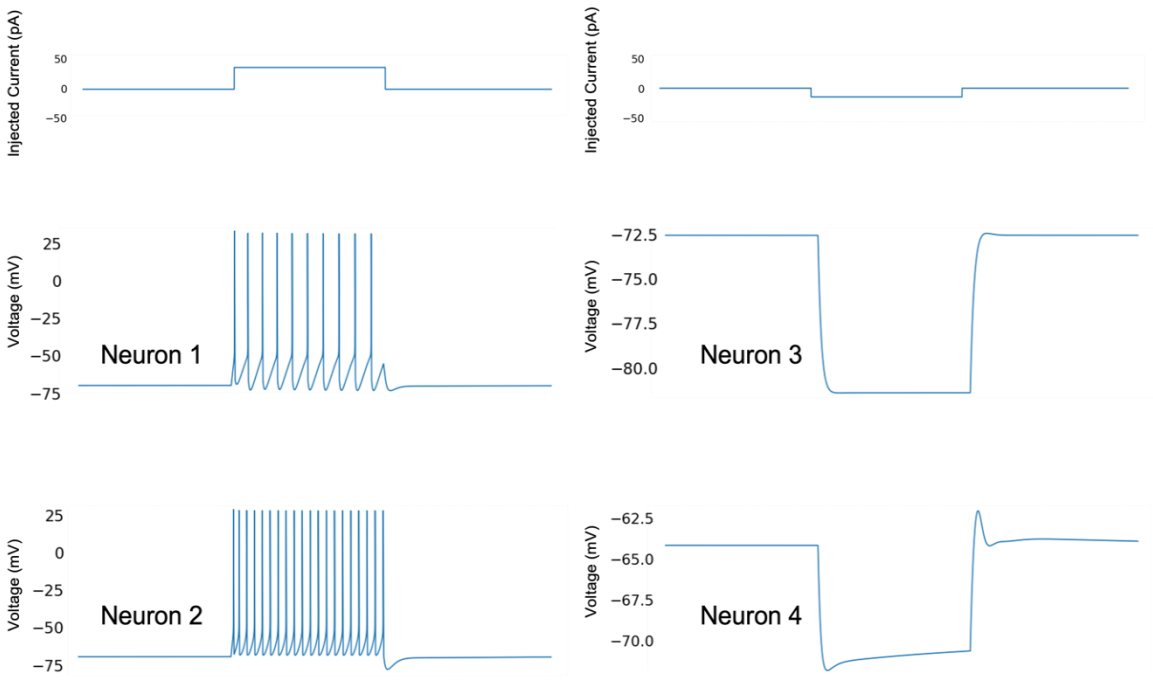

Figure 1.2. Ion channel conductances affect neuron firing properties. Example traces from four Hodgkin-Huxley model neurons to different applied currents (top two panels). Columns are associated with the corresponding trace in the top row: neurons 1 and 2 received the depolarizing current shown on the top left panel. Neurons 3 and 4, received the hyperpolarizing current shown on the top right panel.

Birdsong as a model system

In order to investigate how neuronal IPs contribute to learning, network structure, and behavior, I leveraged vocal production in songbirds. I focused on the stereotyped song of the male zebra finch (Taeniopygia guttata). In zebra finches, song is a critical part of courtship behavior and reproduction. Females judge individual males, form lifelong mating pairs, and raise offspring together. Learning to produce a species typical, 'good' song, is arguably the most impactful part of an individual male zebra finch's life as it relates to their reproductive success (Riebel, 2009).

Zebra finch song consists of multiple spectrally distinct units, or 'syllables', separated by gaps. Each individual sings one song, a series of one or more "motifs" (e.g., two motifs: 'A B C D A B C D'), with each motif comprising the same sequence of syllables. In adulthood, the syntactical and temporal structure of the motif varies very little (Mello, 2014). Under typical developmental conditions, male juveniles form a memory of their tutor's song and undergo a period of practice after which they produce a copy of that song. The juvenile's song copy is characteristically very similar to the tutor's but varies in the degree of similarity. Song copies can include slight spectral differences within a syllable, omissions of entire syllables or inclusions of novel ones. In adulthood, the song becomes crystalized such that birds sing highly reliable renditions of their motif, which is repeated several times during a bout of singing (Tchernichovski et al., 2001). This process leads to individualized behavior that is exceptionally regular (Figure 1.3).

The developmental trajectory of male zebra finches is well characterized (Mello, 2014; Tchernichovski et al., 2001), which facilitates experimental manipulations of the song learning process. Young juveniles can form auditory memories of a tutor's song as early as 20 days after hatching (Adret and Margoliash, 2012; George et al., 1995), and then proceed through a period of vocal exploration that requires auditory feedback (Lombardino and Nottebohm, 2000). Importantly, this learning process is modulated by social context (Bolhuis et al., 2001; Farine et al.,

2015) and is individualized such that different juveniles implement different learning strategies (Liu et al., 2004). Some focus on improving all syllables in a motif simultaneously while others work on perfecting individual syllables at a time, then their order. While spectral features of song are very salient to young practicing males, zebra finch song has temporal structure that is highly stereotyped and regulated. In fact, zebra finch song is so temporally stereotyped that it is difficult to separate elements of timing (neural coding that represents arbitrary time) and motor control in premotor brain areas: The two are inextricably linked. Occasional variation in singing patterns of individual finches is particularly valuable to address such questions (Yu and Margoliash, 1996; Dave and Margoliash 2000). Other species, like Bengalese finches, whose songs have more temporal and syntactical variability are more likely to be useful to address questions about motor and temporal neural representations of song. Bengalese finch present technical limitations as compared to zebra finches, however.

These aspects of zebra finch development and behavior provide a useful model system with many advantages and increase the potential to provide clear answers about how learning is represented in the brain. Specifically, we can ask questions about how cellular level mechanisms of plasticity are involved in the production and learning of complex behaviors that require regulation at multiple timescales. Additionally, this point highlights another general interest of this thesis: how neural circuits overcome challenges of timing and integration of feedback over long periods of time (hundreds of milliseconds). While rapid dynamics are often highlighted in descriptions of complex behavior, holding static positions is equally an important part of behavior.

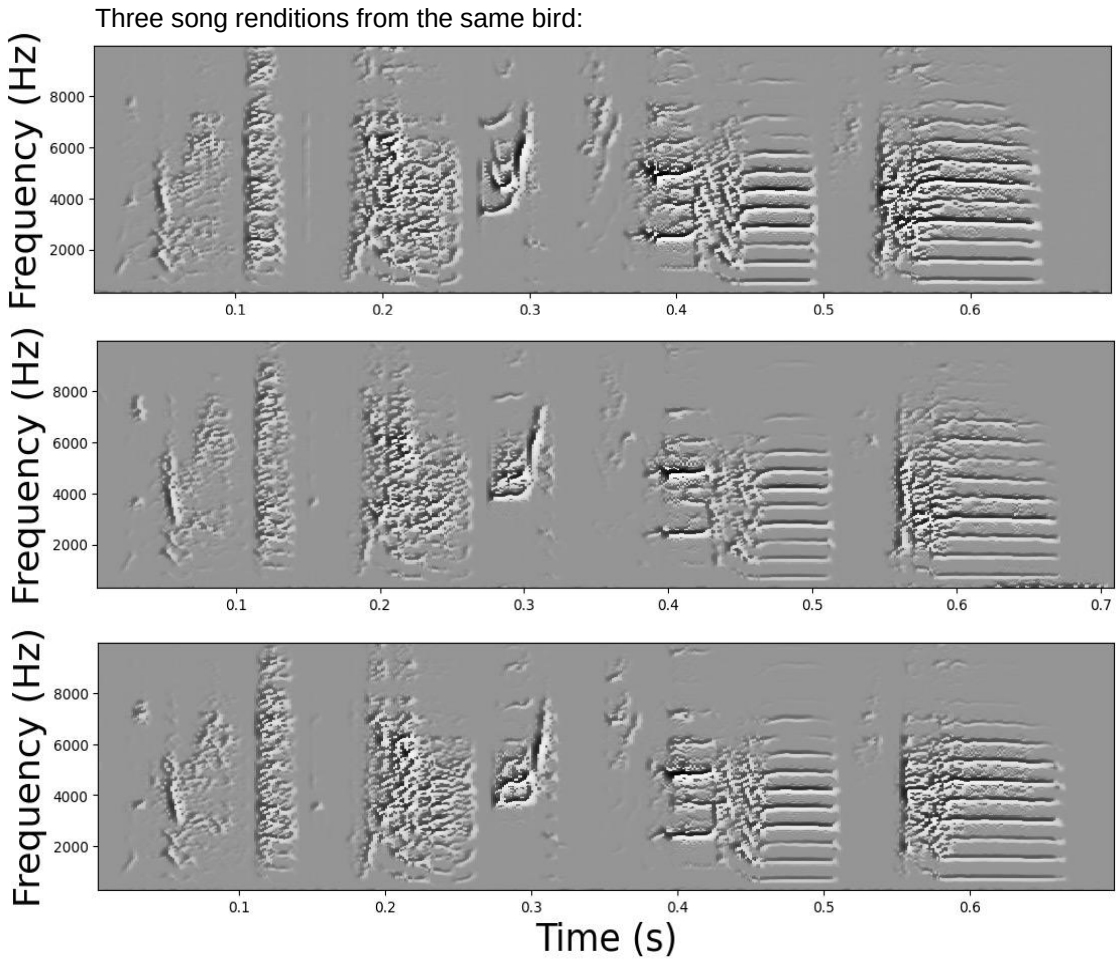

Figure 1.3. Zebra finch song is highly stereotyped. Three song motifs from the same bird.

The Song System: motor and basal ganglia pathways

Unlike the mammalian cortex, with its columnar cortical structure, the bird brain is made up of densely interconnected nuclei. These nuclei express similar connectivity to mammalian cortex (Vates et al., 1997; Doupe et al., 2005), and in songbirds, a specialized set of brain areas underlie the production and acquisition of song. Those nuclei involved in song production and song learning (and which may also contribute to song perception) are colloquially referred to as the "song system". There are two major forebrain pathways within the song system. One pathway is a motor pathway that descends from the forebrain to the brainstem (and associated ascending pathways from the brainstem). A second pathway is a cortico-basal ganglia-thalamo-cortical pathway, called the anterior forebrain pathway (AFP) (Figure 1.4).

Both the motor pathway and the AFP are largely interconnected and overlap in a forebrain nucleus called HVC (proper name). HVC is analogous to premotor cortex in mammals and is critical for learning and production of stereotyped song. HVC contains neurons that project to one of three targets. HVC_{RA} neurons project to the robust nucleus of the arcopallium (RA), HVC_{X} project to the song system component of the basal ganglia, area X, and HVC_{Av} neurons project to the auditory nucleus avalanche (Av) that is important for song learning (Ikeda et al., 2020). A small number of neurons have been found to have axons that project to both RA and area X, but the evidence on whether that is a permanent state is unclear (Benezra et al., 2018). Additionally, HVC_{Av} neurons are small in number (less than 5% of all HVC neurons). Thus, the vast majority of neurons in HVC can be categorized into one of three classes: Exclusively RA projectors (HVC_{RA}), exclusively basal ganglia projectors (HVC_{X}), or inhibitory interneurons (HVC_{int}). Roughly 50% of all HVC neurons are HVC_{RA}.

Nucleus RA is analogous to primary motor cortex in mammals, and its projection to the hypoglossal nucleus (nXIIts) and midbrain and thalamic structures is functionally equivalent to

motor cortex layer V neurons with descending projections. Activity in RA coordinates (and drives) syringeal muscle contractions. In the song system, RA is the most direct link between a neural code of an individual bird's song and movements in the syrinx (the vocal organ of birds). Activity in RA is highly regular, with neurons firing at high frequencies at baseline and bursting strongly during singing and their bursts are time-locked with muscles activity in the syrinx with a motor delay (Doupe and Konishi, 1991).

Area X is the basal ganglia component of the song system and is necessary for song learning and plasticity. Lesions of area X in juveniles prevent tutor song copying, while the same lesions in adults prevent song deterioration that typically results from deafening (Scharff and Nottebohm, 1991). Importantly, Area X is involved in the assessment of feedback, error correction, and juvenile vocal exploration (Ölveczky et al., 2005). Likewise, other nuclei in the AFP have similar effects on song. For example, lesioning the forebrain nucleus LMAN in adults leads to decreased spectral variability of adult song. From classic experiments like these, the AFP has been thought to 'inject' variability into the motor system. Behavioral variability, especially during early learning, is useful in optimizing motor strategies and finding motor solutions to produce desired outputs (Doupe and Konishi, 1991; Ölveczky et al., 2005). In that view, the AFP facilitates exploration of the motor space and adjusts based on feedback to slowly 'nudge' the motor system into generating the precise motor commands that produce a bird's unique song. Without the AFP, the motor system is rigid and inflexible, rendering song learning impossible. The AFP is functionally and structurally like the basal ganglia-thalamo-cortico loops seen in the mammalian brain (Vates et al., 1997; Xiao and Roberts, 2021), which are also intimately involved in learning, and depend on error signals from the dopaminergic system to error correct (see general discussion in Chapter 6).

With its projections to both pathways (motor and AFP), HVC plays a key role in the neural orchestration of song. Consequently, HVC's privileged position makes it a convenient nucleus in

which to investigate questions of motor control, feedback integration, and maintenance of temporal precision.

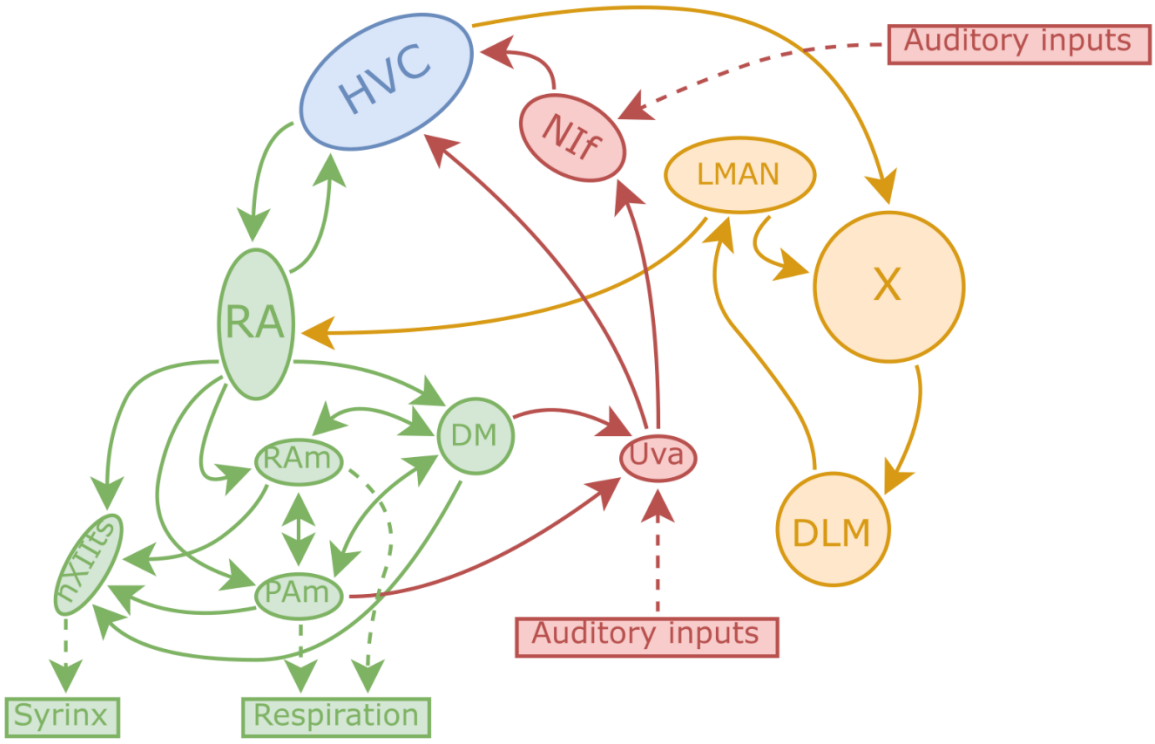

Figure 1.4. Diagram of the song system nuclei. Sensory pathways drawn in red, the anterior forebrain pathway (AFP) in yellow, and the motor pathway in green. Nuclei are not drawn to scale. Taken from Fetterman, 2020.

HVC Network Properties

HVC projection neurons burst sparsely during singing with exquisite temporal precision. We have known for some time that HVC neurons' bursts are time-locked to the motif and can occur multiple times within it (Margoliash, 1983; Lewicki, 1996; Hahnloser et al., 2002). However, in the early descriptions of HVC temporal properties, the identity of neurons, and consequently

differences between projection classes, was not known. In 2002, Hahnloser et al. were the first to record extracellularly from antidromically identified HVC neurons in singing birds. They reported that HVC_{RA} neurons burst once per motif, while HVC_X can burst multiple times (some up to 6 times during a motif). This distinction in burst number between HVC_{RA} and HVC_X allowed for the attribution of previous results to specific cell classes. In Lewicki 1996, for example, neurons recorded during song playback that showed characteristic hyperpolarization to syllable sequences were likely HVC_X neurons. Similarly, in Margoliash 1983, the sequence sensitive neurons with large integration times are likely HVC_X neurons as well. Furthermore, in Mooney 2000, sharp electrode recordings from anesthetized, head-fixed birds showed markedly different subthreshold properties of HVC_X and HVC_{RA} neurons. One such difference is the fact that at song onset HVC_{RA} become depolarized for the duration of the bout of singing, while HVC_X become hyperpolarized. For both neuron classes, the bursts occur on top of these subthreshold changes. This means that the network environments in which the neurons integrate inputs and produce spikes are different and suggests the same may be true of their underlying circuits and (or) cellular properties (further discussed in Chapter 2). From these observations of bursting properties during singing and song playback experiments, emerged several models of HVC that included neuron classes with distinct functional properties yet similar temporal specificity (Lewicki, 1995, 1996; Mooney 2005; Long et al., 2010; Amador et al., 2013).

The HVC_{RA} population should have a clear correspondence to behavior because they project directly to motor nucleus RA and drive activity in the muscles with a motor delay of 20 to 30 ms. However, as mentioned earlier in this document, the lack of temporal variability in zebra finch song makes it difficult to differentiate aspects of temporal coding and motor coding in HVC. Despite that, several experiments have tried to distinguish between the two. In 2008, Long and Fee cooled down HVC and found that the song slowed proportionally to cooling. They concluded that HVC_{RA}

neurons, with their sparse firing, represented a time code. It goes beyond the more cautious interpretation that these cooling results demonstrate that timing (not time) is represented in HVC and has been challenged by subsequent cooling experiments (Hamaguchi et al., 2016). The Long and Fee, 2008, interpretation was consistent with the conclusions from Hahnloser et al.., 2002, that viewed HVC_{RA} sparse coding as absence of a clear correspondence between burst times and spectral features of song. Of course, at a surface level, a time code is consistent with their results, but they do not conclusively prove that HVC activity is randomly distributed and carries no motor information.

Additional work from Lynch et al.., 2016, furthered the interpretation and constructed a model of HVC that represents arbitrary time. In their paper, Lynch et al. reported that, collectively, all neuron bursts continuously tiled the duration of the song. Their model, canonically referred to as the 'clock model', describes HVC_{RA} neurons as falling dominos in a unidirectional chain of activity, or synfire chain (Herman et al., 1995), that provide continuous coverage of the motif: Each burst represents a timepoint in the motif. Critically, in Lynch 2016, while the cellular identity of each neuron was confirmed with substantial experimental effort, all the bursts from both HVC_{RA} and HVC_X were combined for purposes of analysis. The majority of bursts (arising from any neuron) in the continuous representation came from HVC_X neurons whose bursts were treated independently. This analysis is more difficult to reconcile for two reasons. First, chronic ablation of HVC_X neurons did not directly impact song production (Scharff et al., 2000). In the photo-excitotoxicity approached used there, however, some HVC_X survived in each animal, and singing was assessed only days after the experimental manipulation. Second, HVC_X neurons that burst multiple times in a motif contribute to multiple timepoints in the chain. While the statistical mode of burst number of HVC_X is one, roughly half of HVC_X burst two or more times per motif (Lynch et al., 2016; Kozhevnikov and Fee, 2007). This second point is not addressed in Lynch 2016 whatsoever, and no

mechanism is proposed to disambiguate bursts downstream in Area X. Moreover, HVC_X and HVC_{RA} are distinct classes, with different firing properties and distinct microcircuits within HVC (Mooney, 2000; Mooney and Prather, 2005; Daou et al., 2013). They clearly play different roles in HVC network function during development and in relation to behavior (Aranov 2008) and presumably do so in the adult. I will address these points further in Chapter 3, where I propose a network model that aims to remedy these issues and consolidate existing observations of HVC network structure and function as well as the differences in IPs of HVC neuron classes.

Intrinsic Properties of HVC neurons

Decoding the cellular mechanisms involved in storing and processing information in neural networks is a key component of understanding learning and memory phenomena. Beyond well-studied synaptic plasticity mechanisms, non-synaptic changes to neuronal excitability are implicated in engram formation, network function, and behavior. While many examples of experience-dependent changes to intrinsic excitability are documented, there has not yet been a description of a complex learned behavior that captures fundamental cellular and network mechanisms at different scales to produce a model in which intrinsic and synaptic properties fit together cohesively.

Peculiarly, HVC_X and HVC_{RA} have very different intrinsic properties (Figure 1.5, an example trace from an HVC_X and an HVC_{RA}). In vitro, HVC_{RA} are transiently activated, firing few spikes at the onset of stimulation (strongly adapting), followed by stable depolarized plateaus (top panel in Figure 1.5). They tend to have small capacitances, high spiking thresholds, and very little hyperpolarization activated current (Ih), resulting in little to no voltage sag when hyperpolarized (insert of top panel in Figure 1.5) (Daou et al., 2013). For such small cells, they require remarkably large amounts of injected current to elicit spiking (100-500 pA).

Contrastingly, in vitro, HVC_X fire continuously to depolarizing current injection, have modest spike adaptation and large capacitances (Daou et al., 2013; Ross et al., 2017). Interestingly, HVC_X express significant Ih and voltage sag (inset of middle panel in Figure 1.5). In fact, most HVC_X express rebound depolarization when released from hyperpolarization (post inhibitory rebound excitation) (Daou et al., 2013). Rebound excitation refers to additional depolarization beyond the resting membrane potential after the removal of inhibition or hyperpolarization. In many HVC_X, the rebound depolarization is strong enough to trigger spikes (rebound spikes). HVC_X require modest amounts of injected current to elicit spiking (50-100 pA). In these ways, HVC_X are opposite to HVC_{RA}. In the general discussion (Chapter 6), I discuss how these differences could be suggestive of their roles within the HVC network.

Recent work showed that HVC_X IPs are developmentally regulated and differ among individual adult animals. HVC_X ion channel expression is affected by early experience and song exposure, and in adulthood HVC_X IPs are plastic and sensitive to auditory feedback (Daou and Margoliash, 2020; Ross et al., 2017; Ross et al.l 2019). In young males, HVC_X IPs of neurons within the same bird are different from each other (high variability). By post hatch day 90 (early adulthood), neurons have converged on a common set of IPs within an individual male bird (no work has been done in females to determine whether this is solely a property of male HVC). Critically, the differences in adult HVC_X IPs across individuals are related to song differences. This suggests that HVC_X intrinsic excitability is tied to specific features of song and to birdsong learning. Birds who sing nearly identical songs (often siblings) have very similar HVC_X IPs. Birds who sing different songs have HVC_X whose IPs differ by how different the songs are (Daou and Margoliash, 2020). In Daou and Margoliash, 2020, IPs were quantified by fitting HH, conductance-based, models to recorded traces from HVC_X neurons and extracting the conductance values from the model fits. The model was adopted from Daou, 2013, and included pharmacologically confirmed ionic currents: voltage

activated sodium (INa), voltage activated potassium (IK), ISK, Ih, and low voltage activated calcium (ICa-T). The modeled conductance value estimates were cast into a multidimension 'conductance space' where all neurons were represented. In that conductance space, all neurons from a bird represent a volume with a centroid. The distance between the centroids of any two birds was related to the differences between their songs. These results emphasized individual variability, which is an ethologically relevant and experimentally useful feature of birdsong learning.

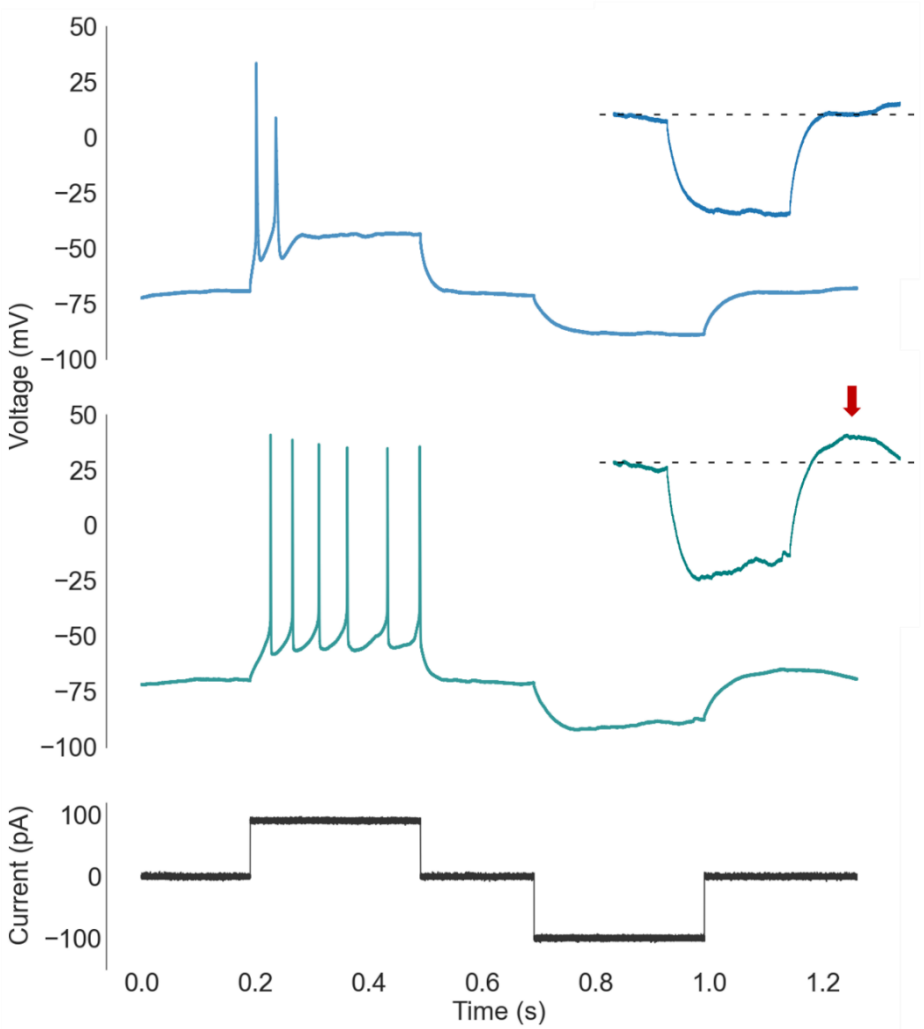

Figure 1.5. HVC projection neurons have distinct IPs. A whole-cell intracellular recording from an HVC_{RA} (blue) and an HVC_X (green) who received the same injected current (black trace in bottom panel). Inserts for each neuron show a zoomed in view of the voltage response to the hyperpolarized portion of the current injection and illustrate the amount of post-inhibitory voltage depolarization above baseline (dashed lines). For the HVC_X a noticeable amount of post-inhibitory rebound depolarization is shown (red arrow).

Fundamental units of song

The song of adult zebra finches has structure that spans multiple timescales. This is most evident in the canonical motif because it is repeated multiple times in a bout of singing. In a larger timescale, finches sing multiple bouts back-to-back, often separated by gaps of multiple seconds, which Graham Fetterman (Fetterman, 2022) named "phrases". What is less clear, however, is how to define within-motif structure. Although we do not yet understand how neural dynamics underlie song, the evidence to date indicates that syllables fit the requisites of a discrete behavioral unit. Birds take breaths in the gaps between syllables, often in the larger gaps in sound production (> 10ms). Work describing the peripheral movements (syringeal and respiratory) that a bird makes to produce song also segregates the song into distinct vocal "gestures", that may subdivide syllables but never cross syllable boundaries. Some juveniles approach song learning by practicing and perfecting one syllable at a time. Birds sometimes drop portions of song, almost always, one (most commonly) or more complete syllables at the end of the motif are dropped. In playback experiments, loud white noise (an aversive stimulus) has been used to disrupt song production. In those cases, the motif was interrupted after completing a given syllable (i.e., during the gaps between syllables) and never in the middle of a syllable. That is, birds tended to finish a syllable if they had already started it. These points support a perspective of organization of neural dynamics that is centered around syllables. Thus, it is highly pertinent that we do not know what the neural representation of a syllable is (particularly in HVC). And furthermore, how are intra-syllabic elements represented in such a temporally stereotyped behavior? I discuss this further in Chapter 4, where I describe temporal structure that spans the entire motif.

Syllable combination selectivity

HVC projection neurons burst at precise moments during singing (Hahnloser et al.., 2002). This can also be further investigated in anesthetized or sleeping birds by playing back the birds own song (BOS) (Amador et al., 2013; Fetterman, 2022). The same time-locking phenomenon occurs in the non-singing preparations. However, if the BOS spectral or temporal features are modified, the selectivity of the bursts decreases substantially (Margoliash, 1986; Amador et al., 2013; Fetterman, 2022). HVC_X neurons are selective to the sequence of syllables (Margoliash and Fortune, 1992), similar to how Margoliash, 1983, reported that the neurons were sensitive to the gaps between whistles of the white-crowned sparrow. These two results describe important features of HVC_X neurons' functional properties: long integration times and "combination selectivity". Combination selectivity refers to the selective encoding of specifically timed and ordered events. In zebra finch HVC, some neurons burst only after the bird sings (or hears) a sequence of syllables which can span a period of hundreds of milliseconds. White-crowned sparrow putative HVC_X neurons could detect a sequence of whistles even when the gaps reached 300 ms (Margoliash, 1983).

Extracellular single unit recordings in HVC of lightly anesthetized zebra finches share the long integration times seen in white-crowned sparrows. Units that responded to syllables 'B-C', for example, could still detect the sequence even if the gap was increased. The response waned as the gap duration increased but was sustained up to nearly 100 ms in some neurons (Fortune and Margoliash, 1992).

Lewicki, 1996, made in vivo sharp electrode recordings in the HVC of anesthetized zebra finches. Using this approach, he described how two-syllable selective HVC neurons were hyperpolarized by playback of the first syllable and depolarized by the second syllable. If played back in the correct sequence (one that matched the BOS), and with the correct relative timing, the sequence produced a burst in the selective neuron. Playing the depolarizing syllable twice, or

altering the relative timing of the two syllables, did not reproduce a stereotyped response in the neuron (instead producing unreliable and often subthreshold activity). Lewicki's 1995 and 1996 papers address the mechanisms of sequence selectivity and suggest that inhibition is a critical component. In Lewicki's model of syllable selectivity, the magnitude of the inhibition caused by the first syllable predicted the amount of excitation and strength of bursting produced by the second syllable. In his 1996 paper, Lewicki addressed the model proposed in Margoliash, 1983, which suggested that the release from inhibition could generate a rebound that could then interact with depolarization from the second syllable. Thus, the earliest systematic extracellular and intracellular studies of HVC responses to song playback converged on the same basic model for burst timing regulation.

Goals of this thesis

In my thesis work, I was driven by two curiosities. One is general to neurobiology and signal processing, and another that is grounded in a neuroethological perspective. The first, is an interest in the fundamental rules that underlie information storage and processing in biological systems. The second is a specific curiosity about the inner workings of the song system, and specifically, in the function of a group of neurons in the premotor nucleus HVC that project to the basal ganglia (HVC_X). These two general questions drove the organization and design of my experiments, such that results that inform either provide clarity to both. All experimental chapters hereafter should be interpreted through the lens of both questions.

The interest in the fundamental rules of information processing in neurons stems from a desire to understand things well enough to reproduce them. As it relates to neuroscience, it is not sufficient (and hopefully not necessary!) to know every connection in a brain to understand its function; we also need to understand the basic rules of computation within neurons and across

synapses. Ideally, we would understand neural computations at such a fundamental level that we could run simulations of biological networks that are indistinguishable from the real things. This perspective underlies my approach to tie together features of intrinsic properties in single neurons to network properties and ultimately to behavior. I believe that to do this, we must leverage different experimental techniques (and modeling) to produce comprehensive models of individual biological networks. In Chapter 5, I discuss future directions that stem from my work and address this goal of modeling individualized behavior by using multiple experimental modalities and network modeling in the same animal.

CHAPTER 2

TEMPORAL FEATURES OF SONG CORRELATE WITH HVC_X REBOUND EXCITABILITY

Introduction

The contributions of ion channel expression to cellular properties, and therefore signal processing within neurons, are relatively well understood. Yet, there is a substantial lack of understanding as to how to extend our intuition of phenomena at the level of intrinsic properties to how they influence network properties and whole organism behaviors. This is of course true (if to a lesser extent) of the much more intensively studied synaptic connectivity and synaptic plasticity mechanisms, and it is not surprising that embracing multiple levels of analysis makes it difficult to construct a comprehensive model that links ion channels to behavior. This is a daunting task especially in systems of networks with complex internal and external feedforward and feedback interactions among multiple classes of neurons, so progress has been greater in studies of smaller networks. The work on intrinsic neuronal properties regulating rhythmicity of small networks within the stomatogastric ganglion of the spiny lobster is a standout example (Marder and Prinz, 2002).

Another approach has worked in the backward direction by identifying aberrant behaviors or pathologies and looking for associated neural structure. There too, we find links with neuronal excitability (Pilarski et al., 2011; Oginsky et al., 2016). Despite important progress in both approaches, no specific example has been described that lays out a direct path from features of intrinsic properties to complex learned behavior: one where every aspect of the neural activity, network architecture, and behavior are modeled.

An important step forward in this research was recently reported when Daou and Margoliash, 2020, reported on the characteristics of IPs of HVC_X neurons of male zebra finches. The study demonstrated that HVC_X neurons express considerable uniformity of IPs within individual animals. Neurons from the same bird show similar spike waveform morphology and evoked firing patterns that are different from neurons of other birds. To understand these results from the perspective of HVC_X ion currents, a subset of neurons were quantified by fitting Hodgkin-Huxley models to recorded intracellular traces of HVC_X neurons responding to depolarizing and hyperpolarizing current injections. This provided a model estimate of the maximal conductances of five channels (Na, K, Ca-T, SK, HCN) for each neuron. HVC_X neurons of the same bird clustered tightly within the N-dimensional conductance space (where N was the number of modeled conductances) and defined a volume with a centroid. The centroid volume for any given bird occupied a small volume of the total volume defined by all birds. The distance between any two birds' centroids was strongly related to the differences between the two birds' songs, generally. Furthermore, the data indicate that the IPs of HVC_X are maintained dynamically, for example the IP homogeneity rapidly degraded upon exposure during singing to disruptive delayed auditory feedback, slowly changed with age, and was not present in relatively old juvenile birds still learning to sing (Daou and Margoliash, 2020). This result represents the novel and exciting possibility of linking individual behavior to individual expression of IPs in a complex system involved in learned vocal production. A central reason for this success is likely to be related to the highly stereotyped songs that individual zebra finches sing. This predicts that such IP homogeneity maybe observed in other species in more stereotyped regimes of singing – a prediction that has yet to be tested.

Focusing on zebra finches, one limitation of the analysis from Daou and Margoliash, 2020, is that they used a measure of song similarity which condensed all spectral and temporal features of song into a single percent similarity score (Tchernichovski et al., 2001). Thus, the question

remains whether there are specific relations between features of song and different features of IPs. How do the IPs of the HVC_X population in a given bird reflect a network level solution to learning of that bird's particular song? Furthermore, Daou and Margoliash, 2020, did not track parentage for any birds, except the 4 adult and single juvenile sibling pairs of birds, which leaves unresolved questions about the potential role of heredity in HVC_X IP expression. To explore these questions, I recapitulated the results from Daou and Margoliash, 2020, while bringing the song learning experience under experimental control and extending the relationship of HVC_X IPs to features of song.

Timing is critical

As mentioned in earlier chapters, HVC neurons are highly sensitive to temporal structure of song during playback experiments, and the timing of their in vivo bursts is locked to moments in the motif. HVC_X neurons show this exquisite precision in their burst times and yet they integrate inputs over hundreds of milliseconds. At the same time, the behavior itself is highly precise across motif renditions, and requires tight control and coordinate of syringeal muscles and air sac pressure. It is thus unsurprising that the premotor nucleus that plays a role in the production of song is equally precise in its neural activity. Despite that, we do not know what HVC bursts encode (though models of motor or time coding have been proposed, see introductory chapter). In summary, tight temporal control is essential for singing behavior in zebra finches (as in humans), and HVC network properties reflect it but the connection is unclear.

We see another form of this trope of tight regulation in the expression of IPs of HVC_X neurons. And just as we don't fully understand the network properties of HVC, we don't know how HVC_X IPs relate to behavior explicitly. Daou and Margoliash, 2020, showed that differences in HVC_X IPs comparing pairs of birds are related to a summary measure of song similarity (comparing the

pairs of songs). This does not identify whether specific acoustic features of song are related to specific features of HVC_X IPs. Motivated by the long integration time that HVC_X express, the regulation of the related HVC_X IPs via juvenile learning (Chapter 2) and adult maintenance (Daou and Margoliash, 2020), and the potential that these IPs are related to long, continuous vocal elements of motifs (harmonic stacks), I investigated the sub-motif structure and correlations of spectral and/or temporal features of song with specific HVC_X IPs. To this end, I evaluated the hypothesis that specific IPs are related to specific song features by manipulating the tutoring experience of birds to introduce controlled changes in song features. The results indicate an explicit link between rebound excitability and temporal features of song (duration and continuous harmonic vocalization), but not others (amplitude modulation, entropy, pitch).

Investigating plasticity of IPs in vitro

In the course of these studies, I also discovered that the IPs of HVCx in my recordings are quite sensitive to the amount of stimulation a cell receives. As described below, I modified my analyses (and protocols) to reduce that variation as a source of noise in these Chapter 2 experiments. Given this perspective, I also investigated these unanticipated effects of HVC_X intrinsic plasticity by presenting them with somatic stimulation protocols previously shown to induce changes in intrinsic excitability in slices (Paz et al., 2009; Gill and Hansel, 2020).

Methods

Animals and housing

All procedures were performed in accordance with all relevant ethical regulations for animal testing and research and approved by the University of Chicago Institutional Animal Care and Use

Committee (IACUC). Zebra finches were obtained from the Margoliash lab breeding colony and housed on a 14:10 h light/dark cycle. Food and water were provided ad libitum. All birds used for electrophysiological experiments were adults older than 90 days.

Natural and instrumental song learning

I used three different breeding designs that had varying degrees of control over the tutoring experience (Figure 2.1). All birds who reached adulthood and produced a stereotyped song were included in electrophysiological experiments.

In the first design, zebra finches were raised by their parents in individual cages where they could hear birds from other breeding cages as well as nearby flight aviaries. Birds were housed with their siblings and parents until post hatch day 80, at which point they were moved to a flight aviary. Adult male zebra finches whose parentage was known were collected from the general colony and used for experiments.

In the second, zebra finches were bred in sound attenuation chambers with their parents and siblings only. The father was removed when hatchlings reached 15-20 days of age and housed separately. At 40-45 days of age, juvenile males were identified by their chest and cheek plumage and separated to another sound attenuation chamber for live tutoring. Live tutoring involved the introduction of an unrelated adult male into the sound chamber of a song-naïve juvenile. Tutor and tutee were housed together until the tutee reached 90 days of age.

Finally, the third design used instrumental tutoring in the absence of other birds (Figure 2.2, picture of a juvenile bird using the setup). I used triggered playback of pre-recorded song through a speaker positioned behind the string and controlled by the software Sound Analysis Pro (SAP) (Tchernichovski et al., 2001). Sound files used for instrumental song learning contained one, three-motif, bout of either naturally occurring song, or a manipulated song. For the manipulated song, I selected a long harmonic stack from a bird that sang a very long song (and had the longest

stack in my dataset). I maintained the overall temporal structure of the original song in the manipulated version by using a method for finding rhythm in song (Norton and Scharff, 2016; and replicated in Chapter 4).

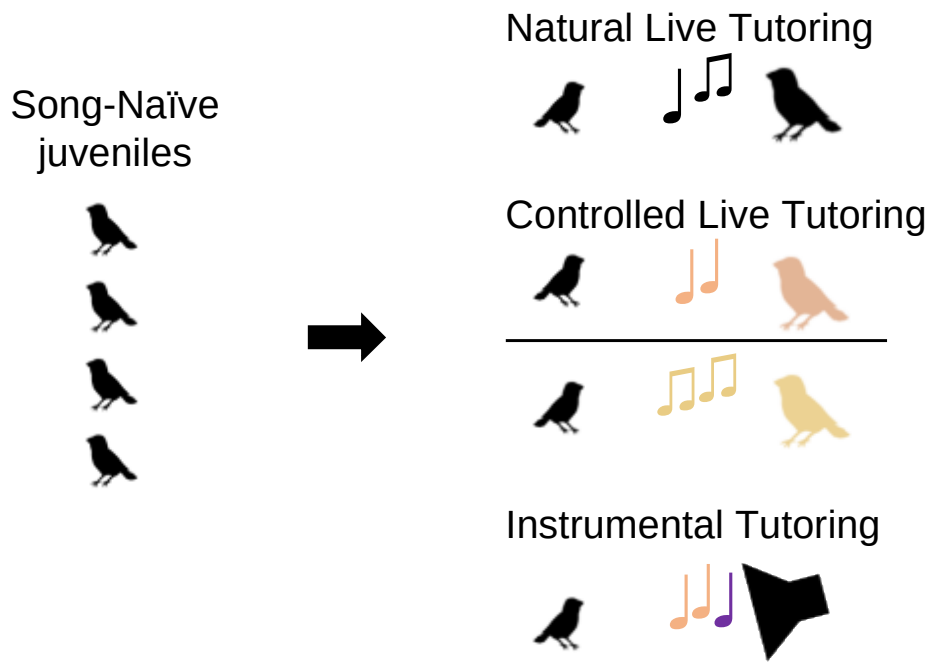

Figure 2.1. Diagram of experimental designs. Shows the three experimental designs used to control the tutoring experience and generate birds for electrophysiological experiments.

Figure 2.2. A juvenile listening to song playback. Picture of a male juvenile zebra finch interacting with the instrumental song learning setup.

Song analysis and segmentation

A representative motif for each bird was chosen from song bouts that occurred in the days prior to slice electrophysiology experiments. All analyses were performed on the representative motif. Sub-motif elements, such as syllables, were hand labeled using Audacity or SAP (http://soundanalysispro.com/manual). Syllable segmentation was verified in a semi-automated way using Chipper (https://github.com/asearfos/chipper), using the normalized amplitude signal and taking the 95th percentile of amplitude as the threshold to define onsets and offsets. Harmonic stack durations were verified algorithmically with custom code that relied on Resin (https://github.com/margoliashlab/resin), a python library that was based on SAP. I used Resin to quantify amplitude and frequency modulation (FM) of songs, which were then used to identify moments of high amplitude and low FM. As defined by SAP, FM is the angular component of squared time and frequency derivatives. To identify harmonic stacks, the FM signal (ranging from 0 to 1) was smoothed (running average with a 5-value window) and an arbitrary threshold was set at 0.2 FM, where 0 is a perfectly straight line in the spectrogram (Figure 2.3).

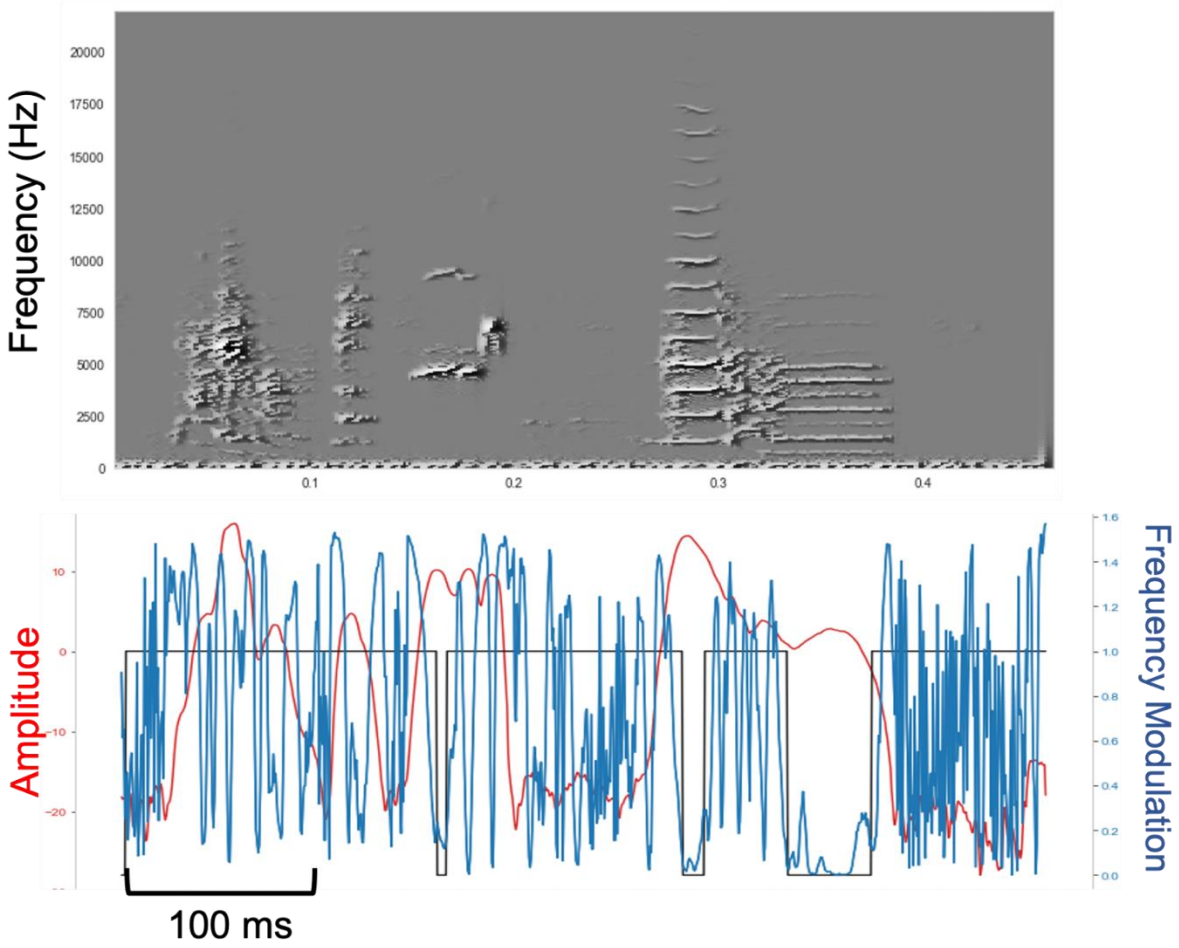

Figure 2.3. Automatic detection of harmonic stacks. A spectrogram of a zebra finch song (top panel) and the extracted signals for amplitude (red), frequency modulation (blue), and predicted location of harmonic stacks (black).

Slice preparation

Birds were anesthetized with isoflurane, checked for loss of peripheral reflex with a foot pinch and then decapitated. A razorblade was used to block the brain through the skull behind the eyes (front) and at the cerebellum (back). The blocked brain with skull still attached was placed in ice-cold (slushy consistency) sucrose-ACSF (225 mM sucrose, 2 $MgSO_4$, 2 $CaCl_2$, 1.25 NaH_2PO_4, 26 $NaHCO_3$, and 10 glucose, 3 KCl, ph: 7.2-7.3) while the rest of the brain was removed. One could quickly remove the brain by cutting through the bone on the sides and of the blocked skull and lifting off the top layer. Horizontal slices (200-300 uM) were cut from both hemispheres using a Vibratome 1000 and moved to incubate in a warm (32-34 °C) NMDG-ACSF (93 NMDG, 2.5 KCl, 1.2 NaH_2PO_4, 30 $NaHCO_3$, 20 HEPES, 25 glucose, 5 sodium ascorbate, 2 thiourea, 3 sodium pyruvate, 10 $MgSO_4.7H_2O$, 0.5 $CaCl_2.2H_2O$) for 10-15 minutes before being moved to another incubation chamber containing standard recording ACSF (124 NaCl, 2.5 KCl, 1.2 $NaH2PO_4$, 24 $NaHCO_3$, 5 HEPES, 12.5 glucose, 2 $MgSO_4.7H_2O$, 2 $CaCl_2.2H_2O$). All ACSF solutions were bubbled continuously with 95% O_2 5% CO_2. Slices were left to incubate for at least additional 30 minutes before being moved to the recording chamber.

Whole-cell recordings

Recordings were conducted at moderately elevated temperatures of 28-32 °C, controlled with an inline heater (Warner Instrument). Recordings were made using a Multiclamp 700B and digitized with a Digidata 1550B at 50 kHz (axon instruments), using a 10 kHz low-pass Bessel filter. HVC was first identified under wide-field illumination as a dark region in the horizontal slice at 4x magnification (Figure 2.4) then by the presence of the characteristic electrophysiological responses of the two main classes of projection neurons in HVC (verified with retrograde labeling). Data collection was controlled using pClamp 10.4 (Molecular devices). Recordings were made with fire

polished glass pipettes (4-8 MΩ) and visually guided using a camera (Olympus Oly-150IR, or Hamamatsu Orca Fusion C15440). Pipettes were filled with 100mM K-gluconate, 5mM $MgCL_2$, 10mM EGTA, 2mM NA_2-ATP, 0.3mM Na_3-GTP, 40mM HEPES (pH: 7.2-7.3, osmolarity 290-300 mosM).

A giga-Ohm seal was formed before break-in for all cells, and a period of 1-2 minutes was given before presentation of experimental protocols. Series resistance, membrane resistance, and time constant were calculated from a -10 mV step in voltage clamp. Series resistance was calculated as $R_s = V/I_{peak}$, membrane resistance was calculated as $R_M = \Delta V/I_{steady\ state}$, τ was calculated by fitting a polynomial (Python's numpy-polyfit function) to the current trace and finding the time where the current reached 63% of its steady-state value. Capacitance was measured as $C_M = tau/R_M$. The median series resistance of cells was 22 MΩ with a standard deviation of 13.39, 73% of cells had R_S < 30 MΩ).

Cells were then held to -70 mV in current clamp and presented with depolarizing and hyperpolarizing square current injections of varying amplitudes (-120 to -60 pA hyperpolarizing, 100 to 50 pA depolarizing, 300 ms duration). A holding current to bring cells to -70 mV was chosen because this is the in vitro resting potential of HVC_X observed at break-in in a large population of HVC_X previously reported (N=370 neurons, break-in potential –70.49±2.3 mV, Daou and Margoliash, 2020). This also provide a common voltage reference point from which to analyze the neuronal responses. Firing frequency was calculated as the number of spikes divided by the time between the first and the last spikes. Sag ratio was calculated as the ratio between the most hyperpolarized voltage during the hyperpolarizing current injection (illustrated later in this chapter in Figure 2.13 as a black triangle) and the voltage before release of hyperpolarization (a black square in Figure 2.13). In 20 cells from 4 birds (3, 3, 5, and 9 cells respectively), I performed voltage clamp

experiments to produce I/V plots, stepping voltage from -100 mV to -60mV, with step sizes of 10 or 5 mV.

For a set of neurons (N=33), I presented a protocol of somatic stimulation at 10Hz (10 pulses over the course of 1 second). The protocol was modified for each neuron so that every pulse produced 2-3 spikes. Additionally, in a subset (N=10) of those neurons, I collected evoked currents at different voltage steps (-100 mV to -60 mV in 10 mV steps) and produced current-voltage (I/V) curves.

Figure 2.4. A brain slice containing HVC. HVC can be seen as a darker myelinated region within the slice.

Inclusion and analysis criteria

All cells that fired consistent trains of spikes (no depolarization block), with spikes passing 0 mV were recorded and included in analysis. Features of cells that significantly varied with R_S were not considered for analysis (e.g., spike amplitude, or peak of the first spike. Examples shown in Figure 2.5).

Retrograde labeling

While the firing patterns of HVC neurons were characteristic and helped to identify the different classes, as an independent confirmation we also retrogradely labeled HVC neurons in several birds. Birds were anesthetized with isoflurane and head-fixed using a stereotaxic frame. Bilateral craniotomies over Area X, or Nucleus RA were made using predetermined coordinates (relative to Y Sinus with head angle of 18°. Area X: 1.5-2 latera, 3.5 rostral, 3.5 deep, RA: 2.3-2.4 lateral, 1-1.1 caudal, 1.5-1.9 deep). Three birds were bilaterally injected with retrograde tracer (tetramethylrhodamine dextran from invitrogren, 10-20 nL) using a Nanoject 2.0 or Nanoject 3.0. Similarly, in one bird we injected a self-complementary AAV carrying a GFP construct (sc-AAV9-GFP, UNC Vector core, 300-350 nL at 5nL/s) into Area X, and tetramethylrhodamine into RA. A 7–10-day period was allotted for transport, or viral expression, before slice experiments. Retrogradely labeled cells within HVC were identified with epifluorescence during slice experiments and used to confirm the identification of HVC using wide-field illumination.

Data Processing and Analysis

Data files were exported from PClamp as axon binary files (.abf), which included multiple sweeps of a square wave current injection protocol (Figure 1.4, black trace in the bottom panel). Each sweep consisted of a small hyperpolarizing step (-20 pA), a 300 ms depolarizing step of varying magnitudes (50 to 100 pA), and a 300 ms hyperpolarizing step of varying magnitudes (-60 to -120 pA). Files were opened using python code (PyABF, written by Scott W Harden: https://github.com/swharden/pyABF), and the raw traces were extracted and saved in Bark format (https://github.com/margoliashlab/bark). Features of the raw data were extracted and analyzed using custom python code written by me.

Results

Each tutoring paradigm produced birds with varying degrees of success. The second and third design, which controlled the tutoring experience, were particularly low yielding, and required 3 years to produce the numbers of birds that are included in this thesis. Removing the father at PHD 15-25 often resulted in the ejection of the juveniles by the mother. Design 1 (home cage raised and tutored) produced 18 birds, design 2 (controlled but live tutored) produced 12 birds, and design 3 (instrumental song learning) produced 8 birds. None of the results in the first two sections that follow were related to the tutoring paradigm used and birds from all three tutoring paradigms were collapsed together for purposes of analysis.

Regarding the electrophysiological recordings, I analyzed features of the raw voltage traces (spike amplitude, firing frequency, voltage sag, etc.) and found that several of them (spike amplitude and spike width) varied significantly with the series resistance of the recording. Series resistance (also called access resistance) is a physical property of the recording itself and relates to the access of the tip of the pipette with the intracellular medium. Hence, I limited my analysis to those features of the IPs that were not strongly affected by the recording conditions (Figure 2.5).

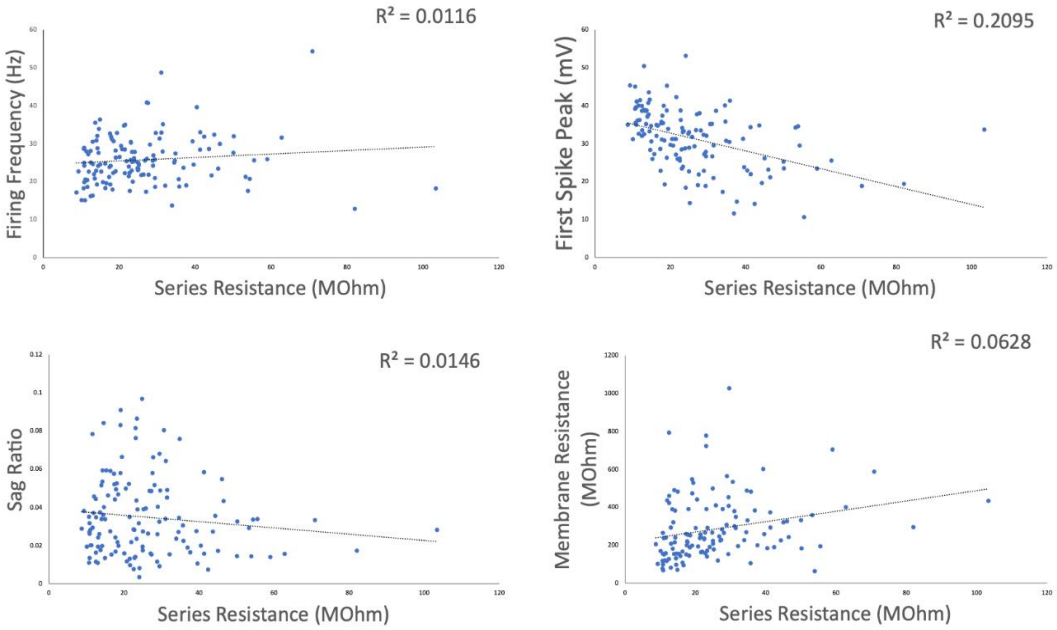

Figure 2.5. Features of recordings covary with series resistance. Distributions of features (voltage sag, membrane resistance, firing frequency, and peak of the first spike) and their relationships to series resistance. Each point represents a recording from one neuron.

Within-individual uniformity of IPs

In order to evaluate whether my data showed the same pattern of organization reported in Daou and Margoliash, 2020, I grouped neurons by bird and evaluated the variance of IPs within each bird. If neurons recorded from the same bird are more similar to each other (centered on the same mean), then the variance of IPs among cells from the same bird should be lower in my dataset than a dataset that has no relationship (randomly shuffled data).

Holding the numbers of cells per bird constant, neurons were randomly reassigned, thus generating 1,000 shuffled data sets. I then compared the average within-bird variance of the real

and bootstrapped data for firing frequency, sag ratio, and membrane resistance (features that varied minimally with series resistance, see Methods) and evaluated where the real data fell within the bootstrapped distribution. This showed that the real neurons were significantly less variable within birds for firing frequency (p=0.002) and sag ratio (p=0.012) but not for membrane resistance (p=0.269) or holding current (p=0.102) (Figure 2.6). Thus, neurons from the same bird shared more similar firing frequency and sag currents than neurons from other birds.

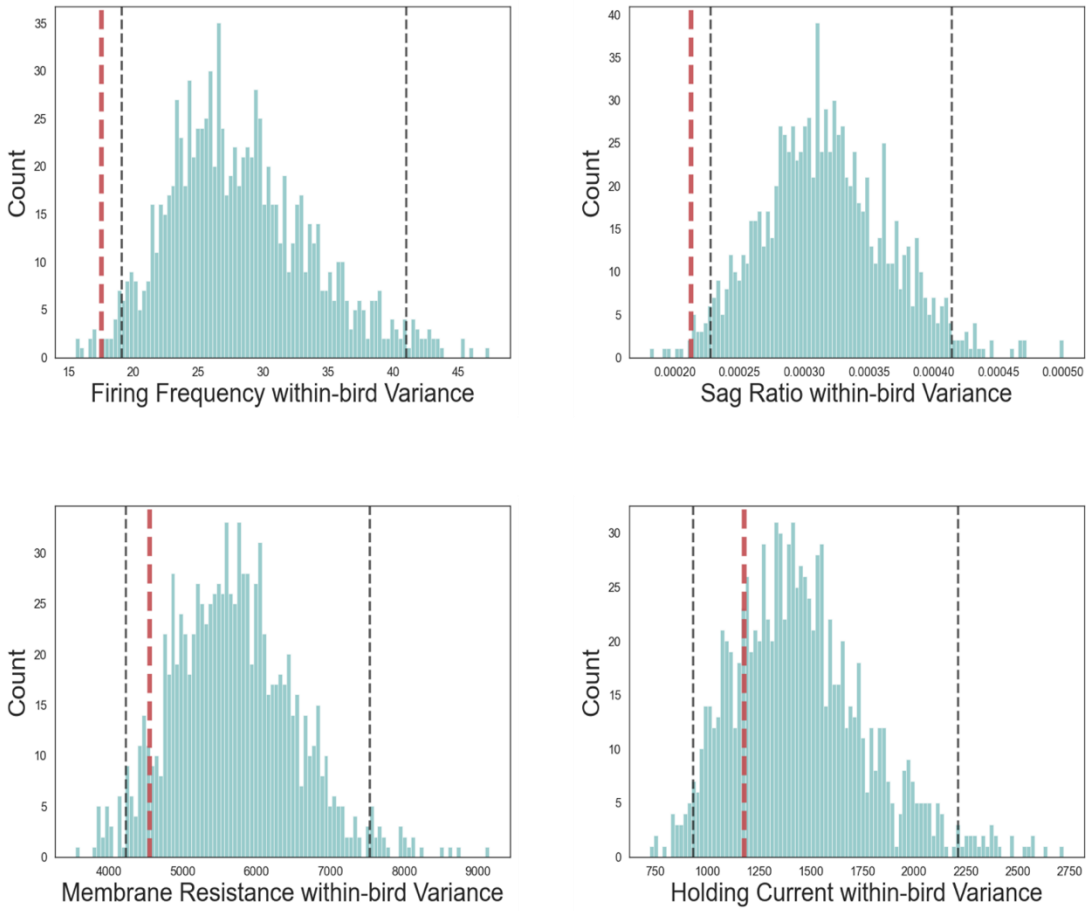

Figure 2.6. Within-bird similarity of intrinsic properties. Real (red dashed line) and bootstrapped (light blue) within-bird variance for firing frequency, sag ratio, membrane resistance, and holding current. The 95% confidence intervals are shown as black dashed lines.

IP expression is determined by song learning

To evaluate the relative contribution of heredity and song learning to the IPs of the neurons I examined the effects of features of songs and parentage on the measured IP values. To this end, I used mixed effects linear models (MixedLM) to examine the interactions between sag ratio, firing frequency, motif duration, the duration of the longest harmonic stack, and family as an indicator variable assuming random effect. I ran two MixedLMs (153 neurons, 4 neurons per bird on average, 38 birds, 13 families): one using evoked firing frequency (100 pA) as the dependent variable, and another using the sag ratio (-100 pA) as the dependent variable. All values were normalized before being run through the model. Only the duration of the longest harmonic stack was significantly correlated with sag ratio ($p = 0.018$) and firing frequency ($p=0.008$) (Tables 1 and 2). It is important to note, that to date I have not estimated statistical power for the mixed linear model. Nonetheless, the result points to the contribution of temporal song features to IPs of HVC_X.

Mixed Linear Model Regression Results

Model:	MixedLM	Dependent Variable:	SAG_stand
No. Observations:	154	Method:	REML
No. Groups:	38	Scale:	0.6971
Min. group size:	1	Log-Likelihood:	-208.7421
Max. group size:	11	Converged:	Yes
Mean group size:	4.1		

	Coef.	Std.Err.	z	P>|z|	[0.025	0.975]
Intercept	-0.202	0.206	-0.979	0.328	-0.606	0.202
Motif_stand	-0.052	0.128	-0.404	0.686	-0.303	0.199
Family	0.020	0.024	0.832	0.405	-0.028	0.068
Stack_stand	0.334	0.141	2.367	0.018	0.057	0.610
Group Var	0.266	0.744				
Group x Family Cov	-0.007	0.097				
Family Var	0.000	0.010				

Table 1. Mixed Linear Model Regression Results for sag ratio. MLM results regressing sag ratio on the duration of the motif, the duration of the longest harmonic stack, and family identity.

Mixed Linear Model Regression Results

Model:	MixedLM	Dependent Variable:	FF_stand
No. Observations:	154	Method:	REML
No. Groups:	38	Scale:	0.5885
Min. group size:	1	Log-Likelihood:	-199.4111
Max. group size:	11	Converged:	Yes
Mean group size:	4.1		

	Coef.	Std.Err.	z	P>|z|	[0.025	0.975]
Intercept	-0.412	0.222	-1.852	0.064	-0.848	0.024
Motif_stand	0.046	0.131	0.348	0.728	-0.211	0.302
Family	0.053	0.033	1.606	0.108	-0.012	0.117
Stack_stand	0.324	0.122	2.660	0.008	0.085	0.563
Group Var	0.710	0.524				
Group x Family Cov	-0.101	0.078				
Family Var	0.015	0.012				

Table 2. Mixed Linear Model Regression Results for firing frequency. MLM results regressing firing frequency on the duration of the motif, the duration of the longest harmonic stack, and family identity.

Plasticity of intrinsic excitability in vitro

During most of my recordings of HVC_X neurons, I observed a decrease in the evoked firing frequency over time. This was most noticeable in the period 5-10 minutes after the initial recording. To mitigate this possible confound, I restricted analysis to the first 11 traces for each cell that focused on IPs (for all analyses throughout this thesis), which correspond to the most stable part of the recordings and usually the first 5 minutes of stimulation (e.g., Figure 2.7, green neuron). Beyond 5 minutes of continuous stimulation, the rate of evoked spike loss increased for some cells (Figure 2.7, yellow neuron). This may relate to features of activity-dependent plasticity, or it could be artifactual and related to tissue health, or have elements of both.

To evaluate the potential role of activity-dependent plasticity in these changes, in a smaller subset of neurons (N=33), I recorded responses to a 10 Hz stimulation protocol to investigate whether the decrease in excitability was activity dependent. I noticed that using a stimulation protocol of 10 Hz for 1 second followed by a 1 second gap (example trace shown in Figure 2.8) caused a hyperpolarization in the neurons and a decrease in evoked spikes. This effect was quantifiable after 2 minutes of stimulation, after which neurons often fired 2-3 fewer evoked spikes to a 100 pA, 300 ms square pulse (Figure 2.9).

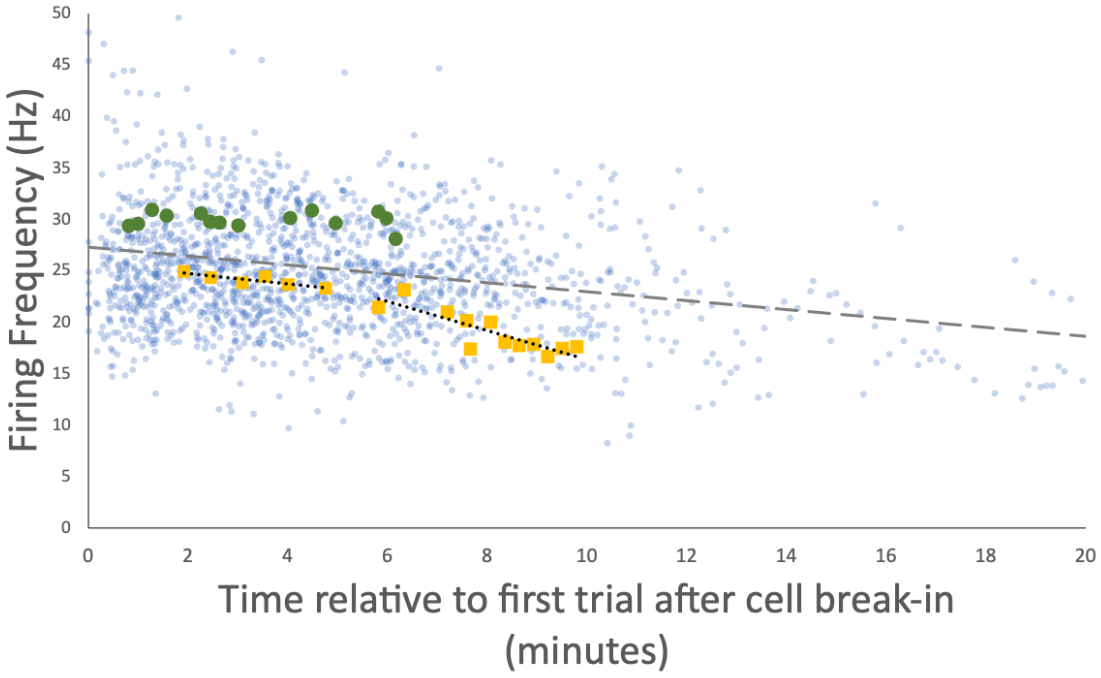

Figure 2.7. Time and activity dependent loss of evoked firing. Evoked firing frequency of HVC_X neurons from all birds (blue dots) over the course of their recordings. One cell shows consistent evoked firing frequency over a period of 5 minutes (green), while another shows a rapid decrease in firing frequency after 5 minutes (yellow).

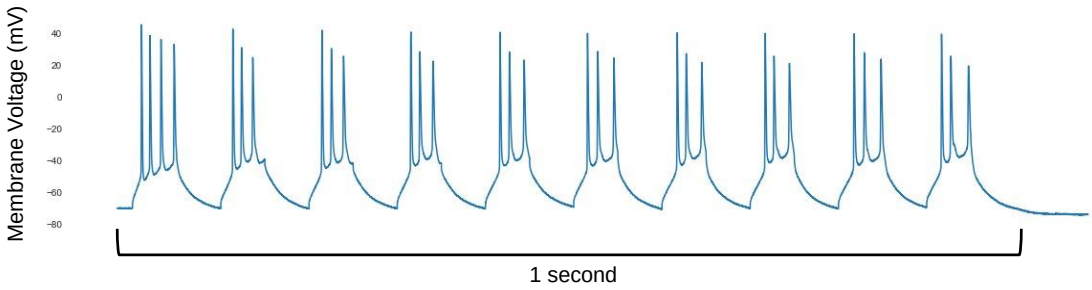

Figure 2.8. Somatic stimulation protocol. An example voltage trace from an HVC_X during one second of 10 Hz stimulation.

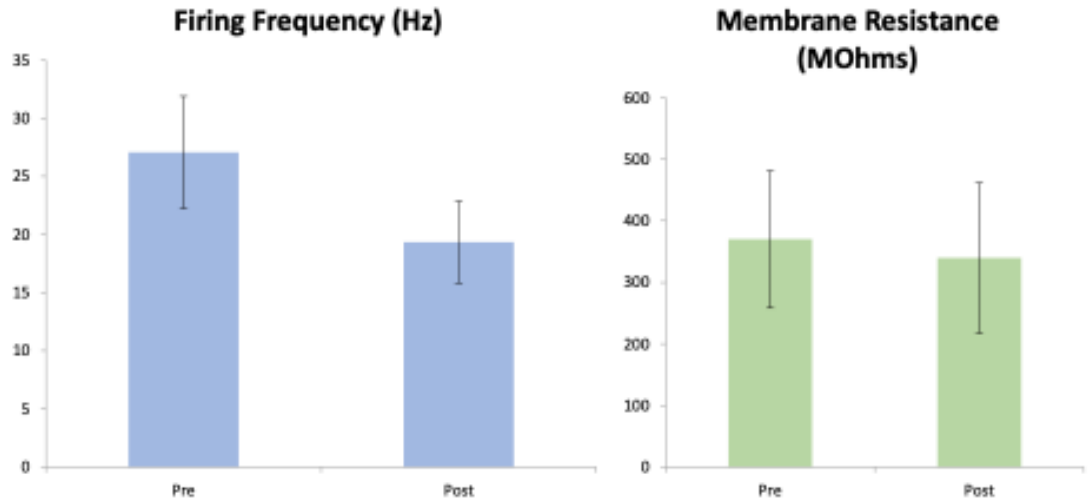

Figure 2.9. Stimulation decreases evoked firing frequency. Changes in HVC_X firing frequency (blue) and membrane resistance (green) after two minutes of 10 Hz somatic stimulation.

The stimulation induced hyperpolarization of the resting membrane potential occurred as quickly as one trial (1 second) and can be seen in the first few trials (Figure 2.10). Note that many pulses produce one fewer spike after each subsequent trial. A zoomed in view of the resting membrane potential (RMP) for one example neuron (black box, Figure 2.10) shows a hyperpolarization of 1-2 mV after each trial (Figure 2.11). Figure 2.12 shows a summary plot for the first 15 ms of the first 6 trials for 33 neurons (black dots) and the average membrane voltage of all neurons at each trial (blue line). The average pre-trial RMP was -70.83 mV, which hyperpolarized to -72.7 mV, and -74.1 mV for the second and sixth trial respectively. Additionally, qualitatively, the after-hyperpolarization of each spike train seemed to have become steeper when comparing the first trial to the last trial. Figure 2.13 illustrates the first (blue) and last (red) traces for three example neurons.

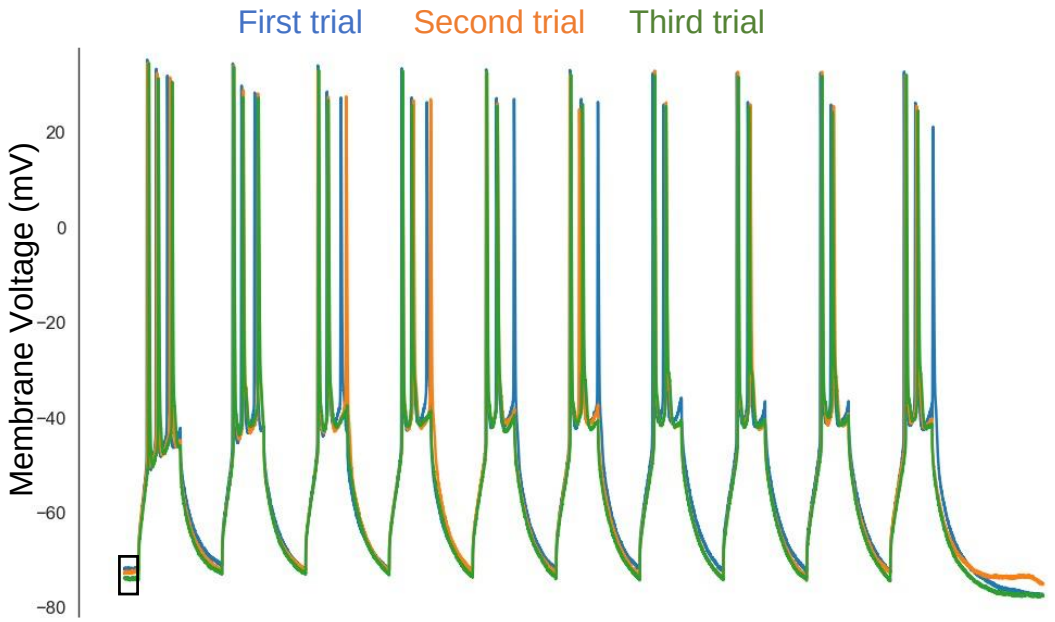

Figure 2.10. Example traces from a stimulated neuron. The first (blue), second (orange), and third (green) trials from one neuron during the somatic stimulation protocol. Black box focuses on the resting membrane potential of each trace (see Figure 2.10).

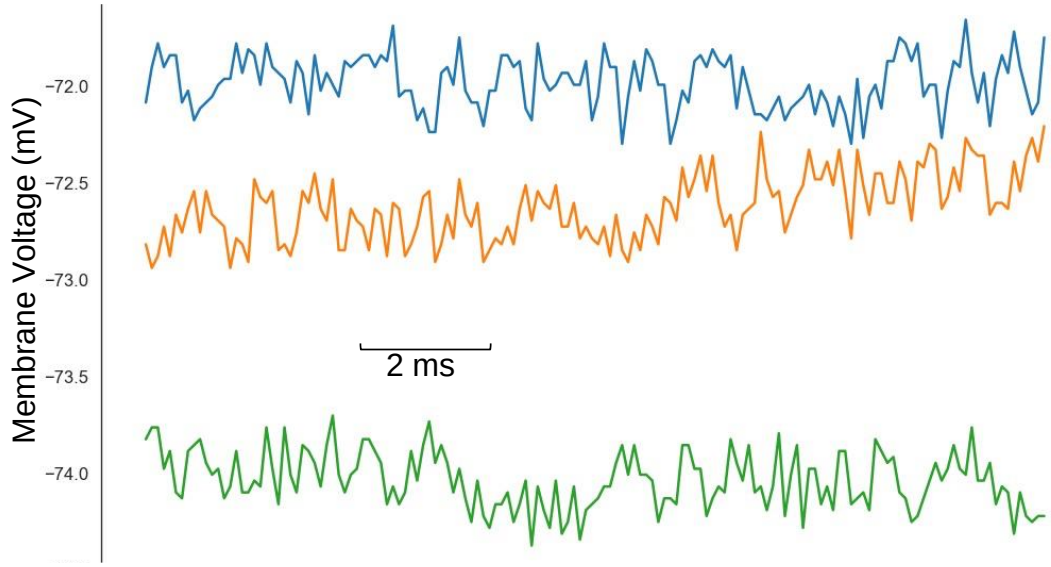

Figure 2.11. Stimulation induced hyperpolarization. A zoomed in view of the first three stimulation traces from within the black box in Figure 2.9.

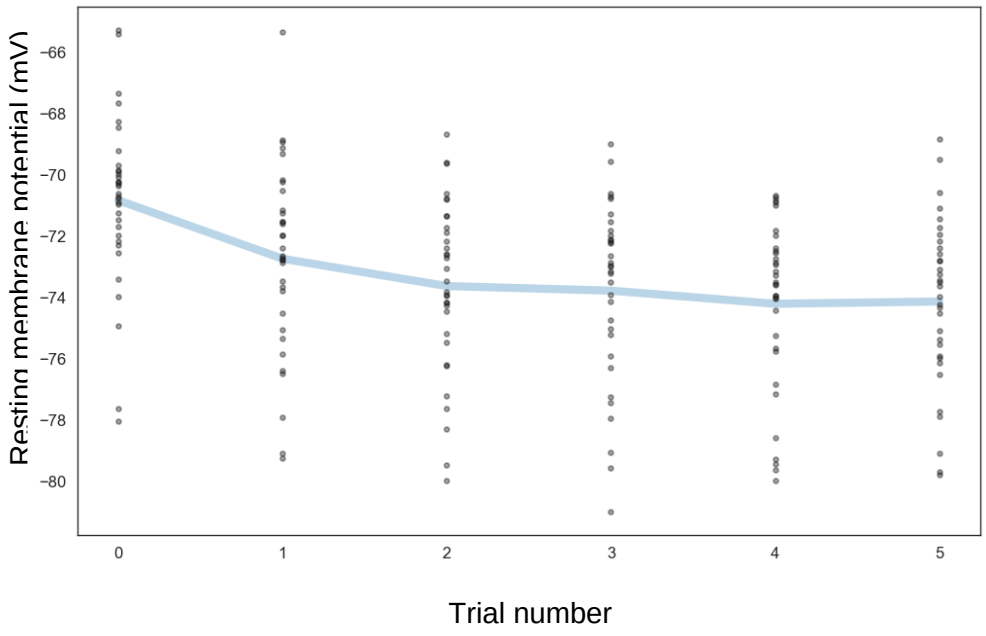

Figure 2.12. Summary of rapid resting membrane potential hyperpolarization. Resting membrane potential measured before the first stimulation pulse for the first 6 trials for 33 HVC_X (black points) and the average resting membrane potential for all HVC_X at each trial (blue line).

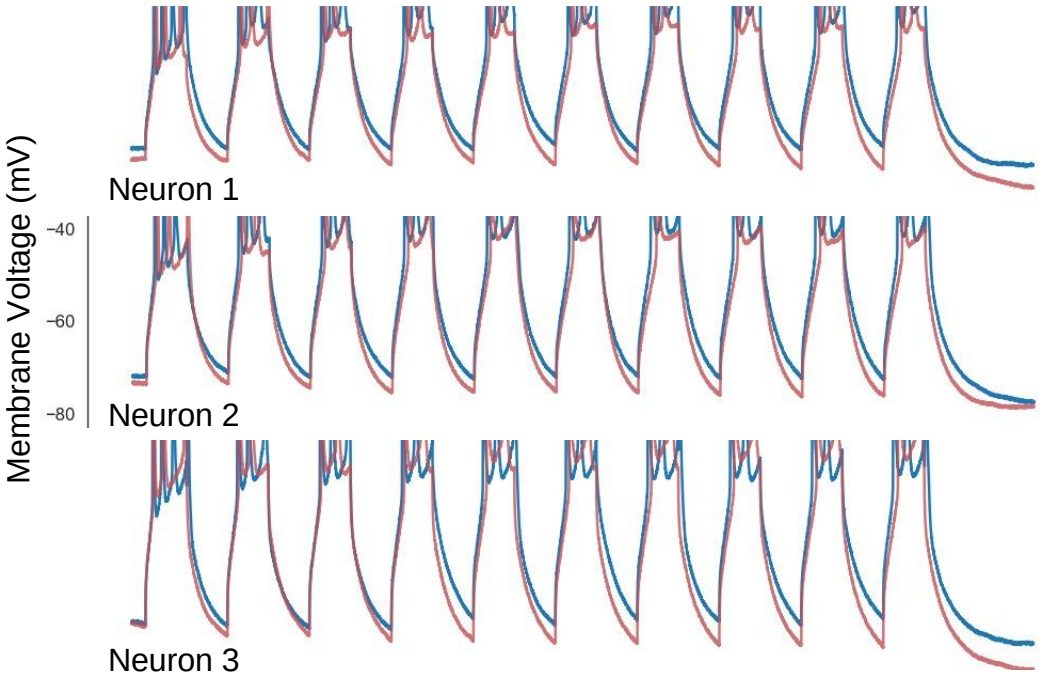

Figure 2.13. Post-stimulation changes in afterhyperpolarization. The first (blue) and last (red) trials of the stimulation protocol for three neurons.

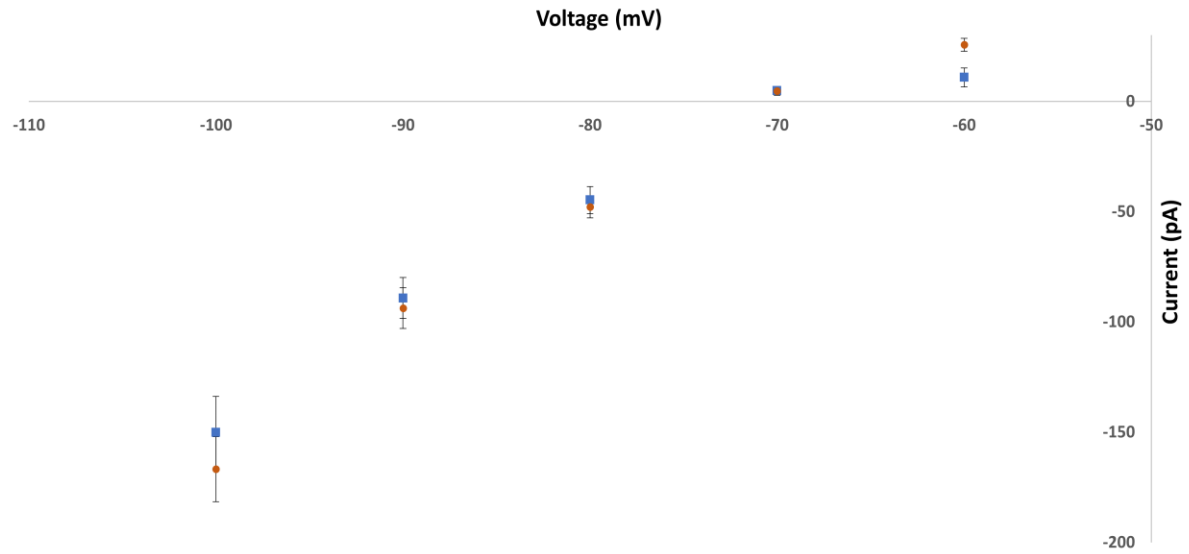

Figure 2.14. Post-stimulation changes in I/V relationship. The average evoked currents for 10 mV voltage steps (from -100 to -60 mV) for 10 HVCX neurons before (blue) and 5 minutes after (orange) somatic stimulation (error bars represent the standard error of the mean).

Lastly, I wanted to investigate the currents that were underlying the changes in excitability that occurred after stimulation. To do so, I recorded currents in voltage clamp, and presented a protocol that stepped from resting (-70 mV) to -100, -90, -80, and -60 mV, before and after 5 minutes of stimulation. Stimulation caused a slight increase in the evoked inward current at -100 mV. At -60 mV, there was an increase in the evoked outward current. This increase was completely absent in many cells prior to being stimulated (Figure 2.14). This stimulation-dependent outward current, as well as the prior mentioned hyperpolarization (Figure 2.12), points to a shift in some potassium conductance.

HVC_X IPs are learned and related to temporal features of song.

I performed whole-cell recordings in horizontal HVC slices (195 neurons from 38 birds) and assessed the intrinsic excitability and passive membrane properties of the neurons recorded via somatic depolarizing and hyperpolarizing current injections. HVC was identified as a dark myelinated region under brightfield illumination and confirmed with retrograde labeling using GFP or rhodamine (n=4 animals, 8 slices, see Methods). This definition of HVC was also independently verified by the presence of canonical firing patterns of HVC projection neurons (see below).

HVC_X and HVC_{RA} were distinguished by their characteristic firing properties, as previously reported (Daou et al., 2013; Daou and Margoliash, 2020; Ross et al., 2017 and 2019; Mooney and Prather, 2005; Mooney, 2000). HVC_{RA} neurons showed robust spike adaptation to my standard set of applied depolarizing currents (100 – 150 pA square pulses, 10 pA steps, 300ms), firing few spikes at the stimulus onset riding atop a large, depolarized plateau (20 mV or more). HVC_X (n = 154) had distinct firing properties that included continuous (tonic) firing (Figure 2.15, dotted line) with smooth spike after-hyperpolarization, modest spike adaptation, voltage sag (note the difference between the black triangle and black square in Figure 2.15) and post-inhibitory rebound depolarization to negative applied currents (Figure 1.5, red arrow; Figure 2.15, black dashed box). The membrane capacitances of the HVC_X were larger than for HVC_{RA} ($p < 1^{-15}$) (Figure 2.16) (Ross et al., 2017), whereas there were no differences in the membrane resistance between the two classes ($p = 0.21$). Finally, only the HVC_X showed post-inhibitory rebound.

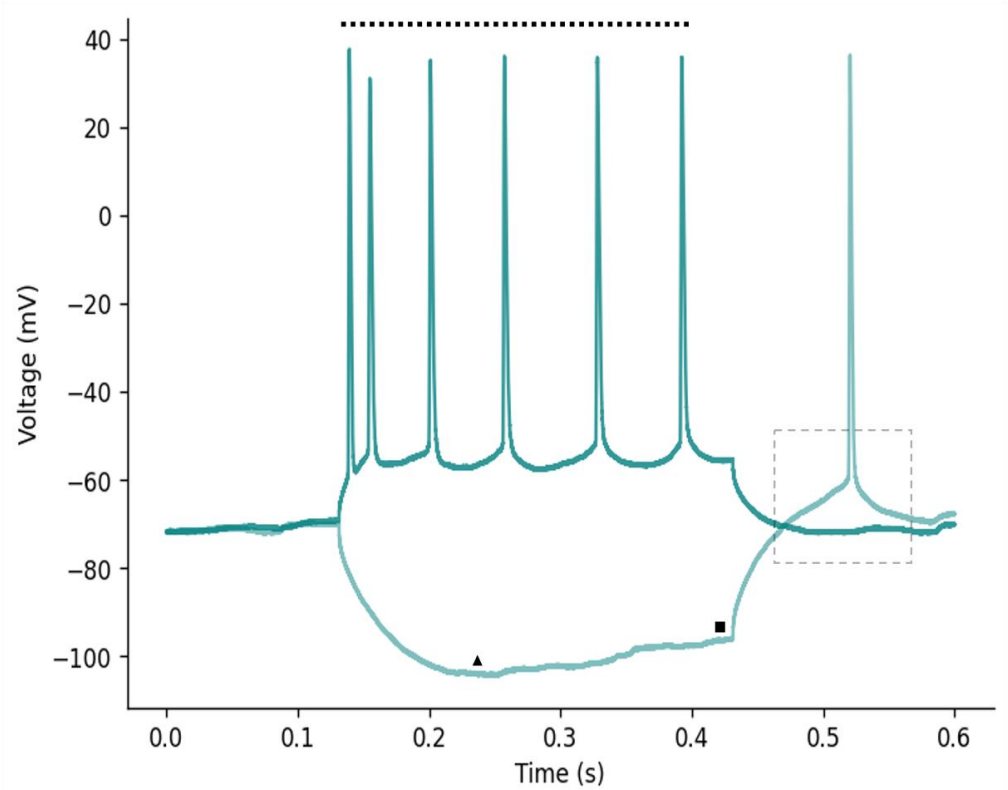

Figure 2.15. HVC$_X$ IPs evaluated from the raw data. An HVC$_X$'s evoked response to a depolarizing (100 pA) current injection (top, darker green trace) and a hyperpolarizing (-100 pA) current injection (bottom, lighter green trace). Dotted black line represents the time from the first to the last spike in the evoked train. Black triangle represents the most hyperpolarized point while black square represents the point immediately before the release of inhibition. Black dashed box denotes post-inhibitory rebound depolarization and its associated rebound spike.

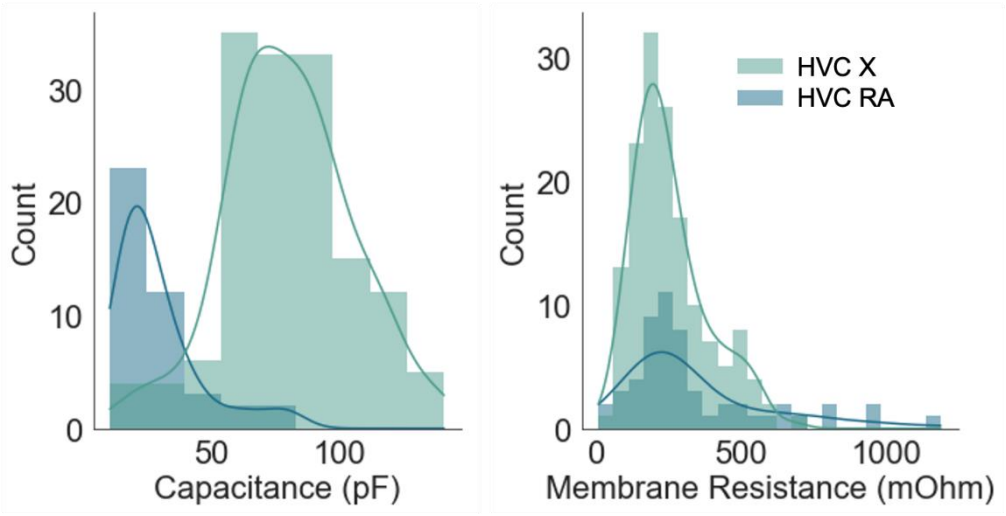

Figure 2.16. HVC$_{RA}$ and HVC$_X$ are distinguishable by their membrane capacitance. Distributions of membrane capacitance (left panel) and Membrane resistance (right panel) for HVC$_X$ (light green) and HVC$_{RA}$ (dark green).

Over the course of these experiments, I deployed three experimental designs (described earlier in the methods of this chapter) as the structure of the data set emerged. In the first design, birds were raised by their parents in individual cages but in acoustic contact with birds in the other cages and in a flight aviary in the same room. This resulted in (14 birds) from which I obtained electrophysiological data. Siblings raised under such conditions tended to show only small variations in song copying (less than we had hoped for), confounding my ability to relate differences in IPs with differences in songs. In the second design, birds were raised in sound isolation chambers with their parents until post hatch day 15, at which point I removed the father. Once juveniles were identified as having male plumage, they were placed in a separate sound isolation box with an adult male tutor. Over the course of these experiments, a relation between features of song timing and HVC_X IPs emerged. Thus, I pursued a third design with stronger control over the structure of the tutor songs that the birds heard. Female–raised males (at 32-40 DPH) were transferred to a sound isolation chamber arranged so that pulling a string provided instrumental access to hearing song playback (Tchernichovski et al., 2001). The songs these birds heard were chosen to explore the relation of IPs and features of syllable timing.

First, I explored a relationship between rebound excitation and features of the entire motif. For the spectral analyses, I extracted features from sound analysis pro (SAP) and investigated their relationship to the average firing frequency and sag ratio of the neurons recorded from birds from the first and second design (no modified songs). A number of SAP features correlated with firing frequency and sag ratio, including pitch, frequency modulation, and goodness of pitch. Amplitude, amplitude modulation, and entropy were not correlated (Figure 2.17).

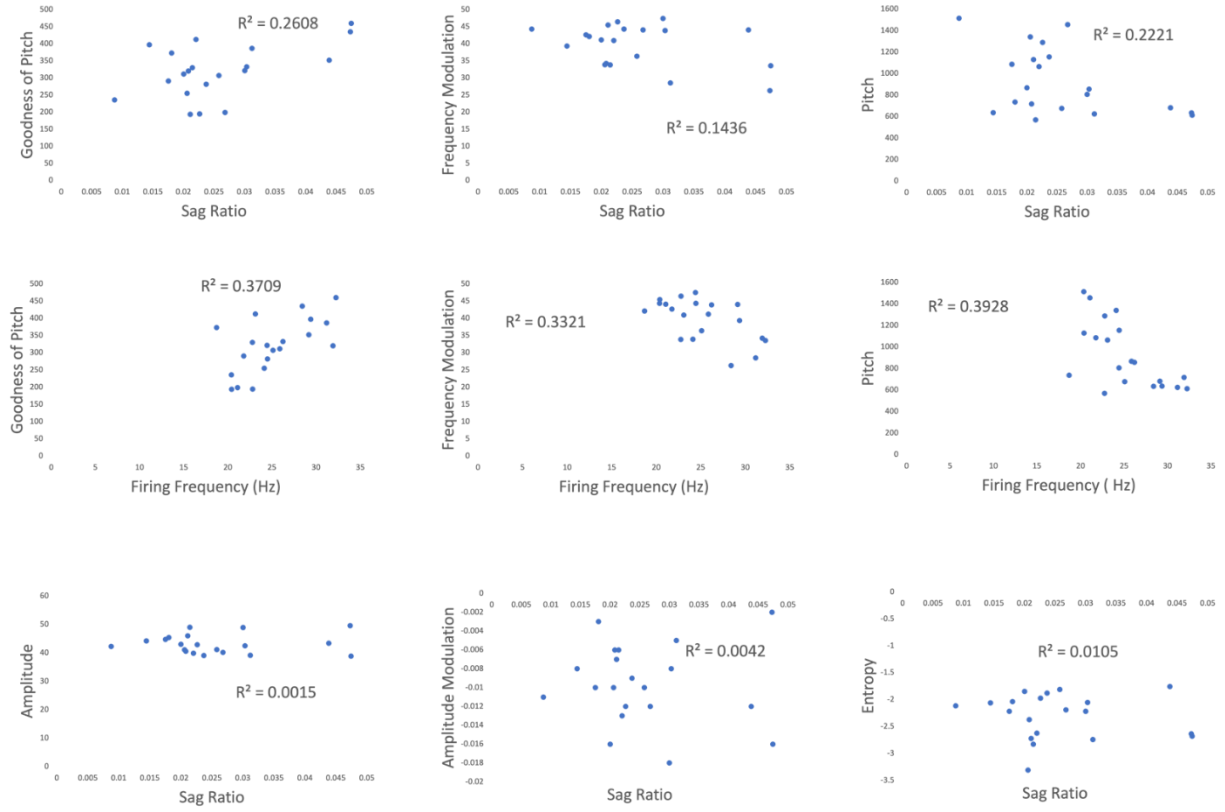

Figure 2.17. Correlations of spectral song features with HVC_X IPS. Features of song extracted from SAP and plotted against the mean firing frequency and sag ratios of all neurons from each bird (blue points).

Notably, all features of song that showed a correlation with electrophysiological features are explained by the amount of harmonic stack vocalizations within the motif. Harmonic stacks are continuous spectrally invariant vocalizations. They have low frequency modulation and high goodness of pitch. This means that songs that include many harmonic stacks have lower average FM for the motif, and their longest harmonic stack is on average longer.

Harmonic stacks also have low pitch relative to other syllable types, which results from biophysical constraints on peripheral song production mechanisms. We confirmed this independently by examining the pitch of harmonic stacks and other syllable types in a randomly chosen set of birds (N = 9) from the first two designs (Figure 2.18). Thus, if HVC_X firing properties

are correlated with temporal features of harmonic stacks (a property presumptively encoded in the forebrain), by the biophysical constraints they would also be correlated with song pitch. If, however, HVC_X firing properties were encoding song pitch directly, they should not be correlated with temporal features of harmonic stacks.From this point, I focused the analysis of temporal features of HVC_X IPs on harmonic stacks, the duration of the song motif, number of syllables, the duration of the longest syllables, and the longest duration harmonic stack in the motif of each bird (blue shaded regions, Figure 2.19). The duration of the longest harmonic stack varied over approximately 5–fold (40 ms to 200 ms).

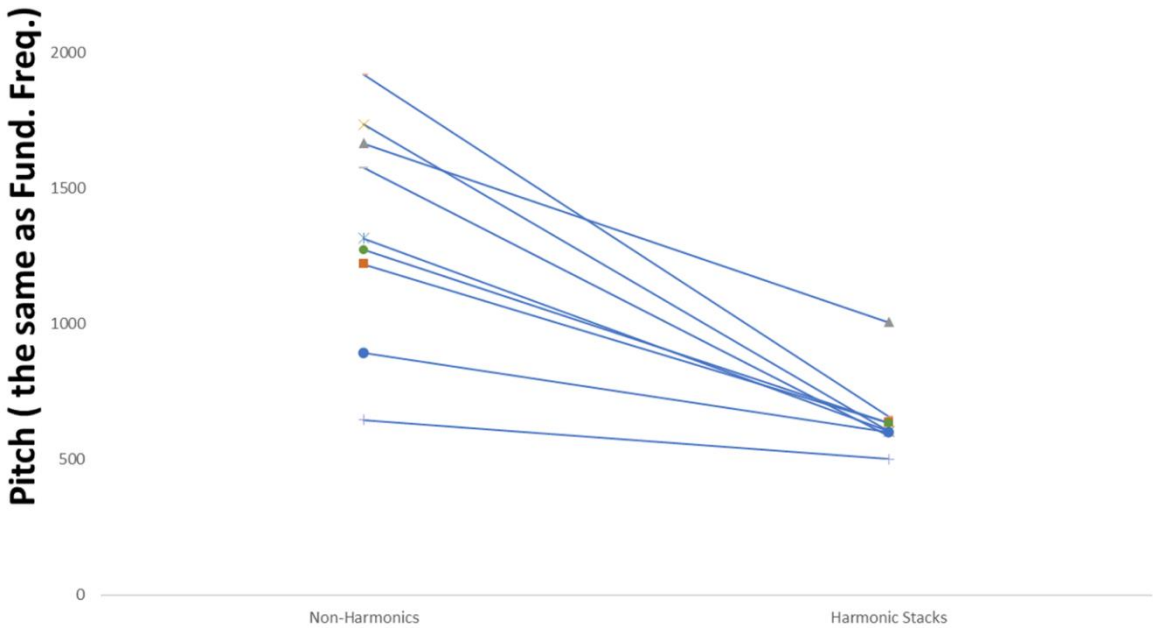

Figure 2.18. Harmonic stacks have lower pitches than other syllable types. Average pitch (or fundamental frequency) of non-harmonic syllables and harmonic stacks for 9 randomly chosen birds' songs.

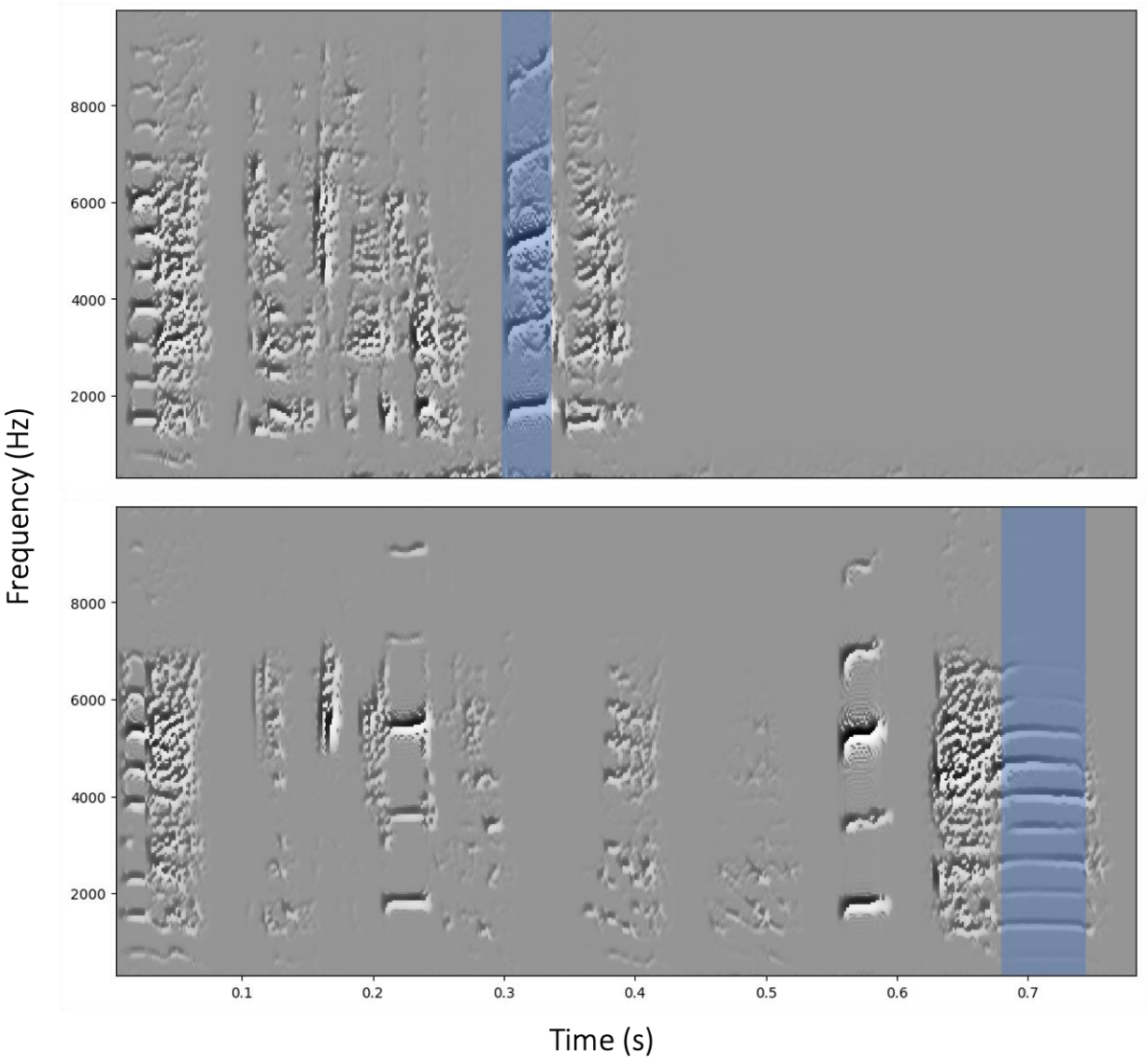

Figure 2.19. Harmonic stacks reflect temporal structure. Example spectrograms from two different songs, one short (top panel) and one long (bottom panel) with their respective longest harmonic stacks denoted (blue shaded regions).

The mean sag ratio and firing frequency of the HVC_X from each bird were positively correlated with the duration of the longest harmonic stack (Pearson's R: 0.59 and 0.2, p values: 0.0003 and 0.02; Figure 2.20) as well as the remainder of the motif (total motif duration – longest stack) (Pearson's R: 0.38, p value: 0.03, Figure 2.20). Average HVC_X membrane capacitance was inversely correlated with the duration of the longest harmonic stack of each bird (Pearson's R: -0.50, p value: 0.004, Figure 2.20). I also tested whether a relationship between sag ratio, firing frequency, and stack duration was present in the 18 birds with song data from our lab's previous study (Daou and Margoliash, 2020) by looking at the modeled ionic conductances associated with firing frequency and sag (1/gSK and gH, respectively). There was a positive relationship between mean gH/gSK of each bird and the longest harmonic stack in those data as well, though it did not reach statistical significance with a linear regression (Pearson's R: 0.42, p value: 0.08, Figure 2.21). One bird from those data however, had a harmonic stack of 11 ms (unusually short), and may be an outlier. Excluding that bird, the fit of the linear regression improves (Pearson's R: 0.59 , p value: 0.012). The results suggest the possibility that the duration of the longest stack was also correlated with the duration of the remainder of the motif. I confirmed this result for the 38 songs in my dataset (Pearson's R: 0.77, $p < 2^{-7}$), and further confirmed the result in a dataset of 52 songs from other labs (people.bu.edu/timothyg/song_website/index.html), which included zebra finch songs provided by Frederic Theunissen, Luke Remage-Healy, Kathy Nordeen, Ofer Tchernichoski, Sarah Bottjer, and Elizabeth Regan (Pearson's R = 0.58, $p < 9^{-6}$, Figure 2.22). Thus, zebra finches with longer songs tend to have longer harmonic stacks. Additionally, I found a tendency for the longest harmonic stack to appear near the end of the motif, with 78% of songs having their longest harmonic stack in the second half of the motif, and 55% of songs having the longest harmonic stack in the last third of the motif.

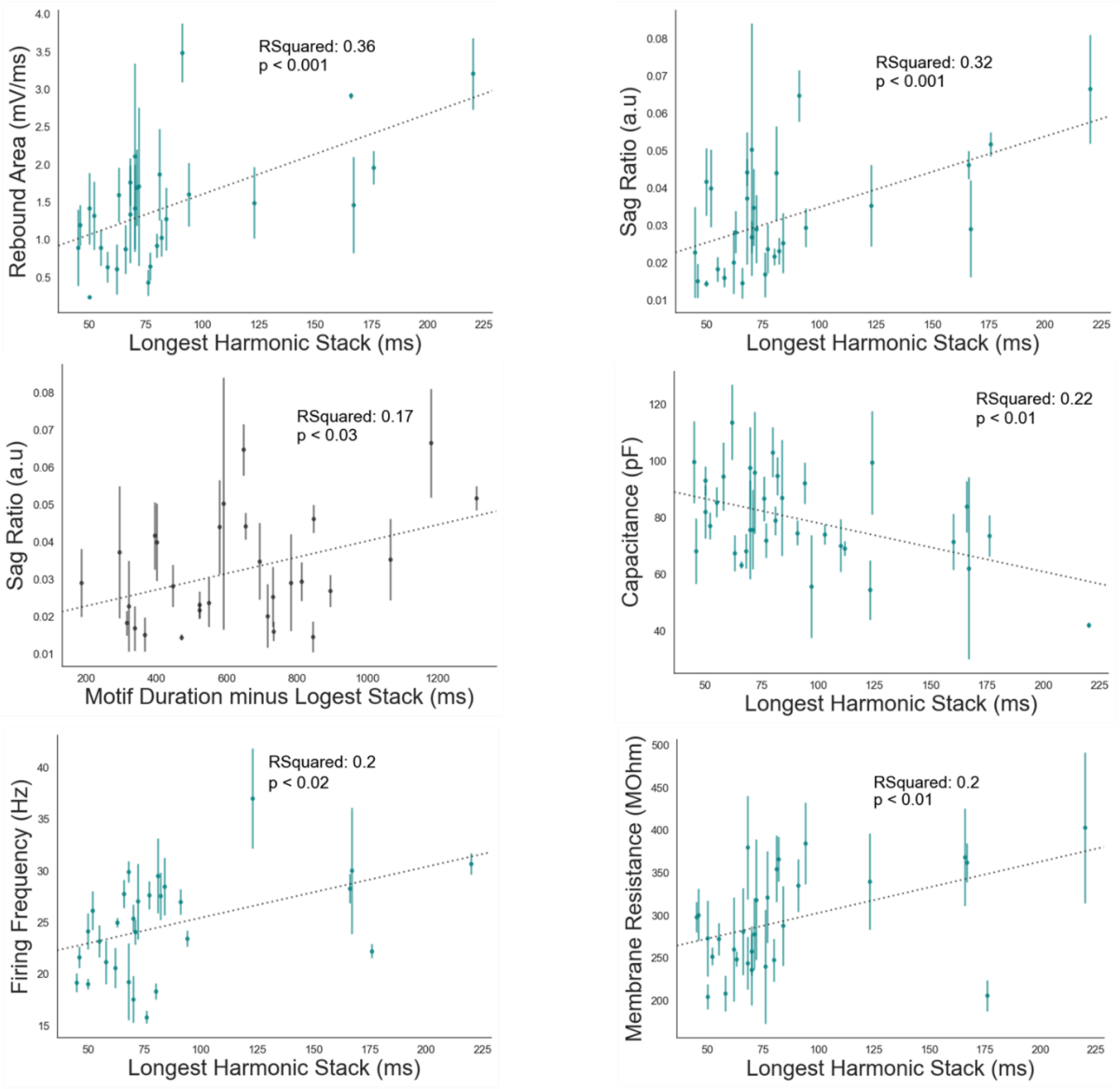

Figure 2.20. Features of rebound excitation relate to temporal song features. Scatter plots of mean analyzed parameters for all HVC_X for each bird, plotted against temporal features of song (error bars are standard error of the mean).

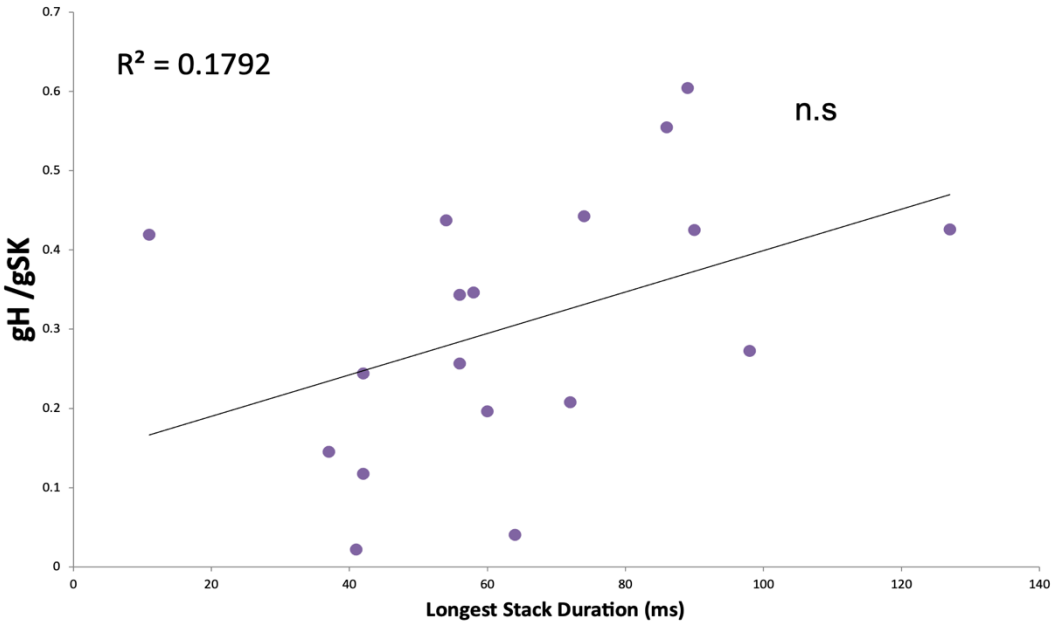

Figure 2.21. Revisiting data from Daou and Margoliash, 2020. Average conductance values for HCN channels and SK channels (plotted as gH divided by gSK) from modeled neurons from Daou and Margoliash, 2020, regressed on the duration of the longest harmonic stack of the corresponding birds' songs.

I then leveraged the zebra finch's ability for song learning to gain control over the songs the birds sang as adults. To do this I used a combination of live tutored birds (second design) and the instrumental learning protocol (third design) that allowed me to manipulate the songs used for tutoring (Figure 2.23). With this approach, I generated two groups of birds who sang nearly identical songs, except one group's song includes an additional long harmonic stack as their last syllable (~100 ms) (song B, Figure 2.23). My aim here was to limit potential effects of spectral differences on intrinsic excitability. I found that HVC_X neurons from birds who sang the unmodified song, which had a short harmonic stack and short overall duration had lower sag ratios and firing frequency (Figure 2.23, C, p values: 0.001 and 0.0001 respectively) when compared to those from birds who sang the modified song. Additionally, I find that though the membrane capacitance

trended towards smaller values for cells from the modified song group, it was not statistically significant (Figure 2.23, C, p = 0.08).

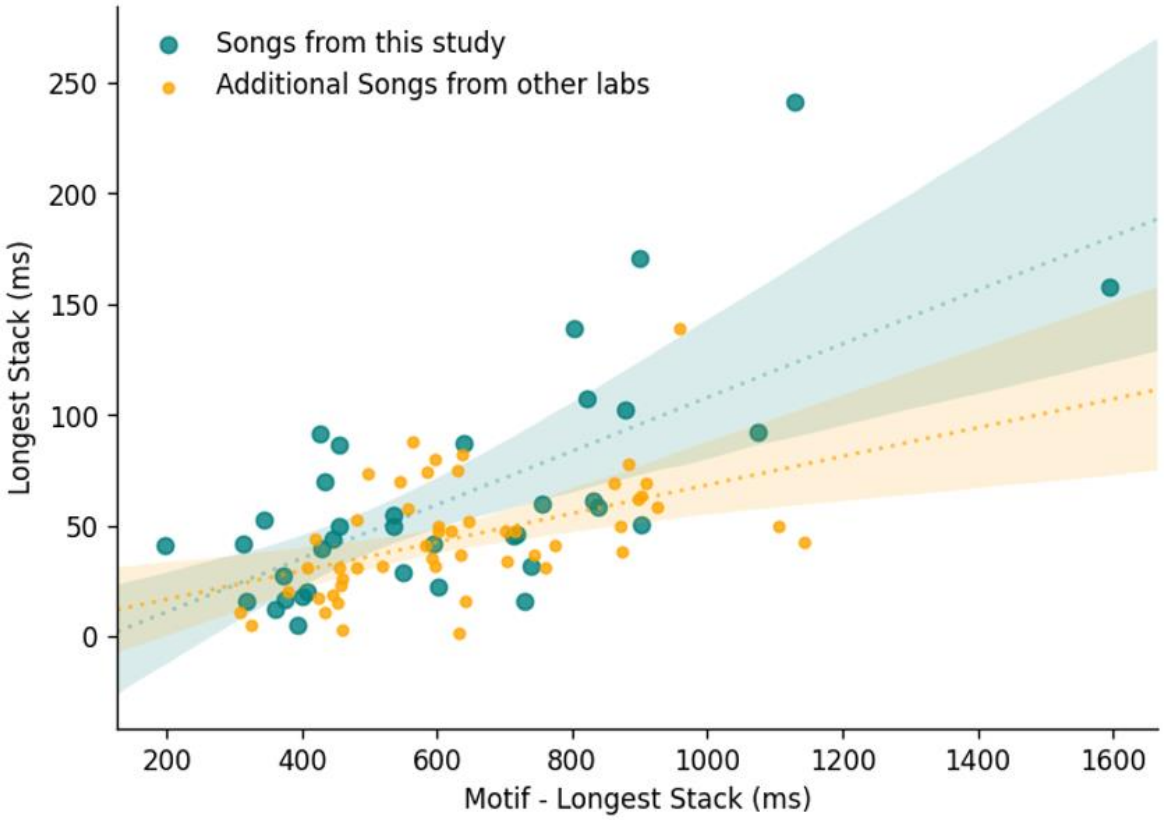

Figure 2.22. Duration of song motif and longest harmonic stacks covary. Correlation between the duration of the longest harmonic stack and the remainder of the motif duration (motif minus longest stack) for two groups of songs: songs from my own work (green) and 52 songs from other labs (yellow).

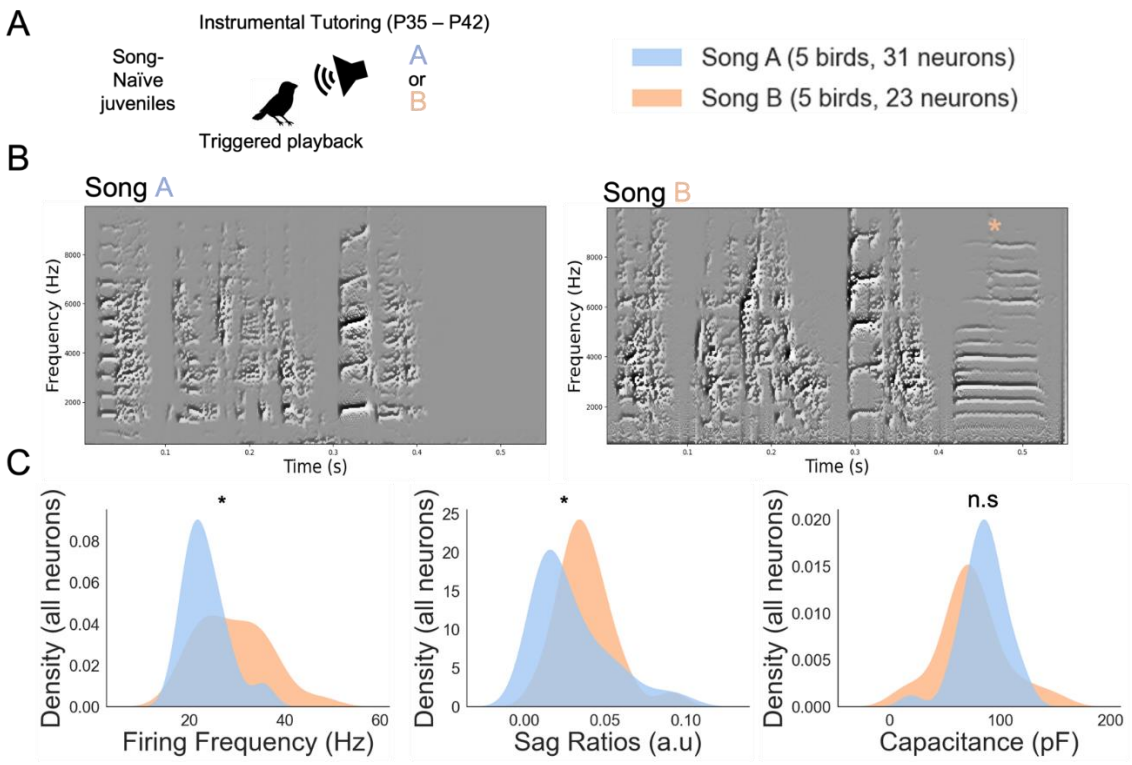

Figure 2.23. Instrumental tutoring with modified songs changes HVC$_X$ IPS. A: Diagram of tutoring paradigm, depicting a juvenile who can pull on a string to get song playback (see methods in this chapter). Birds were tutored with either Song A or Song B (not both). B: Spectrograms of example motif from one bird from each group. C: Distributions (kernel density estimations) for all HVC$_X$, grouped by song type, for evoked firing frequency, sag ratio, and membrane capacitance.

I also collected voltage-clamp data from four birds (20 neurons) to further evaluate the relationship between voltage sag and temporal features of song. Birds who sang longer songs had HVC_X with larger inward currents at hyperpolarized potentials (Figure 2.24). Two of the four birds, L174 and L176, sang songs A and B respectively (Fig. 2.23, B). L176's average inward currents were consistently greater than L174's across all membrane potentials below -70 mV. Two other birds, L89 (longest stack of 91 ms) and L148 (longest stack of 66ms) had greater inward current magnitudes. Notably, L148 who has the greatest evoked inward currents, has a total motif duration of 910 ms, while L89 has a motif duration of 738 ms. L176 came from the instrumental tutoring design in which birds heard playback of a short song with an added stack, and as a result, has the longest harmonic stack of the four birds (97 ms) but a short total motif duration (512 ms).

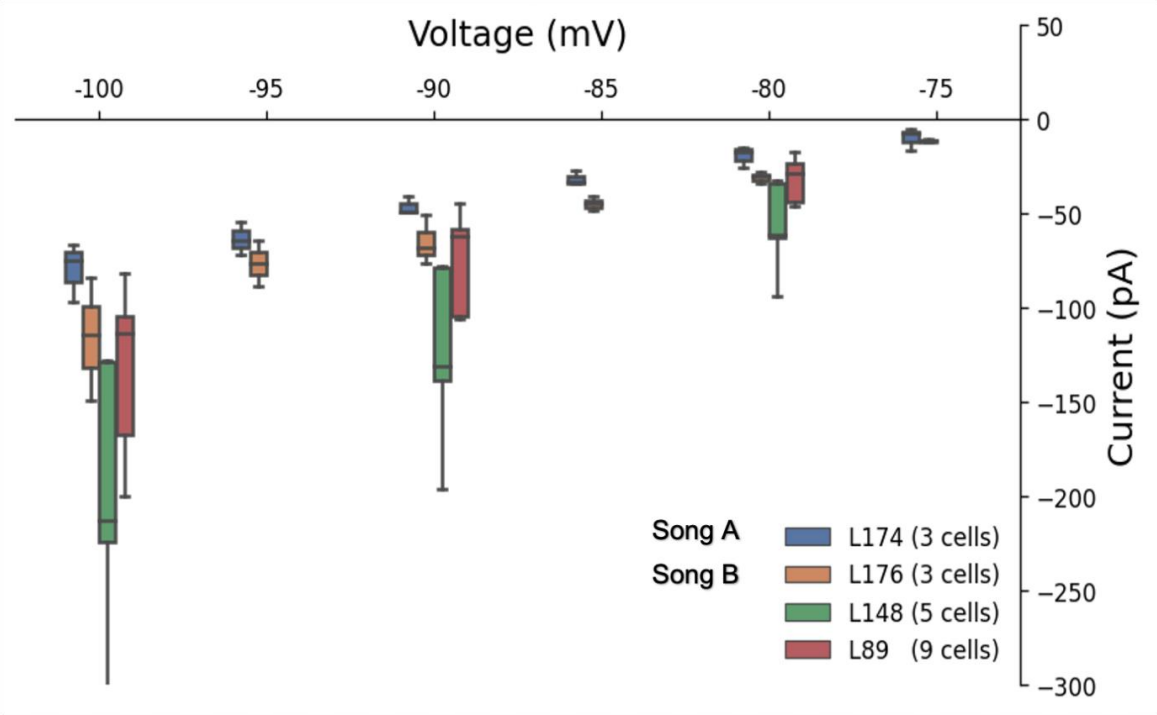

Figure 2.24. Evoked inward currents relate to song duration. Current/voltage curve for HVC_X from 4 birds, two of which sang the unmodified and modified songs from Figure 2.21: L174 (orange) and L176 (blue), respectively).

In two birds (one neuron each) I blocked Ih with ZD7288 and produced current/voltage curves. I subtracted the remaining currents after Ih blockade from baseline to reveal the contribution of the HCN channel. In Figure 2.25 I plot the Ih currents at various voltages for those two neurons, and show that the neuron from bird L176, who sang the modified song with a long harmonic, had larger Ih.

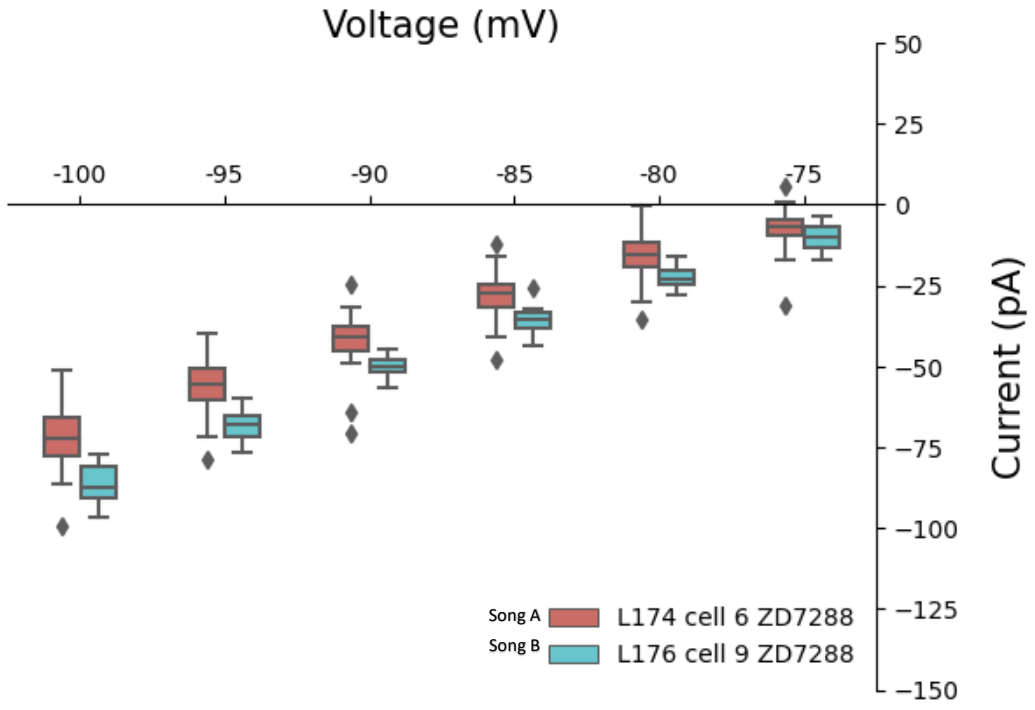

Figure 2.25. verified HCN currents for one cell from two birds. Current values shown are the baseline values with ZD7288 subtracted**.** The remaining HCN Current/voltage curve for one HVC_X from two birds that sang the unmodified and modified songs from Figure 2.21: L174 (red) and L176 (blue), respectively). Each box and whisker plot represents every trial presented to the neuron. Diamonds represent trials with more than two standard deviations from the mean.

Discussion

Reflections on Daou and Margoliash, 2020

In my initial planning of these analyses, I anticipated taking a similar approach to Daou and Margoliash, 2020, and evaluate IPs based on modeled maximal ion channel conductances. This entails first fitting models to raw voltage traces by manually varying ionic conductance values in the model (gNa in equation 2, for example) until the model fits the real data and makes correct predictions of non-fitted traces. My preliminary analysis and exploration of my hand-fitted models, however, revealed that many local solutions were easy to find, but achieving a global minimum, 'good', predictive fit was more challenging. Additionally, many parameters such as capacitance and time-step in the model significantly changed the output. This is not surprising, as capacitance has a measurable effect on neuron electrophysiology, and as such, HH models should capture that as well. I found that because I had recorded capacitance values in my dataset, I did not necessarily need to hold capacitance constant in the model. This realization emphasized the utility of the modeling approach, which in my perspective, is to be used as a tool to bring the real IPs into a space where they can be quantified and represented: Meaning that the modeled conductances are a reflection of the state of the model (and its non-varying parameters) and not absolute biological values. This evokes caution when interpreting the modeled neurons and their differences within the conductance space. Below I provide two examples of this from my own journey of discovery and interpretation of Daou and Margoliash, 2020.

The first example is related to the interpretation of the results from their juvenile data. In their data, the within-bird similarity of HVC_X IPs seen in adults is absent in juvenile birds. All HVC_X modeled conductances from juvenile birds, instead, take up a common area in conductance space and show high within-bird variability. Compared to the adult space, however, the total juvenile conductance volume only takes up a fraction of the volume. From this, the interpretation that arose

suggested that over the course of development, juvenile HVC_X IPs clustered and migrated beyond the limits of the juvenile conductance space to some common, song learning depended, solution. This interpretation is valid given the approach, yet I believe that a different interpretation evaded observation as a result of the constraints of the HH model. Another paper by Ross et al., 2017, reported on IPs of multiple classes of HVC neurons at various developmental timepoints. Ross et al. used a similar modeling approach but also reported on features of the IPs evaluated directly from the voltage traces. These raw features included estimates for the membrane capacitance and membrane resistance. The membrane capacitance of HVC_X from juveniles during early learning (DPH ~50) was double that of their adult counterpart (after DPH 90). Now, consider the effect that capacitance has on the magnitude of modeled conductances in the HH model: As capacitance increases, larger ionic currents are necessary to produce an equivalent voltage response, meaning that for a model neuron with a 100 pF capacitance to have the same spike amplitude as a 50 pF neuron, it would need approximately twice the number of voltage gated sodium channels (max gNa in the model). Taking this into account, it is difficult to analyze the juvenile data in the same conductance space as the adult data, and instead suggests that if the capacitance had also varied in the model that the juvenile space would not be as restricted.

The second is related to a control experiment done in Daou and Margoliash, 2020, in which all synaptic activity was blocked to better estimate IPs without contamination from network activity. The observed evoked responses to injected currents in the synaptic blocking condition were more excitable when compared to the intact recordings. This increase in excitability was manifested in the model as a decrease in the SK channel conductance, which as I described above, has an inverse relationship with neuronal excitability. In this case, the SK conductance was unlikely to have changed. Thusly, they interpreted that blocking synaptic activity reduced tonic inhibition onto the neurons and resulted in the only solution the model could reflect, which was a lowering

of the SK currents. This is a plausible interpretation. Yet, a similar increase in excitability would be expected if there had been an increase in membrane resistance (Ohm's Law), which would result in a greater depolarized voltage. Such an increase in membrane resistance is expected from closing ligand gated channels at synapses, and as a such, the increase in excitability is ambiguous: The effects of membrane resistance and decreased inhibition on the cell cannot be separated.

These examples encapsulate the limitations of modeling generally (not specifically those of Daou and Margoliash, 2020) and the reasons I shifted away from a pure modeling approach to one that focused on the raw features of the electrophysiology with modeling as additional explorative tool. Hence, in this thesis, I limit my use of HH modeling to simulations of specific hypotheses of network architecture, and all other data chapters that address IPs focus on the raw data.

Following this approach, my bootstrap analysis above (firing frequency and sag ratio) supports the finding of within-bird IP uniformity of the HVC_X population (Daou and Margoliash, 2020). Furthermore, I wanted to address a possible concern that the within-bird IP similarity arose from features of the recordings on the day of the experiment. I evaluated this hypothesis by doing the same bootstrapping procedure on the holding current for each neuron. The holding current is the current injected to hold a neuron at –70 mV, which is related to the quality of the seal and break-in, as well as ion channels open at rest. The real within-bird variance of holding current fell within the 95% confident interval of the bootstrapped distribution. This suggests that recording quality, as reflected by holding current, does not explain uniformity of IPs within birds. Lastly, the mixed effect linear regression models also support the view that song learning plays a strong role in IP expression and that, at least in my data with my analysis, parentage does not have a statistically significant effect on firing frequency and sag ratio of HVC_X.

Activity dependent changes to excitability in vitro

The slow decrease of evoked firing frequency in my recordings was a concern over most of the data collection process, one that I tried to mitigate by limiting the analysis to the early portions of each whole-cell recording. This arose from conversations with Dan Margoliash and Arij Daou, who raised that such rapid rundown of spiking likely represented problems with the quality of the recordings. Given the experiments and data in this chapter, it seems more likely (but it could be related to both) that there is some effect of stimulation on ion channel conductances in the neuron and not recording quality (likely K^+ channels, given the hyperpolarization and appearance of an outward current at -70 mV). Whether such an effect is a result of the intracellular pipette solution lacking some critical molecule (like cyclic AMP), or whether it's a broader feature of HVC or bird neurons in general, remains to be explored.

If the observed decrease in excitability is indeed a biological phenomenon, however, it begs the question: what is its function? In vivo, when zebra finches sing, the HVC_X neurons hyperpolarize (below -90 mV) and fire sparsely. HVC sparse firing during singing is a canonical feature of the nucleus and even outside of singing HVC projection neurons are not tonically active. It is curious that after stimulation there seems to be a slight increase in evoked inward currents in HVC_X at -100 mV. One possibility is that this plasticity mechanism works to maintain sparse firing, while preserving rebound excitation in HVC_X neurons. This could be a useful feature during development, when the network is plastic and overexcitation may be more common. In this speculative view, activity-dependent intrinsic plasticity in HVC_X could prevent runaway oscillations in a nucleus with strong internal dynamics, which would not be a concern shared by the HVC_{RA} portion of the network because of the remarkably high spike thresholds.

HVC_X IPs are learned and related to temporal features song.

The differences in IPs between neuron classes in HVC are stark. Those differences are likely reflective of their functional properties in the network. HVC_{RA} are transient in their spiking and have high thresholds: features that make them well-suited for onset encoding and precise burst timing. In vivo, HVC_{RA} become significantly depolarized when the bird starts to sing, which facilitates bursting by bringing their RMP closer to their action potential thresholds.

We can learn from the intuition gained from this interpretation of the HVC_{RA} IPs, as they likely facilitate their in vivo function (since we don't yet know for certain). A similar perspective arises for HVC_X and raises a question about the role of the hyperpolarization seen in HVC_X in vivo when birds sing. This question was the initial motivation behind my focus on the rebound excitation of the HVC_X. The in vivo hyperpolarization, together with their ability to fire post-inhibitory rebound spikes, means that at least some component of their bursts during singing involves rebound excitation. Additionally, one of the curiosities that drives my thesis work is the mystery of the function of HVC_X neurons in the song system.

Because HVC has often been associated with timing (sometimes analogized to the conductor of song), and there is vigorous discussion of whether HVC projection neurons encode muscle gestures or time itself, focusing on temporal features of song seemed important. Identifying which aspects of time varying spectral features to analyze was a challenge. Because of that, the non-varying vocalizations made up harmonic frequencies caught my attention. In the gesture trajectory extrema model (GTE) of HVC (Amador et al., 2013), harmonic stacks contain no GTEs and therefore no muscle transitions. This means that the longest harmonic stacks represent the longest period without a new motor command, or without any spectral point of reference, and as such would constitute a significant challenge in temporal integration. To summarize this point in a simpler way: How does HVC know how long a harmonic stack should be, and when it needs to end?

Considering that in my dataset the longest harmonic stacks were upwards of 200ms, this is not a trivial task for the network, or individual HVC_X.

I found that the rebound excitability of HVC_X neurons was related to the total duration of the motif and the duration of the longest harmonic stack. In general, the longer the song, the more moments of low frequency modulation, and the more rebound excitation observed in HVC_X neurons. The correlations themselves are not perfect (they have a fair amount of noise). The region of short song duration (and short harmonic stacks) had particularly high variance for sag ratio and firing frequency, but as song durations increased there were fewer birds with low amounts of sag ratios or low firing frequencies. One possible explanation for this is that longer songs are limiting the IPs of HVC_X, while shorter songs are not as constraining. Strong evidence of the validity of this correlation was the increased rebound excitability of HVC_X from the 5 birds who learned a modified song (100 ms) compared to birds who sang an nearly identical song. Interestingly, the original stack included in the tutor song was 220 ms in duration, yet every bird shortened it to ~100 ms, an effect that merits further investigation through in vivo electrophysiological recordings in juvenile birds as they learn the modified song.

CHAPTER 3

MODELING HVC_X NEURONS NETWORK PROPERTIES

Introduction: A coordinated orchestra keeps time

Spike rebound excitation is a mechanism that integrates intrinsic properties of a neuron with network properties (the timing of release from inhibition). My results from Chapter 2 motivated a modeling effort to construct a network model of HVC that utilizes rebound excitation to capture the in vivo properties of HVC_X. The model assumes that HVC_X neurons integrate subthreshold activity over long intervals (> 100ms) while also being sensitive to sequences of song elements, giving rise to syllable–sequence dependent sparse bursting that has been observed in vivo for presumptive HVC_X neurons (see section on sequence selectivity of the introductory chapter). I hypothesize that Ih and rebound excitation are the intrinsic components of the mechanism that gives rise to sequence selectivity.

I conceptualized HVC_X as coincidence detectors of any two events, which define an interval (interval encoders). As also independently hypothesized by Margoliash in 1983, the first event depends on inhibition, and the second on excitation. In this view, an HVC_X neuron encodes the occurrence of two events: the first event is a release from inhibition which releases Ih as a depolarizing current (manifested as recovery from rebound in vitro), and the second is an excitatory synaptic event. Each HVC_X would have an integration window defined by the magnitude of rebound excitation, which we can visualize by looking at its rebound area (blue shaded region, Figure 3.1). The resulting curve determines a window in time when the first event and a second subthreshold excitatory one (green trace to the right of downward green arrow, Figure 3.1) can sum. If the events are sufficiently distant in time no suprathreshold spike occurs but if the events occur in close

temporal proximity, then they sum to produce an action potential (Figure 3.1, left and right panels, respectively). In this framework, neurons with different rebound excitability can have wide or narrow integration windows (Figure 3.2, example traces from two neurons in the left panel). We can investigate this integration window in vitro by varying the delay between release from hyperpolarizing current injection and subsequent small depolarizing current injection to generate a distribution of delays which produce action potentials (Figure 3.2, right panel).

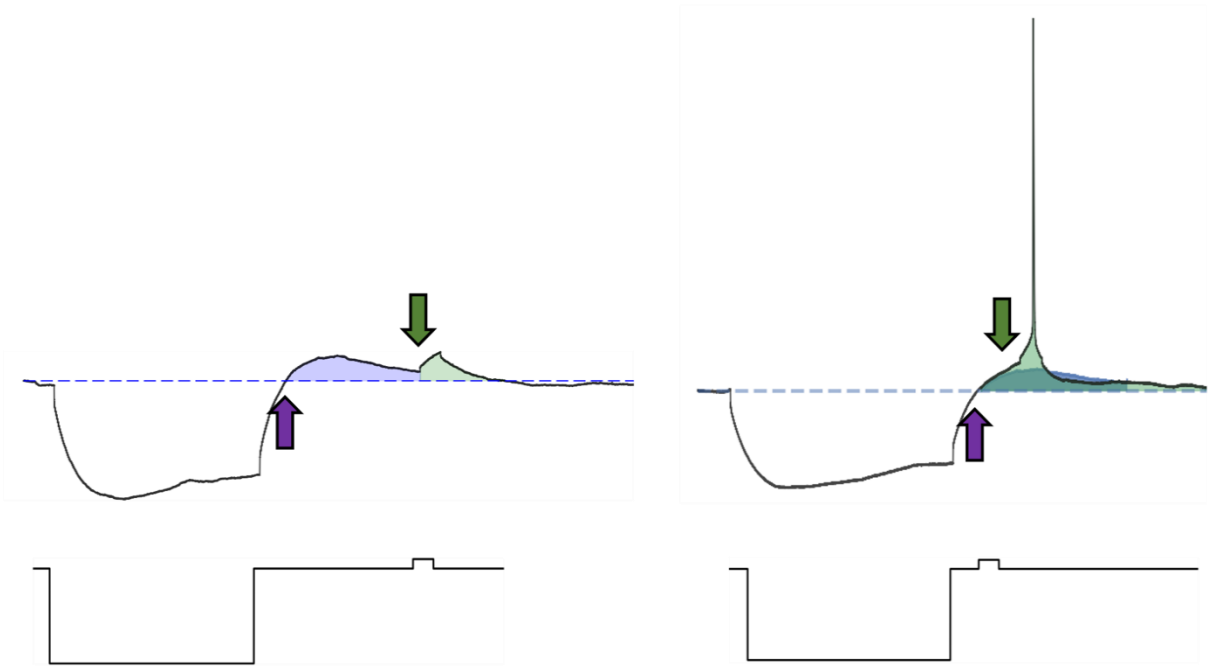

Figure 3.1. HVC$_X$ can function as coincidence detectors in vitro. Traces from a neuron that received a hyperpolarizing current followed by a small depolarizing current at various delays. Purple shows the moment where voltage passes above the pre-inhibition baseline. Green arrow shows the moment of depolarizing current injection. Left panel shows an example subthreshold response to both events (responses colored in the same way as the arrows). Right panel shows a suprathreshold response to a shorter delay.

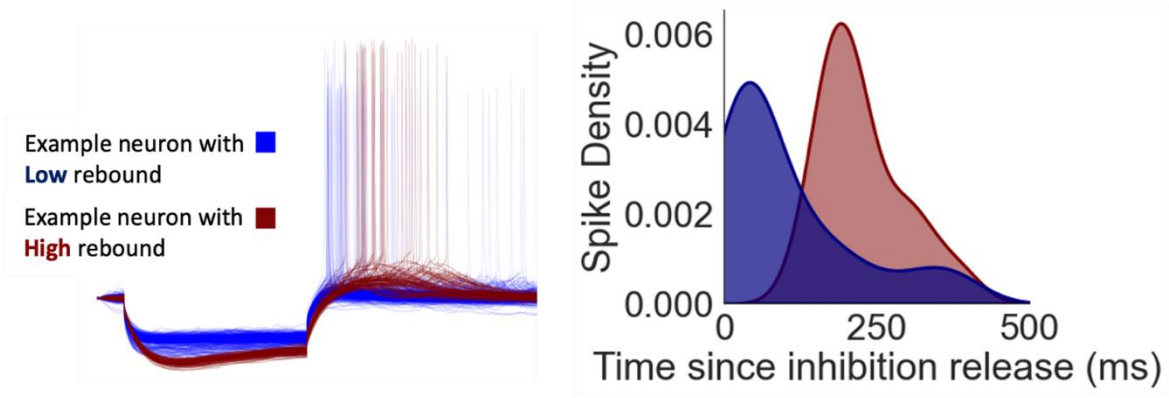

Figure 3.2. Rebound excitation shifts the range of integration. Traces from two HVC_X neurons that received the same protocol depicted in Figure 3.1. The blue neuron elicited low sag and rebound, while the red one elicited large sag and rebound. The right panel shows the distributions of delays that produced at least one spike for both neurons.

Modeling methods and results

I constructed a network where each cell is modeled as a Hodgkin-Huxley neuron with intrinsic and in vitro bursting properties representative of major HVC cell classes (HVC_{RA}, HVC_{int}, HVC_X). I used the HH model (Equations 1 and 2), where each ion current for each class of neurons was pharmacologically confirmed (Daou et al., 2013; Daou & Margoliash 2020). Additional differential equations for excitatory and inhibitory synapses were included to link HH modeled neurons in the model (AMPA, NMDA, $GABA_A$) (Park et al., 2014). HVC_X were modeled with modest values g_h (12 nS / 100 pF) and g_{SK} (7 nS / 100 pF), while HVC_{RA} had high g_{SK} (15 nS / 50 pF) to reflect their high spike threshold. HVC_{int} had modest g_h (3 nS) and either modest (orange trace, Figure 3.3, 2 nS) or low g_{SK} (yellow trace, Figure 3.3, 1 nS). Tonic interneurons (orange) varied in capacitance from 30 pF to 80 pF to add variance in spike timing, while phasic inter neurons (yellow) had a capacitance of 10 pF. An initial pass helped determine values of gH and synaptic strength that

produced coincidence detection in the model (in the same way as recorded neurons do in Figure 3.2).

In the model, HVC_X behave as interval detectors, and have two distinct responses to the onset and offset of said intervals. Below I describe how the first response, and underlying mechanism, relies on a tri-synaptic connection from an HVC_{RA} to an HVC_X, while the second (offset) response is a simple monosynaptic excitatory event. The tri-synaptic connection is implemented by connecting HVC_{RA} to a population of tonically active interneurons, connecting the first population of interneurons to a second population of interneurons, and connecting the second population of interneurons to HVC_X (Figure 3.3). The tonically active interneurons increase their firing rate at song onset. Using this basic structure described above, the model can produce a repolarization window (beginning at release of inhibition, purple arrow, Figure 3.3) whose shape, timing, and magnitude are related to the Ih current (blue shaded region and green bracket, Figure 3.3). The description in Figure 3.3 is foundational for the model and is built upon in later figures.

One constraint on network architecture was to implement different sub-threshold changes that occur during singing: depolarization for HVC_{RA}, and hyperpolarization for HVC_X. This was achieved by connecting every HVC_X to the population of tonically active GABAergic interneurons (orange tonic interneuron population, Figure 3.3). This increases the interneuron firing rate at song onset, hyperpolarizing the HVC_X. I coded the increased background firing of the tonic interneurons as an increased square depolarizing current that spanned the modeled-motif duration. Similarly, an increase in input current was given to HVC_{RA} to simulate the depolarization seen at song onset. Importantly, these constraints serve not only satisfy the in vivo network conditions during singing, but also define the mechanism of coincidence detection within HVC_X which I describe below. The input current into this tonic interneuron included stochastic noise to make the traces less

deterministic and appear biological. Only the tonic interneuron included noise, however, because the additional noise also increased computational time.

The circuitry described so far represents the base components that reproduce the fundamental network environment in which HVC_X neurons burst. The tonic firing interneuron (orange neuron, Figure 3.3) causes the necessary hyperpolarization of the HVC_X neuron, the phasic interneuron (yellow trace, Figure 3.3) then causes a gap in that hyperpolarization, which is a critical component of the rebound excitation mechanism: the two interneuron classes form a tri-synaptic connection from an HVC_{RA} (in this case) and the HVC_X and define the detection of first event of an interval. In the case of Figure 3.3, the first event is the spike of the HVC_{RA}. Using this basic structure, the model can produce a repolarization window (beginning at release of inhibition, purple arrow, Figure 3.3) whose shape, timing, and magnitude are related to the Ih current (blue shaded region and green bracket, Figure 3.3). The description in Figure 3.3 is foundational for the model and is built upon in later figures.

$$\frac{dV}{dt} = \frac{(-I_{Na} - I_K - I_{Ca-L} - I_{Ca-T} - I_{SK} - I_h - I_A - I_L + I_{inj(t)})}{C_m}$$

Equation 1. Hodgkin-Huxley single compartment neuron, adapted from Daou et al. 2013. Currents included: Voltage gated sodium (I_{Na}), Voltage gated potassium (I_K), L-type calcium channel ($I_{Ca\text{-}L}$), low threshold activated T type calcium channel ($I_{Ca\text{-}T}$), small conductance calcium dependent potassium channel (I_{SK}), hyperpolarization activated cyclic nucleotide channel (I_h), A-type potassium channel (I_A), a leak current (I_L) and any additional injected current provided, typically to model experimental current injections (I_{inj}).

$$I_{Na} = g_{Na} m^3{}_\infty(V) h (V - V_{Na})$$

Equation 2. Example of ionic current equation for voltage gated sodium channel. The equation includes terms for maximal channel conductance (g_{Na}), activation parameter (m), neuron voltage (V), inactivation parameter (h), and the driving force as the neuron voltage (V) minus the reversal potential of the ion (V_{Na})

$$\frac{ds_{AMPA}}{dt} = a_{rAMPA}[T](1 - s_{AMPA}) - a_{dAMPA}s_{AMPA}$$

$$I_{AMPA} = g_{AMPA}s_{AMPA}(V - V_{AMPA})$$

$$T(V_{pre}) = \frac{T_{max}}{1 + \exp\left(\frac{-(V_{pre} - V_T)}{K_p}\right)}$$

Equations 3-5. Example of the set of equations used to model ligand gated ion channels. Within the model, the equations used included AMPA, NMDA, and $GABA_A$ and all depend on the pre-synaptic voltage. Tmax represents the total maximum transmission which is related to the presynaptic voltage (V_{pre}) and the voltage for synaptic release (VT). The current provided by the receptor (I_{AMPA}) depends on the maximal conductance (g_{AMPA}) how much release there is at the synapse (S_{AMPA}) and the driving force, modeled as the neuron's voltage minus the reversal potential of the channel ($V-V_{AMPA}$). The amount of synaptic transmission is determnined by T. Additional constants can be found along with the code on the Margoliash lab github page.

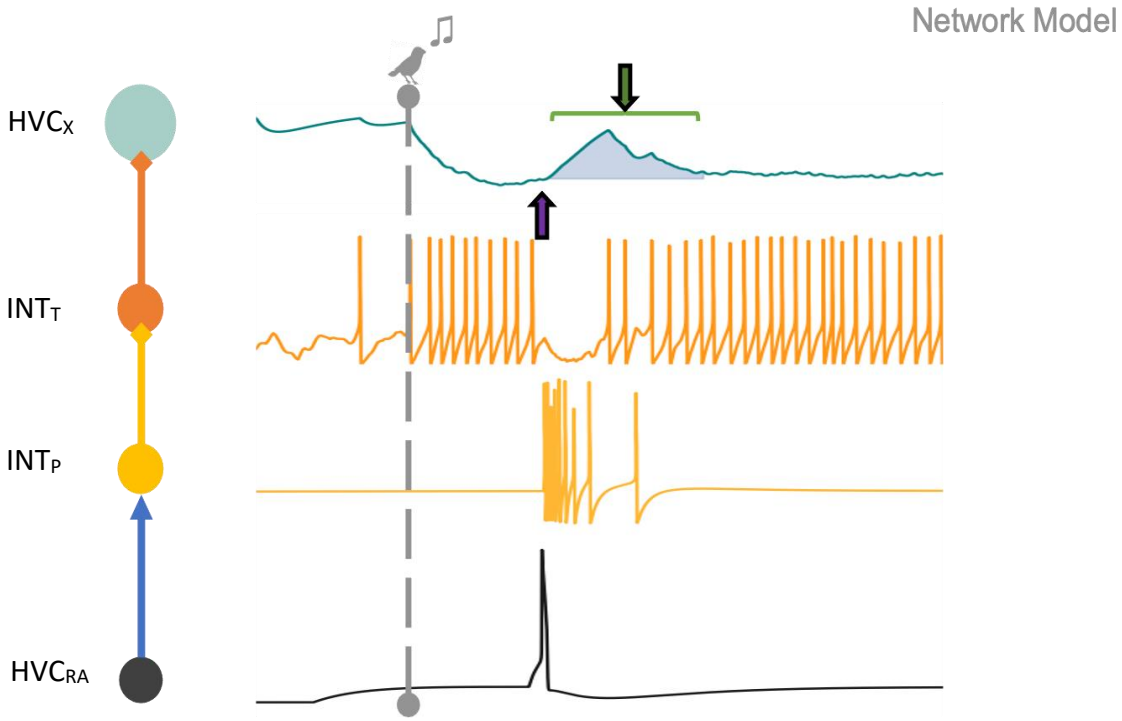

Figure 3.3. The fundamental circuit module of my Hodgkin-Huxley network model. Illustration of the model's synaptic architecture (every trace arises from a Hodgkin-Huxley model): Synaptic connections progress unidirectionally from bottom to top. The first event is a spike within an HVC_{RA} neuron (black, bottom panel), which forms an excitatory synapse (blue arrow) onto a first interneuron population (yellow). The yellow interneuron forms an inhibitory connection (yellow, square arrowhead) onto a second interneuron (orange). The orange interneuron forms an inhibitory synapse with the HVC_X neuron (green, top panel). This synaptic organization gives rise to a momentary release from inhibition (blue shaded region) in the HVCX neuron starting at the time of the spike in the HVC_{RA} neuron (black trace, and purple arrow in top trace). Within this window of time where the neuron is relatively more depolarized (green bracket and arrow) additional inputs can more easily give rise to one or a burst of spikes.

Given these constraints, I first investigated model architectures where bursts from a backbone of HVC_{RA} initiate a process generating bursts in HVC_X through tri-synaptic inhibitory connections, as described in Figure 3.3, and can be incorporated into a larger network comprising multiple neurons (Figure 3.4, left side). A tri-synaptic inhibitory connection exists between an HVC_{RA} (RA1) and the tonic interneuron synapsing onto an HVC_X (X1). Then, another RA projector that bursts later in time (RA2) also connects to X1 via an excitatory synapse. This basic module produces a release from inhibition at one timepoint (RA1) followed by excitation at another

timepoint (RA2) resulting in X1 spiking only if RA1 is followed by RA2 at a certain delay. The duration and shape of the permissive window created by the gap in inhibition is determined in part by the magnitude of Ih and the return of inhibition (HVC_X model trace in top panel of Figure 3.3). A module consists of one tri-synaptic inhibitory connection and a monosynaptic excitatory connection onto the same HVC_X. These can originate from HVC_{RA} neurons, but also from other HVC_X neurons wired as described above (Figure 3.4, solid black box). This results in a series of HVC_X with nested dependencies that encode increasingly longer intervals with sequence specificity. For example, neuron 4 in Figure 3.4, encodes intervals 1, 2, and 3 (also shown as the pink interval numbered 4 within the solid black box in Figure 3.4). Finally, I chose timepoints that create intervals within a two-syllable segment of song and wired them in the modular fashion described here and is depicted in the right half of figure 3.4. The resulting network's behavior includes a neuron which only spikes after the correct sequence of song associated HVC_{RA} bursts, with their appropriate timing. Figure 3.5 shows three such HVC_X neurons (green traces) and their corresponding-colored intervals from Figure 3.4. The behavior of these three neurons relies on post-inhibitory rebound.

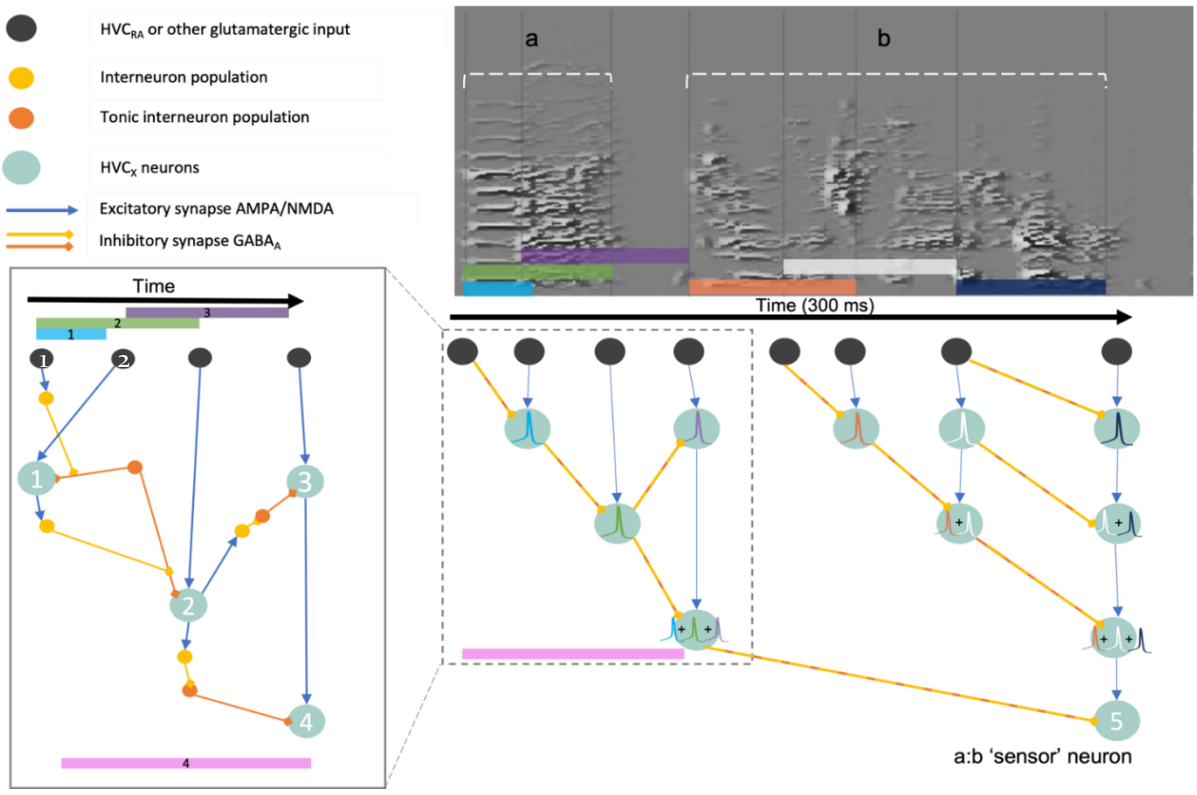

Figure 3.4. A network model uses intrinsic rebound excitation to detect sequences. Using the basic module from figure 3.3, I wire a backbone sequence of excitatory neurons (black) that burst at relative time points chosen from a bird's song (spectrogram in the top right, with vertical lines that mark timepoints in song). Intervals defined by timing differences in backbone bursts are depicted by colored rectangles. A three internal section of the model is shown on the left (solid black box). A simplified view of this is shown in the dashed box on the right.

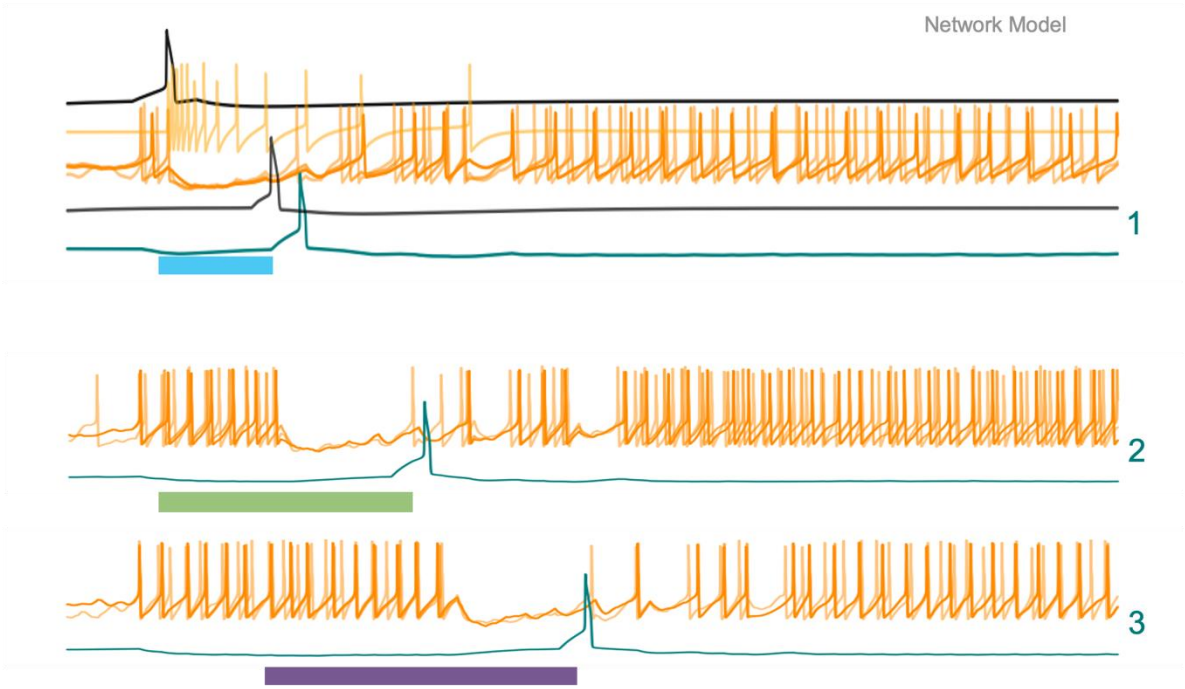

Figure 3.5. Example traces of sequence selective model neurons. Modeled traces from neurons in network depicted in Figure 3.4, which participate in the representation of intervals 1 (teal), 2 (green) and 3 (purple).

Predictions of the model

The architecture of the model was developed with a view of the firing properties of HVC neurons, both in vitro and in vivo, and with a goal to embracing the integration properties of HVC_X neurons to implement interval detection. Because the behavior of the model arises from these many constraints, it is important to point out which aspects arise directly from model fitting, and which are unanticipated ways in which the model fits existing data and makes predictions.

Only the coincidence detection, dependence on rebound excitation and song-induced hyperpolarization of HVC_X were used to constrain the model. As long as the modeled HVC_X encoded an onset and offset utilizing the mechanism described above, it was considered successful. Additional structure, like the nested dependencies, arose from evaluations of this basic mechanism. This then leaves the unexpected ways in which the model fits existing data.

For one, the nested structure meant that neurons that encode long intervals would inherit variations in timing from previous neurons, and therefore suggests that neurons that are selective to long song intervals would tolerate more temporal variation and integrate further out in time. This behavior was seen in Margoliash 1983, Lewicki 1995 and 1996, and Margoliash and Fortune, 1992. For example, consecutive whistles of white crowned sparrows could still be detected by HVC neurons as the gap between them increased (though decreasing in detectability) (Margoliash, 1893). This prediction could be tested with song playback experiments where the gap between two syllables is increased until neurons sensitive to their playback no longer detect the sequence. My model predicts that birds with longer songs should be able to detect sequences with longer gaps.

Second, as I elaborate on in the general discussion, the modular structure of the model means that each neuron can encode multiple intervals, which can give rise to burst structure in the

network activity that relates limits in the inter-burst intervals to temporal features of song (i.e., the duration of the motif, or longest harmonic stacks).

Related to this second point, my model only shows single bursting neurons and hence the interneuron populations within it behave as perfectly tonic (with one gap) or perfectly phasic. In vivo, no interneuron behaves this way. Yet if each HVC_X encodes multiple non-overlapping intervals, then you could get interneuron bursting that is in vivo-like, with multiple gaps and bursts within a single interneuron. From this, the model predicts that the gaps in interneuron bursting are related to the interval durations encoded by HVC_X and relate to temporal features of song. This hypothesis is testable with existing datasets and remains to be addressed.

Finally, the model I present in Figure 3.4 (with only single bursting neurons) predicts that neurons that encode long intervals are far less common than short interval encoding neurons. This is actually inconsistent with experimental data which shows that many (most) HVC_X neurons are sensitive to large portions of song, and the most common number of bursts of HVC_X neurons is one, which in my model would predict to be short. I address this point in the general discussion, where I describe how multiple bursts are incorporated into the model.

Discussion

The model behaves as designed, and so it is not surprising that it succeeds in producing neurons that encode sequences (that was one constraint). Yet, the model does this while also reproducing many of the known network properties of HVC_X, which adds to its biological plausibility. Even so, modeling approaches like this one include assumptions and shortcuts to approximate biology, and as such only serve to generate hypotheses to then test experimentally. One possible outcome of the modeling approach could have been a failure to reproduce the coincidence detection behavior with rebound excitation. In that case, I would have pursued a

different mechanism and it would have separated this chapter from Chapter 2, ideologically. Instead, the model links the IPs result from Chapter 2 and acts as a hypothesis, predicting a tri-synaptic connection between neurons who burst early in a syllable with neurons who burst later or in the next syllable. In Chapter 5, I describe experiments that would provide the necessary behavioral snapshot within HVC network architecture to test this prediction.

Next, I would like to address two caveats in my model. First, the generation of the song induced network environment, i.e., the hyperpolarization of HVC_X, and depolarization of HVC_{RA} and HVC_{int}: I found that the network architecture of the model could support a less artificial mechanism for generating these subthreshold environments by connecting preceding HVC_{RA} neurons to the HVC_{int} tonic population, such that each HVC_{RA} burst would cause depolarization in the interneurons and thus a hyperpolarization of the HVC_X. This, however, required 3 additional differential equations per modeled HVC_{RA} and added approximately 20 hours per simulation. To minimize the runtime, I used the shorthand described above and simply modeled a square pulse of depolarization onto the HVC_{RA} and tonic interneuron populations which defined song onset.

Second, for a similar reason, I only ran portions of the network at a time, which constituted the basic module. Meaning, once a part of the simulation that ended at an HVC_X modeled neuron, I would stop the simulation and run the next portion using the spike times of the previous section as input times. This approach saved hundreds of computation hours, which would be required to run the network of 44 neurons (~440 differential equations, with added stochastic noise, which are solved simultaneously at each timepoint). Below, in the general discussion chapter, I describe additional HVC burst structure replicated by the model which was unexpected and not a result of specifically restricting the underlying mechanism.

Finally, I would like to simply list all that the model accomplishes: it incorporates IPs (and their uniformity within HVC), utilizes HVC_X rebound excitation, achieves long integration times,

replicates the network subthreshold conditions, achieves sequence selectivity, and explains how the longest harmonic stack in a song can be related to rebound excitation in HVC_X (because width of integration windows are related to Ih).

CHAPTER 4

REPLICATION OF SONGBIRD METRONOMICS

Introduction

Coordinated behaviors require precise temporal representation and prediction across multiple systems and organisms. This challenge closely interacts with ideas of rhythm and entrainment, which are crucial for all social behaviors. While feedback is well understood to be necessary for assessment error and behavioral adjustment behaviors, we can also appreciate that errors can rely on prediction. This reliance on feedback, which is often delayed in time, and its integration on a moment-by-moment basis, raises an interesting challenge for neural circuits that are involved in social behaviors, especially those that include vocal production. Song production and perception of songbirds provides a convenient model system to study how neural circuits overcome such challenges to produce highly precise coordinated behaviors, as with call duetting and song-call interactions. Importantly, previous results suggest that internal temporal structure in these behaviors exists and may provide insight into potential solutions to self-motor-output coordination with sensory feedback, and with the behavior of other individuals.

Replication is a critical, yet often underappreciated part of doing science. When we consolidate knowledge to produce models of systems and test assumptions, we incorporate work other than our own and find ourselves first validating methods and results. These efforts regularly go unreported or unappreciated. I found myself in such a position when interpreting and discussing possible implications of prior work from the study of birdsong.

The focus of this chapter is to replicate the findings from Norton and Scharff, 2016 (Guess and Test, or GAT method). Their results showed that the isochronous pulse rate (in Hertz) that

best matched syllable onset times of a particular male zebra finch's song varied across individual songs. Importantly, the generated 'best' pulse rate's additional pulses (pulse times that occur outside syllable onsets used to determine the best pulse rate) aligned with other salient moments in song. This result caught my interest as internal structure in song has strong implications for precise motor-control in neural circuits and in vocal coordination during social interactions. Temporal structure that spans the entire motif could represent global features of song and tie together results about the uniformity of intrinsic neuronal excitability in HVC (Daou and Margoliash, 2020).

Here, I reproduce findings showing adherence to an isochronous pulse in male zebra finch song and expand on the discussion of the results. Additionally, I describe results showing structure in features of duration within song of male zebra finches.

Methods

Syllable onset times were used to define timepoints of interest, which the algorithm then matched by creating isochronous pulse rates (timepoints spaced equally in time) and finding the rate that minimized the root mean squared error (RMSE). The total range of rates tested was between 1 and 100 Hz, separated by 0.01 Hz (9900 total possible pulse rates).

A random array of numbers whose range extended up to the maximum timepoint of the onsets provided (last syllable onset) was then generated. Any array that included fewer numbers than the number of true syllable onsets was discarded. Each remaining pulse rate was then phase shifted by 1 ms until the pulses were 270 degrees out of phase and then the RMSE was calculated for each (a maximum of 819,100 possible combinations). The RMSE value was multiplied by the pulse rate to punish high pulse rates with a higher likelihood of finding matches. The code for this

can be found in the Margoliash Lab Github page (GAT replication). These methods were adapted from, and intend to duplicate, the descriptions in Norton and Scharff, 2016.

Replication

The output of the algorithm returns a single pulse rate for which some but not all of its pulse times fit the syllable onset times with the smallest RMSE. An example of this for one song is shown in figure 4.1, where the red pulses show the syllable onset times, the blue pulses show the timepoints provided by the algorithm, and the black pulses underneath represent all of the pulses for the best pulse rate, in this case 9.83 Hz. Qualitatively, some of these extra pulses happen to fall at spectral transition points of the song (black dashed lines). The RMSE values by pulse rate and phase shift are shown in figure 4.2. These are the fundamental outputs reported in Norton and Scharff, 2016.

Discussion

Scientific works that aim to replicate go underreported, and yet we all rely on them in our own work to validate or push forward new thinking. I as well as others in the Margoliash lab found ourselves in such a position when discussing the results from Norton and Scharff, 2016. For example, Andrew Savoy expressed interest in the internal rhythm of song and how its perception may contribute to female choice. Together with Savoy, I ventured to replicate the 'metronomics' method described in Norton and Scharff, 2016, with nothing more than their descriptions in their methods. For my own work, I think this methodology may have provided additional insight, given that I also found internal structure within the motif (i.e., long songs tended to have long stacks). Future analyses using GAT may identify additional intervals (beyond the longest stack) within song that

relate to rebound excitation of HVC_X. Ultimately, I did not finish pursuing my interests using the GAT tool but others in the Margoliash lab may.

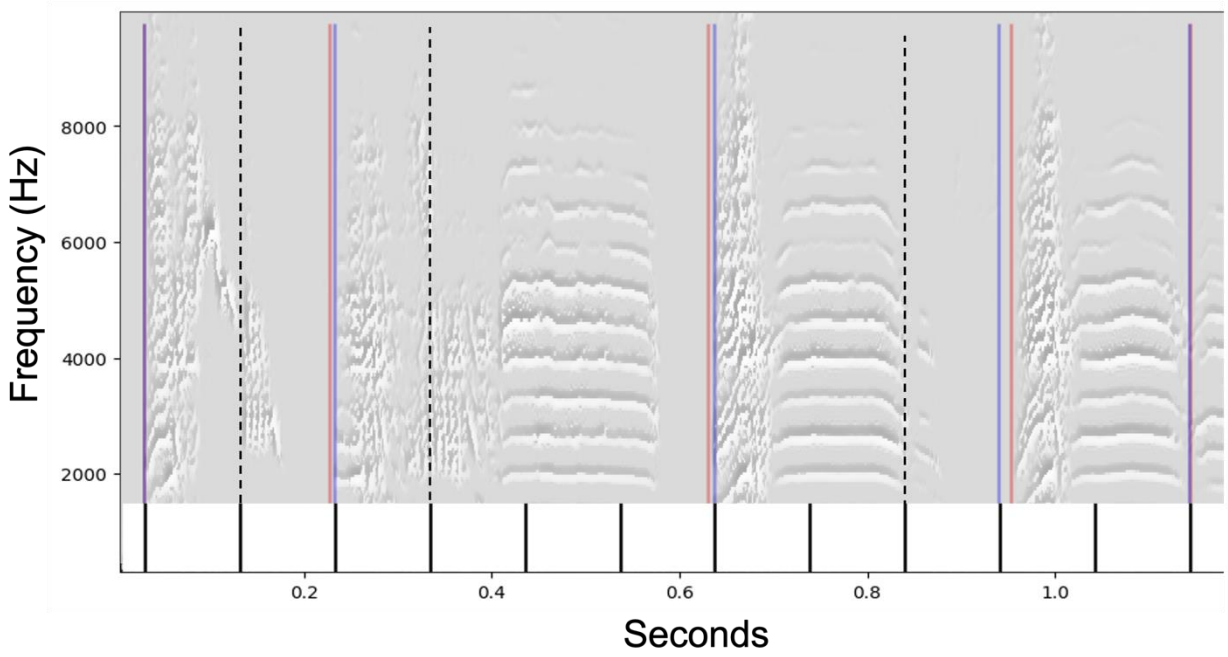

Figure 4.1. Replication of the guess and test method (GAT). An example spectrogram from which onset timepoints (red lines) were used to run the GAT algorithm. The resulting best pulse times are shown in blue, and the rest of the pulses are shown in black as tick marks below the spectrogram. Dotted lines are additional pulse times which qualitatively corresponded to spectral transitions in the song.

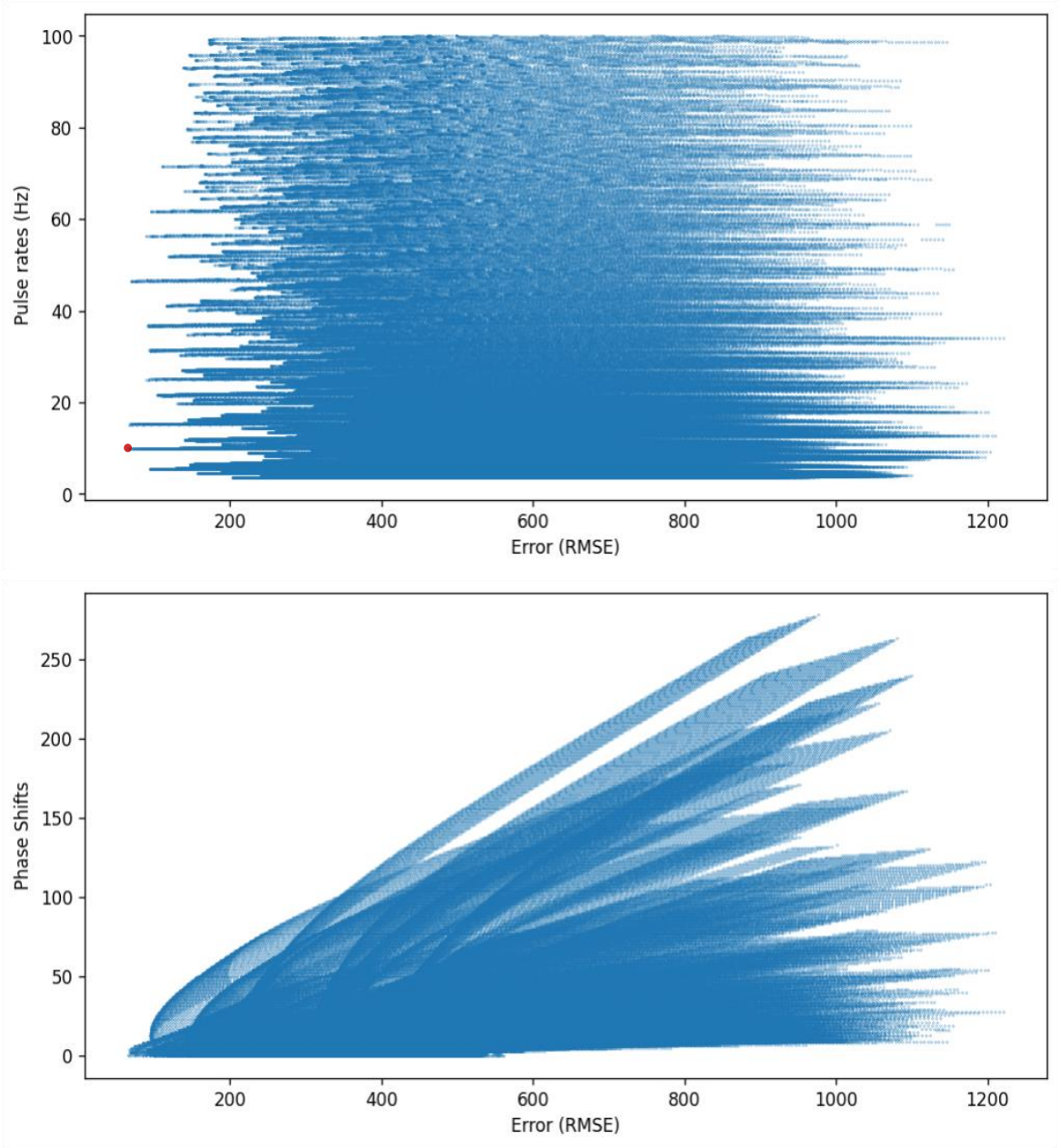

Figure 4.2. Root mean squared error summary plots for one song. All pulse rates searched by the GAT method (top panel) as well as phase shifts in degrees (bottom panel) with their corresponding RMSEs. The best solution (least RMSE) in marked by a red circle (top panel).

CHAPTER 5

SEEING SONG AND OTHER FUTURE DIRECTIONS

Introduction

Central to neuroscience is the pursuit of a rich understanding of the brain at many levels of analysis and time scales, then combine them into a comprehensive model of structure, function, and behavior. This pursuit has greatly benefited from focusing on model organisms that champion profound natural abilities. Zebra finches learn their song during a sensorimotor critical period requiring practice and error correction that results in highly stereotyped song renditions (vary by less than 5% in timing and spectral similarity) made up of sequential syllables, which provides a convenient model behavior to study. In the end of my graduate studies, I proposed and began work on constructing a network model that will tie cellular functional properties and network structure directly to individualized behavior. The novelty of my proposal was the aim to label syllable-specific neurons in HVC for multiple syllables during singing. In addition, I would perform extracellular recordings in vivo to characterize network activity, and patch in vitro to characterize membrane properties and connectivity between labeled neurons.

To label multiple populations of neurons with temporal resolution of terns of milliseconds, I proposed to use the neural activity reporter CaMPARI2. CaMPARI2 fluoresces green at baseline and in the presence of UV light and high levels of calcium (proxy for activation) photoconverts to red. The activity dependent conversion can last weeks, and allows for selecting which moments of behavior to label with concomitant illumination with UV light. Thus, the red-green ratio of labeled neurons is a readout of activation, e.g., a neuron that fires 100 UV-illuminated bursts should have twice the red:green ratio of a neuron that received only 50 UV paired bursts.

Methods

I tested these ideas in neurons in brain slices where I observed gradual increases in red:green ratios with successive combined stimulations with current and UV light. I was not successful in photoconverting neurons in vivo in sleeping birds during acute experiments. During those experiments, I played birds' song (BOS) to them while driving UV illumination in HVC via an optic cannula with a diffuser tip and simultaneously recording extracellularly from HVC (Figure 5.1).

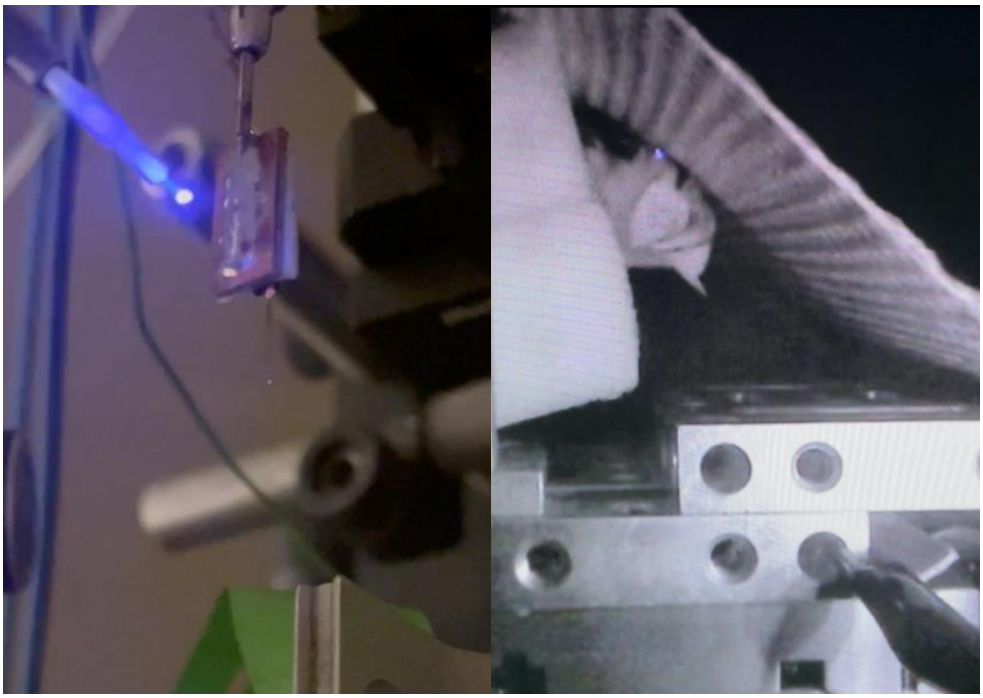

Figure 5.1. Setup for CaMPARI2 photoconversion during song playback. On the left is a picture of the setup without a bird attached, and on the right one of a sleeping bird during an experiment.

Results

One major component of this proposal was the use of viral tools. In the latter portion of my PhD, I piloted experiments using viruses to express eGFP for tracing (Figure 5.2, left panel),

GCaMP6f for calcium imaging, and the activity reporter CaMPARI2 (mentioned here). I was able to get good expression of CaMPARI2 within nucleus HVC after waiting 4-6 weeks (Figure 5.2, right panel). I then patched a small number of green fluorescing cells in-vitro and stimulated them to fire bursts that coincided with UV light to partly convert them to red (one example in Figure 5.3). The photoconvertion I observed in slice was gradual and related to the number of stimulations.

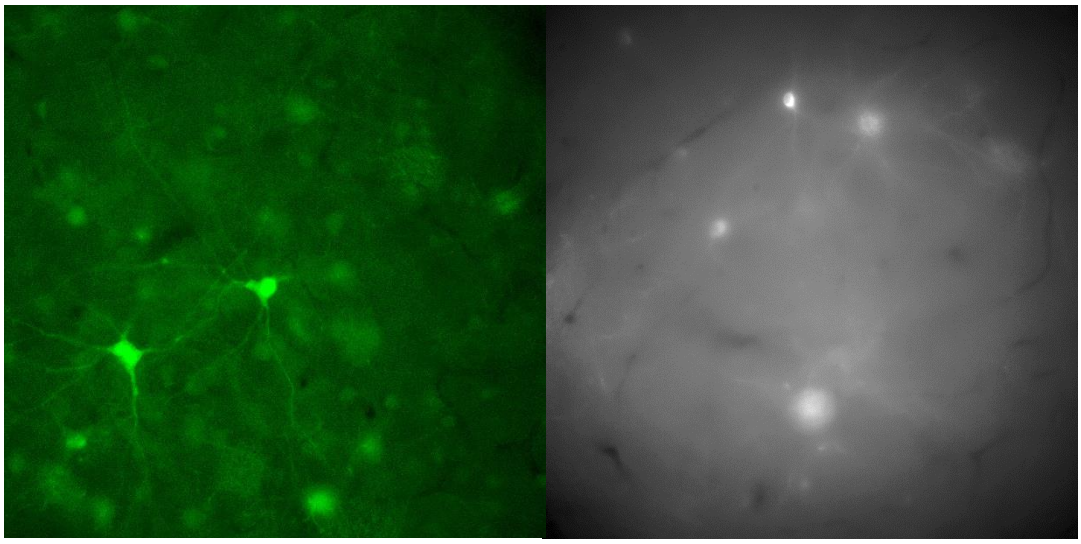

Figure 5.2. Examples of viral expression. A picture of HVC neurons expressing eGFP (green, left panel), and another of HVC neurons expressing CaMPARI2 (greyscale, right panel).

Though I was unable to achieve in vivo CaMPARI2 photoconversion, in the process of performing experiments in a sleeping bird, I noticed interesting structure in the local field potential (LFP) which predicted the occurrence of successful BOS responses in HVC. I saw this structure in the same bird in two separate experiments and used the observation to limit UV illumination only to trials where BOS response was expected (three or more large slow deflections in the unfiltered

extracellular traces). I did this by manually unplugging the cable that delivered the TTL pulse to the LED driver while watching the LFP to predict trials. Out of the 25 trials where the LED was active, only 2 failed.

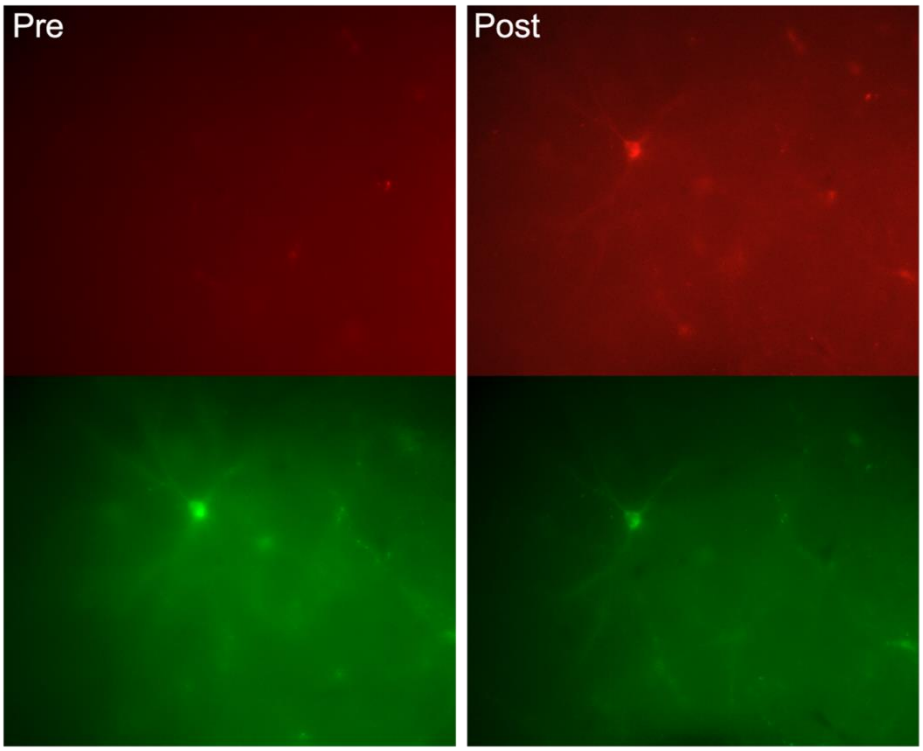

Figure 5.3. In vitro CaMPARI2 photoconversion. Red and green signal from one neuron expressing CaMPARI2 before (left column) and after (right column) 2 minutes of electrical and UV light stimulation in vitro.

Discussion

Studying how songbirds produce songs has provided significant insights into how specialized brain areas produce precisely stereotyped behavior that remains stable over a lifetime. However, analyses of the relationship of networks of neurons to behavior in the song system have

largely focused on characterizing circuit structure averaged across many individuals or over entire songs. While valuable, such data can miss the contributions of individual variability on network structure. I believe that the birdsong community, especially those who study singing in zebra finches, are now at a point where enough is known about the overall architecture of the song system to focus primarily on behaviorally relevant microcircuits. For example, experiments that leverage calcium imaging to identify circuit motifs for different syllables, activity dependent labeling, or optogenetic approaches, are likely to provide the next great strides in this system. Many of the current outstanding questions in the study of motor control in zebra finches require a shift toward studying sub-circuitry at behaviorally relevant timescales. Which neurons within HVC receive inputs from thalamic nucleus Uva? How does activity propagate through HVC_{RA} neurons during syllable transitions and how do they interact with HVC_X neurons that participate in the same or different syllables? These are the kinds of questions that a tool like CaMPARI2 helps address. Particularly relevant to this thesis, are experiments that can address the network model proposed in Chapter 3. Currently, the proposed connections between classes of neurons have been shown to exist (Monney and Prather, 2005), but that alone is insufficient evidence in the support of my coincidence detection model. To test the existence of the network architecture from Chapter 3, we would need to first label neurons at two timepoints during singing and then look for the specific proposed microcircuit in this context. Specifically, whether neurons who burst earlier in song tend to form disynaptic inhibitory connections with HVC_X neurons who burst later in song, while HVC_X neurons tend to receive monosynaptic excitatory connections from neurons who burst at the same time during song. Using CaMPARI2 to label specific neural ensembles, would provide the tool required to test this specific hypothesis.

CHAPTER 6

GENERAL DISCUSSION

The first sets of experiments to describe short-term (Stevens and Wang, 1995) and long-term plasticity (Bliss and Collingridge, 1993) at synapses were done in brain slices (facilitation and depression). In the same way, the fundamental mechanisms of intrinsic plasticity, i.e., plasticity of functional properties that exclude synapses, have been investigated in vitro (Daoudal and Debanne, 2003; Zhang and Linden, 2003. Much of the insight gained from in vitro work arises from manipulations and experiences during behavior. More recent reports have started to probe intrinsic plasticity in vivo (Mahon and Charpier, 2012) and are providing a more comprehensive view of neuronal function that incorporates plasticity at synapses, dendrites, and the whole neuron: a neuron centric view (Titley et al.., 2017).

Neuronal excitability is plastic within a large range of properties and is modulated by an equally diverse set of molecular pathways. Thus, when attempting to model the role for a particular cell-type within a network, as well as its fundamental IPs, one also needs to understand the parameters in which the IPs are plastic. We can appreciate this view from an example from the basolateral amygdala in rats, where positive and aversive stimuli were associated with an increase and decrease in intrinsic excitability of pyramidal neurons respectively (Motanis, et al.., 2014). This kind of relationship reflects the specific organization of the basolateral amygdala (BLA), such that relative firing probabilities of pyramidal neurons encode the valence of a stimulus. We can, however, imagine different rules of plasticity in which the inverse relationship exists. For example, what if instead of BLA pyramidal neurons changing their excitability, it was the interneurons? Would the relationship be inverted in them such that the interneurons decreased their excitability

to encode positive stimuli? From these questions we can see that the internal rules governing how excitability changes are also important when modeling the role of a neuron in the larger context of networks and behavior.

A conductor is not a metronome

The central focus of my graduate studies has been on the fundamental cellular mechanisms that underlie learning, memory, and information processing in neural networks. A practical implication of this is that if we were to construct a realistic simulation of a brain, it is insufficient to model the circuit map (or connectome). We also need to simulate the synaptic rules and firing properties within the network. The physiological rules of brain function extend beyond the twentieth century's ideas of synaptic transmission and structural connections. Since the time of Cajal, neuroscience has tended to focus largely on learning mechanisms at the level of synapses. Yet, neural communication depends fundamentally on the joint behavior of proteins and other electrophysiological properties of cellular membranes. Collectively, network architecture, synapse diversity, and intrinsic properties give rise to behavior and cognition, and thus deserve equal appreciation and scrutiny from neuroscientists. One implication from the importance of intrinsic properties is their effect on spike timing, which is a critical element of all complex behavior.

Summary and Interpretation of results

I replicated results showing that properties of intrinsic excitability (IPs) of a subclass of neurons (HVC_X) in premotor nucleus of zebra finches are more similar within an individual animal than across animals. The IPs of HVC_X are related to the song of an individual bird. I then expanded on this relationship and showed that temporal and not spectral features of song are linked to

rebound excitability of HVC_X. Interestingly, when I chose preliminary song features to investigate, I happened to choose continuous spectrally unchanging vocalizations with harmonic components. I chose these because they were the only parts of song without spectral points of reference over long periods of time. Yet, almost certainly, none of the neurons that I recorded from were involved in encoding of the harmonic stacks. These harmonic stacks later turned out to reflect global features of song timing. This raises a question, and a hint, about the structure that governs uniformity of IPs: Why do all HVC_X have similar IPs? On its own, it is an unexpected result, but the IP uniformity also predicts a common constraint on the network, independent of challenges that may arise from individual syllable differences within the song.

One potential global constraint (one that affects all neurons in HVC) that relates to harmonic stacks, is the challenge of temporal integration. Taking the perspective that events that occur far apart in time are more difficult to integrate than those that occur closer together, we can then interpret my results to mean that rebound excitation may be involved in temporal integration. This perspective also helps explain another of my results which demonstrates a link between the duration of the longest harmonic stack with the duration of the rest of the song, suggesting that there is internal structure within the motif. This agrees with the previous results showing metronomic structure in the motif (Norton and Scharff, 2016). Pursuing this idea, I modeled what would happen to spike timing in a case where IPs were randomly distributed across a population that received identical inputs. I then did the same for a population of neurons with uniform IPs (Figure 6.1). The result showed that holding all else constant, uniform IPs provide precision of spike timing in a population of neurons. Varying the range of possible IPs of a group of neurons by 45% increased the ambiguity in spike time of the population to a 100 ms window (red line, Figure 6.1).

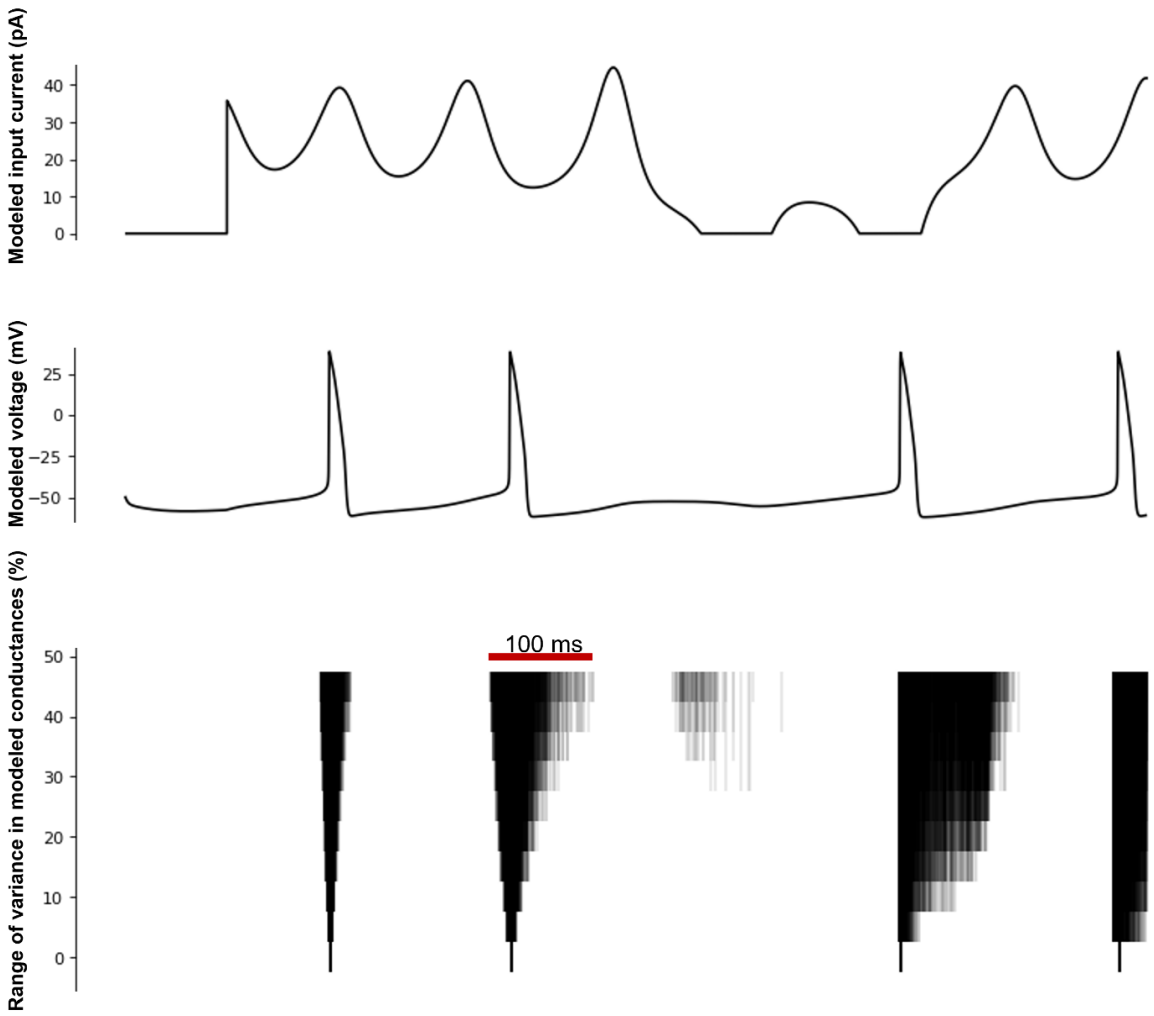

Figure 6.1. Uniformity of intrinsic properties promotes precision in population spike timing. Model neurons receiving identical stimuli (top panel), produce different number of spikes with varying spike times. The middle panel shows an example voltage trace for one such neuron. The bottom panel shows all spike times from 500 neurons per row, where each row is increasing the variance of five conductance (gh, gNa, gSK, gK, gCa-T) values in the Hodgkin-Huxley model among all neurons by 5% per row.

My results provide a framework within the song system for the well-established idea that the premotor projection to the basal ganglia conveys useful information for assessing errors. VTA and HVC inputs converge in the basal ganglia and are critical for song learning and for regulation based on feedback. However, the birdsong literature does not yet have wide agreement on a hypothesis about the information conveyed through the premotor-basal-ganglia projection, or how it is useful for learning. Here I used my results to construct such a framework. My model acts as a hypothesis, providing a biologically plausible mechanism to address HVC_X neurons' well-documented ability to integrate over long periods of time while maintaining selectivity to the sequence of inputs, while also incorporating results of IP uniformity and rebound excitation.

We know that HVC projection neuron bursts are precisely time-locked to behavior and are sensitive to relative timing changes of the bird's own song (BOS). In white-crowned sparrows, HVC neurons (likely HVC_X, though it was not known at the time) selectively burst when a sequence of syllables is played back to an anesthetized bird. This ability for the neurons to detect the sequence wanes as the gap between syllables is increased but does not become abolished until the gap duration is in the hundreds of milliseconds. Similarly, in Zebra finches, HVC_X detect specific sequences of BOS playback. Some neurons respond to specific syllables in isolation, others require multiple syllables, while many only burst to long portions of BOS (Margoliash and Fortune, 1992; Lewicki and Konishi, 1995 and 1996).

Experiments in vivo shed some light into the mechanisms underlying this selectivity. Sharp electrode recordings showed that the selective response expresses itself intracellularly as a hyperpolarization caused by the first segment followed by a depolarization to the second segment (Lewicki and Konishi, 1995 and 1996). Importantly, when zebra finches sing, HVC_{RA} neurons become depolarized, bringing their membrane voltage closer to their relatively high threshold. HVC_X on the other hand become strongly hyperpolarized, opening HCN channels, which provide

the strong inward current that gives rise to rebound excitation. This dichotomy points to their functional differences and highlights my central premise: synaptic properties and neuronal intrinsic properties are inextricable and work together to give rise to functional diversity in neural networks.

My results suggest that post-hyperpolarization rebound excitation in HVC_X neurons is a key mechanism that converts past inhibition into excitation with a delay, which when released can be summed with future excitatory events. This process promotes strong selectivity and precise bursting, as initial events could not accidentally lead to suprathreshold spikes because the neuron is strongly inhibited from song onset. Thus, the window of opportunity for integration of two events is defined by a neuron's intrinsic properties, directly tying HVC_X IPs to timing.

Downstream of HVC, basal ganglia neurons receive differently timed inputs and use them to regulate behavior with exceptional temporal precision. Consider that relative timing of such inputs carries useful information about the timing of song events, and that my results suggest that neuronal IPs affect integration and spike times. In this view, if a nucleus arrives at a global solution for IPs, then differences in EPSP-timing downstream can be interpreted without added ambiguity from the presynaptic neurons' excitability. This realization caused a shift in my thinking away from interpreting syllables as discrete song units, and towards thinking about arbitrary intervals defined by relative timing of events. Many song intervals can then be nested to span the entire song. Intervals of similar durations could be encoded by any neuron in the network with the appropriate IPs. And because different songs have different temporal constraints, different birds would need to express different IPs. This provides a new interpretation of the results from Daou and Margoliash, which showed song related clustering of HVC IPs in zebra finches, and ties in findings about global temporal structure in zebra finch song (Norton and Scharff, 2016) (see Chapter 4). This argument in turn provides an explanation for why the longest stack was correlated with rebound excitation despite it being highly improbable that the neurons I sampled were associated with that specific

syllable. Additionally, the shape of the window of opportunity that results from inhibition release has a shape that permits small differences in timing to produce burst differences (number of spikes in a burst). This would result in a neuron whose bursts provide information about the occurrence of the 'correct' event sequence, but also the relative timing of the events.

The modular structure of the model allows for multiple intervals to be encoded by the same neuron, so long as the intervals do not overlap, and the interval durations are similar. This captures a key feature of HVC_X neurons: Many neurons fire multiple bursts in a single motif. Once a network has a solution for detecting intervals of specific durations, why not reuse them? If one combines this rhetorical question with my results (as well as others') that show that song has internal temporal structure, then many intervals of the same duration may exist within the song, which provides a framework for multiple bursts within my network model. Figure 6.2 illustrates how this would be manifested in the network described in Chapter 3.

These rules, along with some simple optimization (maximizing total song coverage, and minimizing number of neurons), can reproduce newly discovered structure, expressed as parallel burst sequences (Figure 6.3), in reanalyzed data from singing birds (Fetterman 2022). The underlying mechanism in the model demands that HVC_X bursts from the same neuron are treated as non-independent events. To illustrate how the parallel burst structure arises from the model architecture, I coded an algorithm with a few simple rules to generate pseudo spike times (only numbers, not HH neurons). In this simpler toy model, series of numbers corresponding to subthreshold event timepoints were generated and sorted from least to greatest (e.g., 1, 4, 16, 30, 33, 40, 51, 304). Then, numbers were broken into pairs that defined the start and stop of an interval. This approach is computationally simple and guarantees that none of the intervals are overlapping. A sequence with 8 numbers would then correspond to a 4 interval 'neuron', where each interval has a start (release from inhibition) and stop (burst). I then repeated this process one hundred

thousand times and generated a dataset where each row represented a neuron and included n number of intervals (one half of the numbers in the sequence). At this point I introduced two constraints. The first aimed at capturing the uniformity of HVC_X IPs. I do this by requiring that all bursts within a neuron encompass intervals of similar lengths (no greater than a 20% variance of the interval durations). The second constraint was a theoretical one. There are many sets of my fake neurons that cover multiple intervals but do so with large gaps between them. I believe this is inefficient, and unlikely to be a solution in biological systems. Therefore, limited my analysis to the neurons with arrangements of intervals that minimized gaps between them and maximized coverage of the entire range of numbers: encoding the maximal number of intervals with the fewest neurons.

The resulting arrangement of neurons and bursts (only the offset of the interval, as required by my coincidence model, Figure 6.2) reflects parallel burst sequences. This structure excludes neurons who burst once (HVC_X or HVC_{RA}) but illustrates how the underlying mechanism gives rise to structure as described in Fetterman, 2022.

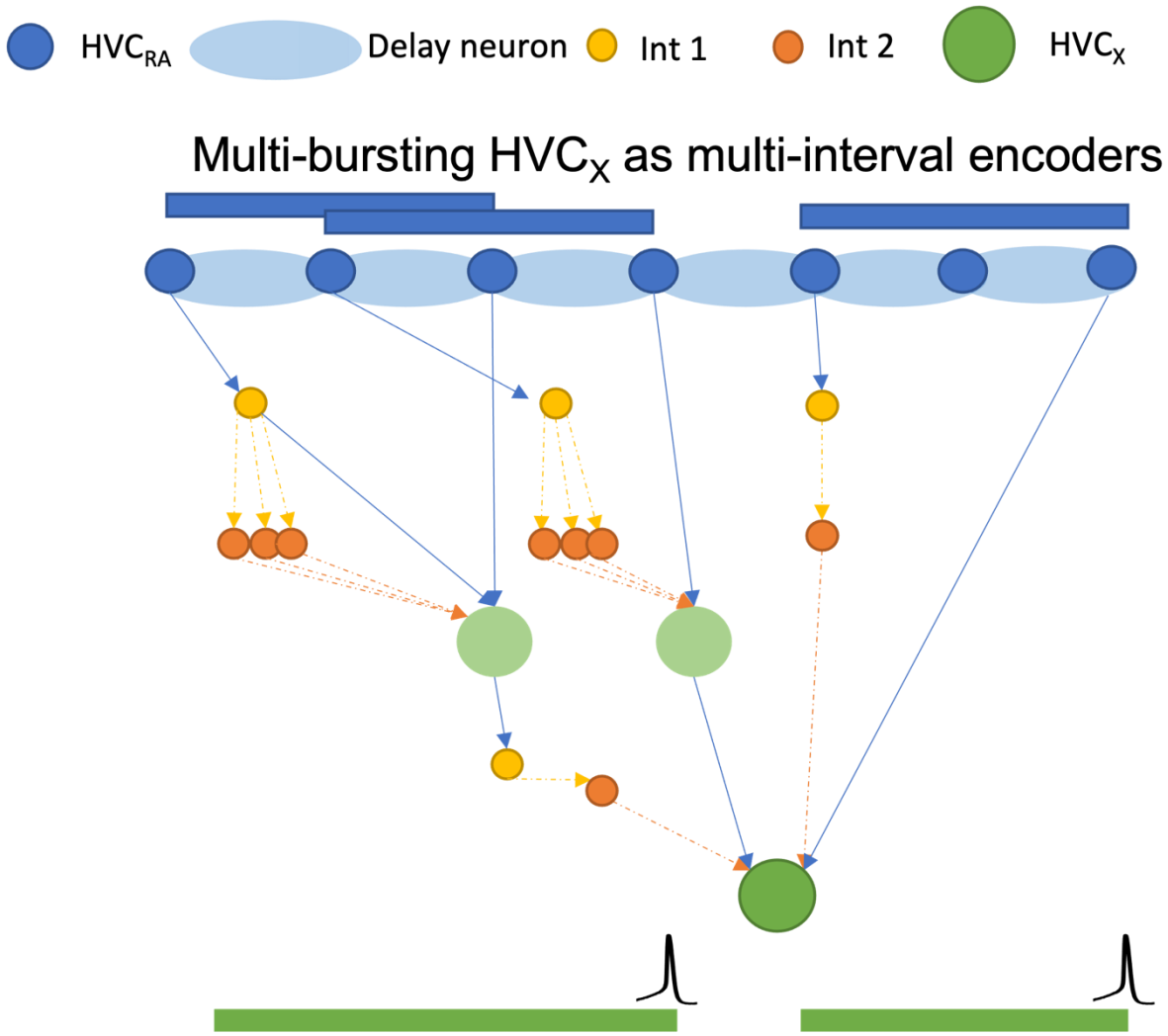

Figure 6.2. Modular network structure supports multiple bursts. Diagram showing how the basic, single burst, module from Chapter 3 can be organized to produce multiple bursts in the same neuron.

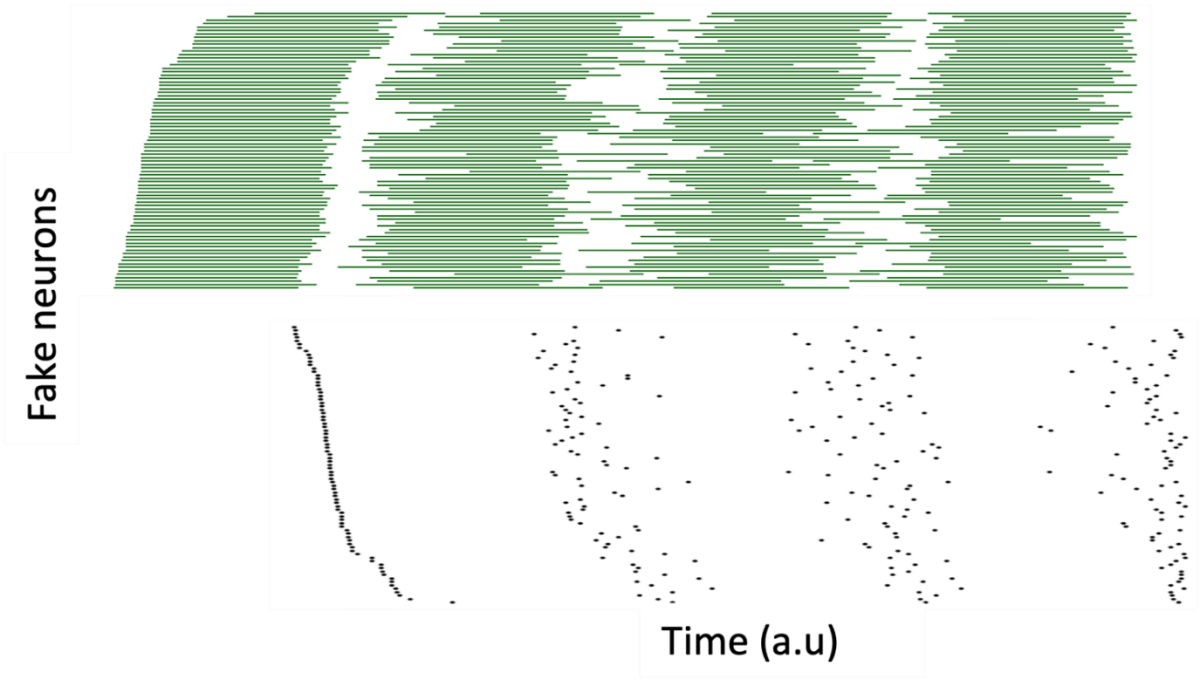

Figure 6.3. Multi-bursting model neurons produce parallel burst sequences. Illustration of simulated (fake), but principled, intervals (green) and burst times (black) where each row represents a four-burst neuron. Each neuron was constructed by a simple algorithm that minimizes overlaps between intervals and uses few neurons.

For my model to hold true, bursts (intervals) would need to be disambiguated at some later point. This could happen in the basal ganglia through specificity of synaptic structure and VTA inputs. A problem does arise from my model, however: If each HVC_X neuron's burst provides information about an interval only at the end, then information about errors that occurred early on would arrive in the basal ganglia with a delay. Critically, this feature of my model actually provides the first explanation for why VTA signals that arise from song errors arrive in the basal ganglia with a substantial delay (Gadagkar et al.., 2016) and predicts that the VTA delay varies by bird and relates to temporal features of song. If both HVC_X and VTA neurons report to the basal ganglia with a delay, then moment by moment song information is preserved and there is no problem with temporal assignment. Alternative models of HVC must address and compensate for this VTA-basal-ganglia delay.

Lastly, I wanted to address problems with the interpretation of my results and provide possible explanation. First, why does song playback produce responses in vivo as described in Lewiki & Konishi, 1996, where one syllable causes inhibition and another excitation? As I briefly addressed this in Chapter 3, my model assumes a 'hard-coded' constant signal for song onset, which acts as a shorthand to reproduce the in-vivo network environment. Instead, if every HVC_{RA} in the backbone produces a burst in the 'tonic' interneurons it can explain how isolated syllables produce strong hyperpolarization and provides a source for the song-induced hyperpolarization of the HVC_X population, which is currently not understood. Secondly, why do I find a weak correlation in the data from Daou & Margoliash 2020? I think this is likely due to a smaller number of birds (18 birds compared to 38), but also to the underestimation of the HCN conductance, which is temperature dependent (the recordings from the prior study were done at cooler temperatures). Finally, these findings support my central assertion that intrinsic neuronal properties are a fundamental

component of network function and studying them provides useful insight that must be fully incorporated into models of neural networks.

Reflections on Neuroethology

It is easy for neuroscientists to undervalue studying specialized behaviors because they are often more challenging to generalize and seldom come from readily available model organisms, like the mouse (though the mouse has more to offer than this view suggests). This perspective (or lack thereof) was one I shared early in my graduate studies and made systems like the retina enticing, with its beautiful, layered structure, and accessible ganglion cells which perform complex computations without the need of the whole animal. Yet, I had missed something essential, which most neuroscientists appreciate: no nervous system exists without influence of the evolutionary history of the whole organism. Later, I learned from the neuroethological perspective that acute focus on the strangest and most unique behaviors can give insight into fundamental systems as they are pushed to the limits of optimization.

REFERENCES

Amador, A., Perl, Y. S., Mindlin, G. B., & Margoliash, D. (2013). Elemental gesture dynamics are encoded by song premotor cortical neurons. Nature, 495(7439), 59-64.

Benezra, S. E., Narayanan, R. T., Egger, R., Oberlaender, M., & Long, M. A. (2018). Morphological characterization of HVC projection neurons in the zebra finch (Taeniopygia guttata). Journal of Comparative Neurology, 526(10), 1673-1689.

Bliss, T. V., & Collingridge, G. L. (1993). A synaptic model of memory: long-term potentiation in the hippocampus. Nature, 361(6407), 31-39.

Bolhuis, J. J., Hetebrij, E., Den Boer-Visser, A. M., De Groot, J. H., & Zijlstra, G. G. (2001). Localized immediate early gene expression related to the strength of song learning in socially reared zebra finches. European Journal of Neuroscience, 13(11), 2165-2170.

Brown, K. J. (2017). Vocal Motor Coding in a Songbird Premotor Nucleus. The University of Chicago.

Caporale, N., & Dan, Y. (2008). Spike timing-dependent plasticity: a Hebbian learning rule. Annual review of neuroscience, 31(1), 25-46.

Daou, A., & Margoliash, D. (2020). Intrinsic neuronal properties represent song and error in zebra finch vocal learning. Nature communications, 11(1), 1-17.

Daou, A., Ross, M. T., Johnson, F., Hyson, R. L., & Bertram, R. (2013). Electrophysiological characterization and computational models of HVC neurons in the zebra finch. Journal of neurophysiology, 110(5), 1227-1245.

Daoudal, G., & Debanne, D. (2003). Long-term plasticity of intrinsic excitability: learning rules and mechanisms. Learning & memory, 10(6), 456-465.

Dave, A. S., & Margoliash, D. (2000). Song replay during sleep and computational rules for sensorimotor vocal learning. *Science*, *290*(5492), 812-816.

Doupe, A. J., & Konishi, M. (1991). Song-selective auditory circuits in the vocal control system of the zebra finch. Proceedings of the National Academy of Sciences, 88(24), 11339-11343.

Doupe, A. J., Perkel, D. J., Reiner, A., & Stern, E. A. (2005). Birdbrains could teach basal ganglia research a new song. Trends in neurosciences, 28(7), 353-363.

Egger, R., Tupikov, Y., Elmaleh, M., Katlowitz, K. A., Benezra, S. E., Picardo, M. A., ... & Long, M. A. (2020). Local axonal conduction shapes the spatiotemporal properties of neural sequences. Cell, 183(2), 537-548.

Farine, D. R., Spencer, K. A., & Boogert, N. J. (2015). Early-life stress triggers juvenile zebra finches to switch social learning strategies. Current Biology, 25(16), 2184-2188.

Fetterman, G. C. (2022). Auditory Feedback and Neuronal Dynamics in the Songbird Forebrain (Doctoral dissertation, The University of Chicago).

Gadagkar, V., Puzerey, P. A., Chen, R., Baird-Daniel, E., Farhang, A. R., & Goldberg, J. H. (2016). Dopamine neurons encode performance error in singing birds. Science, 354(6317), 1278-1282.

George, J. M., Jin, H., Woods, W. S., & Clayton, D. F. (1995). Characterization of a novel protein regulated during the critical period for song learning in the zebra finch. Neuron, 15(2), 361-372.

Gill, D. F., & Hansel, C. (2020). Muscarinic modulation of SK2-type K+ channels promotes intrinsic plasticity in L2/3 pyramidal neurons of the mouse primary somatosensory cortex. *Eneuro*, *7*(2).

Grasselli, G., Boele, H. J., Titley, H. K., Bradford, N., van Beers, L., Jay, L., ... & Hansel, C. (2020). SK2 channels in cerebellar Purkinje cells contribute to excitability modulation in motor-learning–specific memory traces. *PLoS biology*, *18*(1), e3000596.

Hahnloser, R. H., Kozhevnikov, A. A., & Fee, M. S. (2002). An ultra-sparse code underliesthe generation of neural sequences in a songbird. Nature, 419(6902), 65-70.

Hamaguchi, K., Tanaka, M., & Mooney, R. (2016). A distributed recurrent network contributes to temporally precise vocalizations. *Neuron*, *91*(3), 680-693.

Hebb, Donald Olding. The organization of behavior: A neuropsychological theory. Psychology Press, 2005.

Herrmann, M., Hertz, J. A., & Prügel-Bennett, A. (1995). Analysis of synfire chains. Network: computation in neural systems, 6(3), 403-414.

Higgins, E. S., & George, M. S. (2013). *Neuroscience of clinical psychiatry: the pathophysiology of behavior and mental illness*. Lippincott Williams & Wilkins.

Ikeda, M. Z., Trusel, M., & Roberts, T. F. (2020). Memory circuits for vocal imitation. Current opinion in neurobiology, 60, 37-46.

Kao, M. H., Doupe, A. J., & Brainard, M. S. (2005). Contributions of an avian basal ganglia–forebrain circuit to real-time modulation of song. *Nature*, *433*(7026), 638-643.

Kozhevnikov, A. A., & Fee, M. S. (2007). Singing-related activity of identified HVC neurons in the zebra finch. *Journal of neurophysiology*, *97*(6), 4271-4283.

Lewicki, M. S. (1996). Intracellular characterization of song-specific neurons in the zebra finch auditory forebrain. Journal of Neuroscience, 16(18), 5854-5863.

Lewicki, M. S., & Konishi, M. (1995). Mechanisms underlying the sensitivity of songbird forebrain neurons to temporal order. Proceedings of the National Academy of Sciences, 92(12), 5582-5586.

Liu, W. C., Gardner, T. J., & Nottebohm, F. (2004). Juvenile zebra finches can use multiple strategies to learn the same song. Proceedings of the National Academy of Sciences, 101(52), 18177-18182.

Liu, X., Ramirez, S., & Tonegawa, S. (2014). Inception of a false memory by optogenetic manipulation of a hippocampal memory engram. Philosophical Transactions of the Royal Society B: Biological Sciences, 369(1633), 20130142.

Lombardino, A. J., & Nottebohm, F. (2000). Age at deafening affects the stability of learned song in adult male zebra finches. Journal of Neuroscience, 20(13), 5054-5064.

Long, M. A., & Fee, M. S. (2008). Using temperature to analyse temporal dynamics in the songbird motor pathway. Nature, 456(7219), 189-194.

Long, M. A., Jin, D. Z., & Fee, M. S. (2010). Support for a synaptic chain model of neuronal sequence generation. Nature, 468(7322), 394-399.

Lynch, G. F., Okubo, T. S., Hanuschkin, A., Hahnloser, R. H., & Fee, M. S. (2016). Rhythmic continuous-time coding in the songbird analog of vocal motor cortex. Neuron, 90(4), 877-892.

Mahon, S., & Charpier, S. (2012). Bidirectional plasticity of intrinsic excitability controls sensory inputs efficiency in layer 5 barrel cortex neurons in vivo. Journal of Neuroscience, 32(33), 11377-11389.

Marder, E., & Prinz, A. A. (2002). Modeling stability in neuron and network function: the role of activity in homeostasis. Bioessays, 24(12), 1145-1154.

Margoliash, D. (1983). Acoustic parameters underlying the responses of song-specific neurons in the white-crowned sparrow. Journal of Neuroscience, 3(5), 1039-1057.

Margoliash, D., & Fortune, E. S. (1992). Temporal and harmonic combination-sensitive neurons in the zebra finch's HVc. Journal of Neuroscience, 12(11), 4309-4326.

Margolis, D. J., & Detwiler, P. B. (2007). Different mechanisms generate maintained activity in ON and OFF retinal ganglion cells. Journal of Neuroscience, 27(22), 5994-6005.

Mello, C. V. (2014). The zebra finch, Taeniopygia guttata: an avian model for investigating the neurobiological basis of vocal learning. Cold Spring Harbor Protocols, 2014(12), pdb-emo084574.

Mitra, P., & Miller, R. F. (2007). Mechanism underlying rebound excitation in retinal ganglion cells. Visual neuroscience, 24(5), 709-731.

Mitra, P., & Miller, R. F. (2007). Normal and rebound impulse firing in retinal ganglion cells. Visual neuroscience, 24(1), 79-90.

Mooney, R. (2000). Different subthreshold mechanisms underlie song selectivity in identified HVc neurons of the zebra finch. Journal of Neuroscience, 20(14), 5420-5436.

Mooney, R., & Prather, J. F. (2005). The HVC microcircuit: the synaptic basis for interactions between song motor and vocal plasticity pathways. Journal of Neuroscience, 25(8), 1952-1964.

Motanis, H., Maroun, M., & Barkai, E. (2014). Learning-induced bidirectional plasticity of intrinsic neuronal excitability reflects the valence of the outcome. Cerebral Cortex, 24(4), 1075-1087.

Nabavi, S., Fox, R., Proulx, C. D., Lin, J. Y., Tsien, R. Y., & Malinow, R. (2014). Engineering a memory with LTD and LTP. Nature, 511(7509), 348-352.

Norton, P., & Scharff, C. (2016). "Bird song metronomics": Isochronous organization of zebra finch song rhythm. Frontiers in Neuroscience, 10, 309.

O'Hare, J. K., Gonzalez, K. C., Herrlinger, S. A., Hirabayashi, Y., Hewitt, V. L., Blockus, H., & Losonczy, A. (2022). Compartment-specific tuning of dendritic feature selectivity by intracellular Ca2+ release. Science, 375(6586), eabm1670.

Oginsky, M. F., Maust, J. D., Corthell, J. T., & Ferrario, C. R. (2016). Enhanced cocaine-induced locomotor sensitization and intrinsic excitability of NAc medium spiny neurons in adult but not in adolescent rats susceptible to diet-induced obesity. *Psychopharmacology*, *233*(5), 773-784.

Ölveczky, B. P., Andalman, A. S., & Fee, M. S. (2005). Vocal experimentation in the juvenile songbird requires a basal ganglia circuit. PLoS biology, 3(5), e153.

Park, A., Hoffman, K., & Keller, A. (2014). Roles of GABAA and GABAB receptors in regulating thalamic activity by the zona incerta: a computational study. *Journal of Neurophysiology*, *112*(10), 2580-2596.

Paz, J. T., Mahon, S., Tiret, P., Genet, S., Delord, B., & Charpier, S. (2009). Multiple forms of activity-dependent intrinsic plasticity in layer V cortical neurones in vivo. *The Journal of physiology*, *587*(13), 3189-3205.

Pham, T., & Hansel, C. (2022). Intrinsic threshold plasticity: cholinergic activation and role in the neuronal recognition of incomplete input patterns. *The Journal of Physiology*.

Pilarski, J. Q., Wakefield, H. E., Fuglevand, A. J., Levine, R. B., & Fregosi, R. F. (2011). Developmental nicotine exposure alters neurotransmission and excitability in hypoglossal motoneurons. *Journal of neurophysiology*, *105*(1), 423-433.

Prinz, A. A., Bucher, D., & Marder, E. (2004). Similar network activity from disparate circuit parameters. Nature neuroscience, 7(12), 1345-1352.

Riebel, K. (2009). Song and female mate choice in zebra finches: a review. Advances in the Study of Behavior, 40, 197-238.

Ross, M. T., Flores, D., Bertram, R., Johnson, F., & Hyson, R. L. (2017). Neuronal intrinsic physiology changes during development of a learned behavior. eneuro, 4(5).

Ross, M. T., Flores, D., Bertram, R., Johnson, F., Wu, W., & Hyson, R. L. (2019). Experience-dependent intrinsic plasticity during auditory learning. Journal of Neuroscience, 39(7), 1206-1221.

Scharff, C., & Nottebohm, F. (1991). A comparative study of the behavioral deficits following lesions of various parts of the zebra finch song system: implications for vocal learning. Journal of Neuroscience, 11(9), 2896-2913.

Scharff, C., Kirn, J. R., Grossman, M., Macklis, J. D., & Nottebohm, F. (2000). Targeted neuronal death affects neuronal replacement and vocal behavior in adult songbirds. Neuron, 25(2), 481-492.

Scheffer, L. K., Xu, C. S., Januszewski, M., Lu, Z., Takemura, S. Y., Hayworth, K. J., ... & Plaza, S. M. (2020). A connectome and analysis of the adult Drosophila central brain. *Elife*, *9*.
Sjostrom, P. J., Rancz, E. A., Roth, A., & Hausser, M. (2008). Dendritic excitability and synaptic plasticity. Physiological reviews, 88(2), 769-840.

Stevens, C. F., & Wang, Y. (1995). Facilitation and depression at single central synapses. Neuron, 14(4), 795-802.

Tchernichovski, O., Mitra, P. P., Lints, T., & Nottebohm, F. (2001). Dynamics of the vocal imitation process: how a zebra finch learns its song. Science, 291(5513), 2564-2569.
Titley, H. K., Brunel, N., & Hansel, C. (2017). Toward a neurocentric view of learning. Neuron, 95(1), 19-32.

Titley, H. K., Watkins, G. V., Lin, C., Weiss, C., McCarthy, M., Disterhoft, J. F., & Hansel, C. (2020). Intrinsic excitability increase in cerebellar Purkinje cells after delay eye-blink conditioning in mice. Journal of Neuroscience, 40(10), 2038-2046.

Varshney, L. R., Chen, B. L., Paniagua, E., Hall, D. H., & Chklovskii, D. B. (2011). Structural properties of the Caenorhabditis elegans neuronal network. *PLoS computational biology*, *7*(2), e1001066.

Vates, G. E., Vicario, D. S., & Nottebohm, F. (1997). Reafferent thalamo-"cortical" loops in the song system of oscine songbirds. Journal of Comparative Neurology, 380(2), 275-290.
Xiao, L., & Roberts, T. F. (2021). What Is the Role of Thalamostriatal Circuits in Learning Vocal Sequences?. Frontiers in Neural Circuits, 95.

Yu, A. C., & Margoliash, D. (1996). Temporal hierarchical control of singing in birds. *Science*, *273*(5283), 1871-1875.

Zhang, W., & Linden, D. J. (2003). The other side of the engram: experience-driven changes in neuronal intrinsic excitability. Nature Reviews Neuroscience, 4(11), 885-900.